Comments on the CLAS Analysis Note

Deeply virtual Compton scattering off ^{4}He

M. Hattawy, N. Baltzell, R. Dupré , H. Egiyan, L. El Fassi,
F.-X. Girod, K. Hafidi, C. Moody, S. Stepanyan

Nuclear working group, October 12, 2015

Review committee:

Michel Garçon (chair)
Sebastian Kuhn
Zein-Eddine Meziani

This review is based on your 'First version of the Note'. Please put a date on successive versions (on the web page as well as on the Note cover page). You will find hereafter the comments from the three reviewers (after a round of discussions among us). There are some overlapping comments. We left them as such on purpose to reinforce the idea, but you may refer to an earlier answer in your answer to another reviewer.

There are many points to be addressed, but most of them should not take too much time. In short, what seems of particular importance to us is:
- A better explanation of the RTPC drift speed calibration and track reconstruction, and this may entail some rewriting.
- Explain from the start what the RTPC gain calibration is or is not used for and remove the first method which is not used in the end (or just allude to it).
- In several instances raised by the three reviewers, check results with tighter cuts. It does not necessarily mean that the end results should use tighter cuts (e.g. in z-vertex), but that this is a way to study systematic effects.
- The validity of some 'early' pid cuts (Cerenkov, z-vertex, ...) should be checked after exclusivity cuts (for both coherent and incoherent).
- The question of accidentals (especially in e-4He coincidences) needs to be addressed.
- The question of physical background other than exclusive pi0 should be discussed, at least qualitatively.
This is not to say that the other points are to be dismissed ....

1^{st} reviewer

I first have to say that this is of course an unusually complicated and difficult analysis (even by CLAS standards) because of the many idiosyncrasies concerning the RTPC. Many students and other members of the EG6 collaboration have spent an enormous amount of time trying out all kinds of improvements and analysis methods, so it would seem like double jeopardy to also insist on an equally voluminous tome to describe the analysis. However, I do feel that the present version is missing quite a few details that are important for us to fully understand what was done, to assess whether it was done 'well enough' and to give our green light to the analysis.

1) Eq. 2.1, p.16: The second row is missing the charge, q, in front of Bz. This is not trivial, as the next 3 lines contain numerical examples that seem to be wrong. For instance, the range in r_0 quoted for DVCS is 20 - 45 mm - but I find a radius of 100 mm for 260 MeV/c 4He nuclei going radially (q = 2e). Even at some angle, 20 mm is impossible - such a track would never make it through the drift region. (Fig. 2.7 shows a minuscule pedestal below r_0 = 25 mm, but this must be due to some spurious effect - I don't see how you can reconstruct any tracks with $r_0 < 30$ mm). Is this mistake in your software as well (see horizontal scale in Fig. 2.7)?
In equation 2.1, the charge of the particle (q) is indeed missing. Regarding the numerical calculations of r_0 for the elastic and the DVCS ^{4}He, the 0.3 factor is missing only in these calculations while the charge issue is taken into account. In the reconstruction software, both issues are properly implemented. (For example, In a magnetic field of 4.5 T, the recoil 4He nuclei from DVCS (elastic) reaction have kinetic energies in the range [10, 25] ([17, 35]) MeV, from momenta of [260, 450] ([360, 550]) MeV and r_0 [70, 150] ([130,180]) mm.)

2) Section 2.2: The RTPC calibration procedure is described in 2 steps: Event selection (2.2.1)

and actual calibration (2.2.2 - 2.2.4) plus noise rejection (2.2.5). However, the event selection contains cuts on r_0, chi2, z etc. which in turn presuppose some initial calibration already. In other words, the process MUST be iterative - but I couldn't find a clear summary how this iteration was executed (i.e., what was used for the first iteration, how many iterations total, etc.). There is a short mention at the bottom of p. 27, but no details.
The drift paths and drift speed were first extracted using the MAGBOLTZ Monte Carlo simulation. One can find the detailed procedure of a similar extraction in the BoNuS analysis note (https://www.jlab.org/Hall-B/secure/bonus/publication/BonusAnal110117.pdf). Then, we proceeded to derive empirical improvements with many iterations after each change that would affect the drift paths, such as the beam-offset and gain calibrations of the RTPC. Moreover after each pass, the number of elastic events used for calibration increased. Overall, this was a long process that evolved and improved over the years and we concentrated in the note on the description of the final iteration.

3) 2.2.1.1 It would be helpful to have some more background information: What is the longest drift time (from the inner radius) for a good track? What kind of momentum gives you only 4 hits, and are those events important? (see further down, under Fig. 3.19) What is the timing offset between the trigger and the shortest drift time (outer radius RTPC)? What is the average drift velocity and Lorentz angle? Conversion TDC-> time is given p. 15, but it would be much more helpful to have all these basic parameters collected in a single place: 2.1.1 - 2.1.3 are all good places to summarize these parameters.
The longest drift time depend on z but is typically around 6.6 μs. Four is the number of the active pads for a track, not the number of hits. This value has been found to be reasonable from simulation, it mainly help clean the sample and plays very little role after other cuts. The time offset is 15 TDCs (1 TDC= 114 ns), the average drift velocity is 6.14 μm/ns and we did not extract the Lorentz angle, but MAGBOLTZ indicated about 20 degrees.

4) 3rd bullet: There should also be an upper limit on r_0, since it is actually r_0 = +infinity that is indistinguishable from r_0 = -infinity (i.e., charge will be unknown). For the same reason, it would be nice to have a plot of $1/r_0$ instead of or in addition to Fig. 2.7
Figure 1 shows the $1/r_0$ distribution for a sample of the 1.2 GeV data for all the reconstructed tracks without any requirement. Figure 2 presents the same distribution after requiring reading from at least 4 pads, *sdist* and *edist* cuts. We see in figure 2 that selecting $r_0 > 0$ is already cutting the tail of the distribution. Applying a cut for large r_0 would correspond to applying a cut at a larger $1/r_0$. Based on this distribution, we do not see any motivation for this. In particular since exclusivity cut will eventually clean all unphysical results.

5) 4th bullet: How are the points r^{helix}, ϕ^{helix} and z^{helix} determined? Somehow, you have to identify points on a continuous line that are closest to (perhaps) the hits? How are the uncertainties (sigmas) in χ^2 determined? Are those the final values AFTER calibration? If so, how do you select your sample initially? (See above - it must be an iterative process).
$(r^{helix}, \phi^{helix}, z^{helix})$ is the point on the helix that is closest to the reconstructed hit position. The values of the uncertainties are intrinsic detector properties depending primarily on the size and configuration of the readout pads. These uncertainties, $(\sigma_r, \sigma_\phi, \sigma_z) = (0.53mm, 2^\circ, 1.2mm)$, were not derived from our data and were held fixed over all calibration itterations.
Equation 2.2 needs the beam-spot constraint added in quadrature $\left(\frac{DOCA}{\sigma_r}\right)^2$ as follows (changed in the note as well):

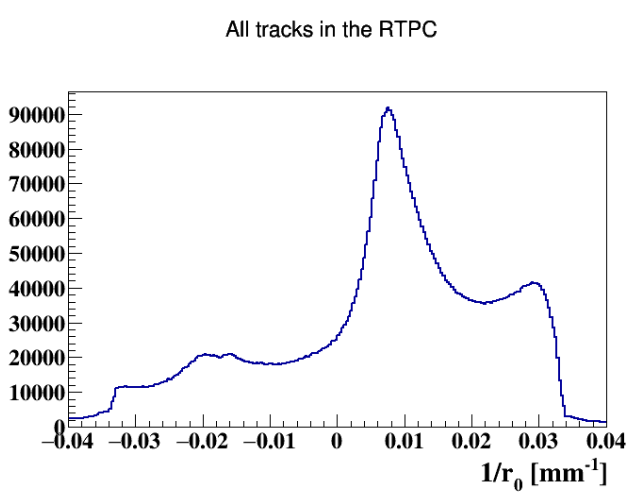

Figure 1: $1/r_0$ for all the reconstructed tracks in the RTPC using 1.2 GeV electron beam.

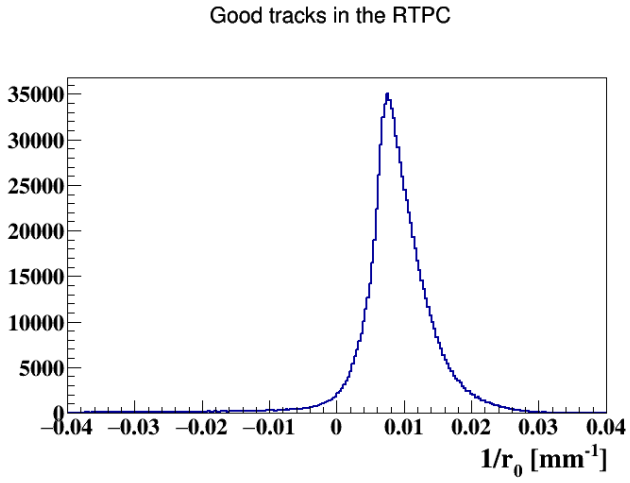

Figure 2: $1/r_0$ for tracks that passed the requirements: reading from at least 4 pads, *sdist* and *edist*.

$$\chi^2 = \frac{\left(\frac{DOCA}{\sigma_r}\right)^2 + \sum_{i=1}^{N_{pts}} \left(\frac{r_i^{pt} - r_i^{helix}}{\sigma_r}\right)^2 + \left(\frac{\phi_i^{pt} - \phi_i^{helix}}{\sigma_\phi}\right)^2 + \left(\frac{z_i^{pt} - z_i^{helix}}{\sigma_z}\right)^2}{N_{pts} - 4} \quad (1)$$

6) 5th bullet: Again, *sdist* and *edist* already pre-suppose a timing calibration. For assessing possible accidental coincidences (see more below), it would be useful to know what time spans correspond to the limits chosen on them.
sdist limits span a drift time equal to 0.68 μs, while *edist* limits span 1.03 μs.

7) Finally, I'm puzzled by the large positive limit on *edist* - supposedly this quantity is easier to measure (shortest 'drift' time), yet there is clearly a tail towards positive *edist* (towards smaller radii??) superimposed on an otherwise sharp peak. Wouldn't you want to cut that tail at least for the purpose of calibration, to make sure you only look at 'golden tracks'? Is it specific to higher momenta?
The positive long tail on *edist* distribution is made of hits out of time mostly due to electronic noise. However, if we do not apply any constraint on *edist* and *sdist* variables and select the elastic He-4 tracks with the other cuts, we observe that most of the tails are removed as can be seen in the figure 3 and 4. Therefore, making tighter cuts would not cause changes in the calibration as the tracks in the tail regions are cleaned by the other cuts. No correlations was observed between the tails and the momentum, as can be seen in figure 5.

8) Last bullet: Again, what are the initial choices on this cut to select calibration tracks? What do you use for the z_0 of the simulated track?
We used similar cuts for all the calibration iterations. z_0 of the simulated ^{4}He is set to be the z-vertex of the scattered electron. The 2σ cut corresponding to ≈ 20 mm.

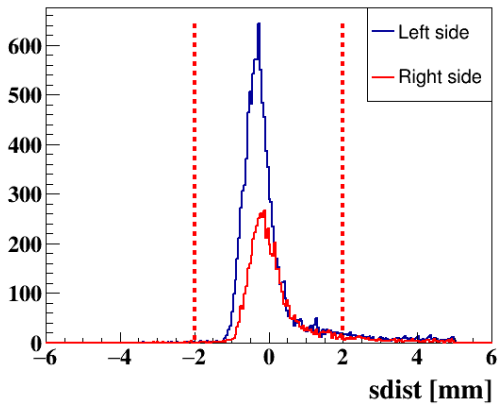

Figure 3: sdist distribution for the selected elastic ^{4}He tracks.

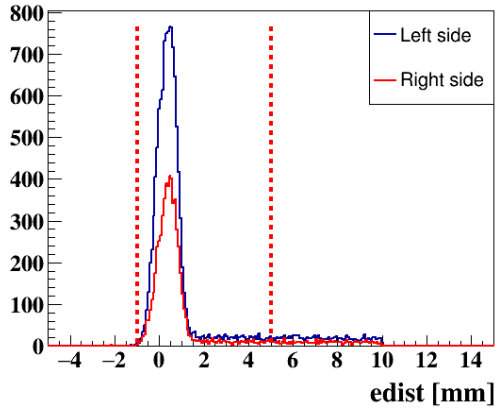

Figure 4: edist distribution for the selected elastic ^{4}He tracks.

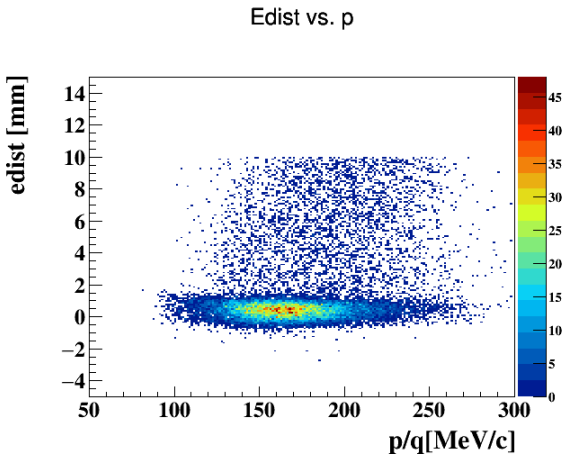

Figure 5: edist as a function of the measured p/q for the selected elastic tracks.

9) 2.2.1.2 Again, these cuts already pre-suppose (good enough) initial tracks.
Yes

10) Fig. 2.11: Do we understand why Δz is not constant? Is this before or after the RTPC alignment (alluded to but not explained)? Is the resolution shown the final result after optimizing the calibration? The exact same questions also arise for Fig. 2.12.
The presented Δz and $\Delta\phi$ distributions are after all the calibration and detector alignments (RTPC alignment is described in CLAS-NOTE-2013-008). The observed remaining dependences are not fully understood and probably arise from field misalignement and variations in the electric and magnetic fields within the chamber.

11) Eq. 2.4: It is much better to use a cut on the reconstructed beam energy from the measured angles θ_e and θ_{He}, since momenta are less precisely measured by CLAS than angles. Peter Bosted has used this method very effectively. Indeed, Fig. 2.13 shows a rather broad distribution, with a cut that barely has any effect. (This is a side comment, not meant to require additional work).
We are indeed aware of this and we do use a $\Delta\theta$ cut as our main selection for this reason, which

we believe is equivalent to your proposition. Note also that $\Delta\phi$ and Δz cuts have already been applied in Figure 2.13's $\Delta\theta$.

12) Fig. 2.14: It's curious that the W distribution 'for the right RTPC module' is wider than on the lhs, given that nothing measured by the RTPC enters this quantity. However, it might be that the corresponding sectors in CLAS have different resolution, as well.
Yes, this is related to the different resolutions of the corresponding CLAS sectors. This effect is large because, the reaction products are emitted back to back resulting in small regions of overlapping acceptances of the RTPC and CLAS. In figure 6, we plot W distributions corresponding to the different sectors in CLAS, one can immediately see the differences of resolution.

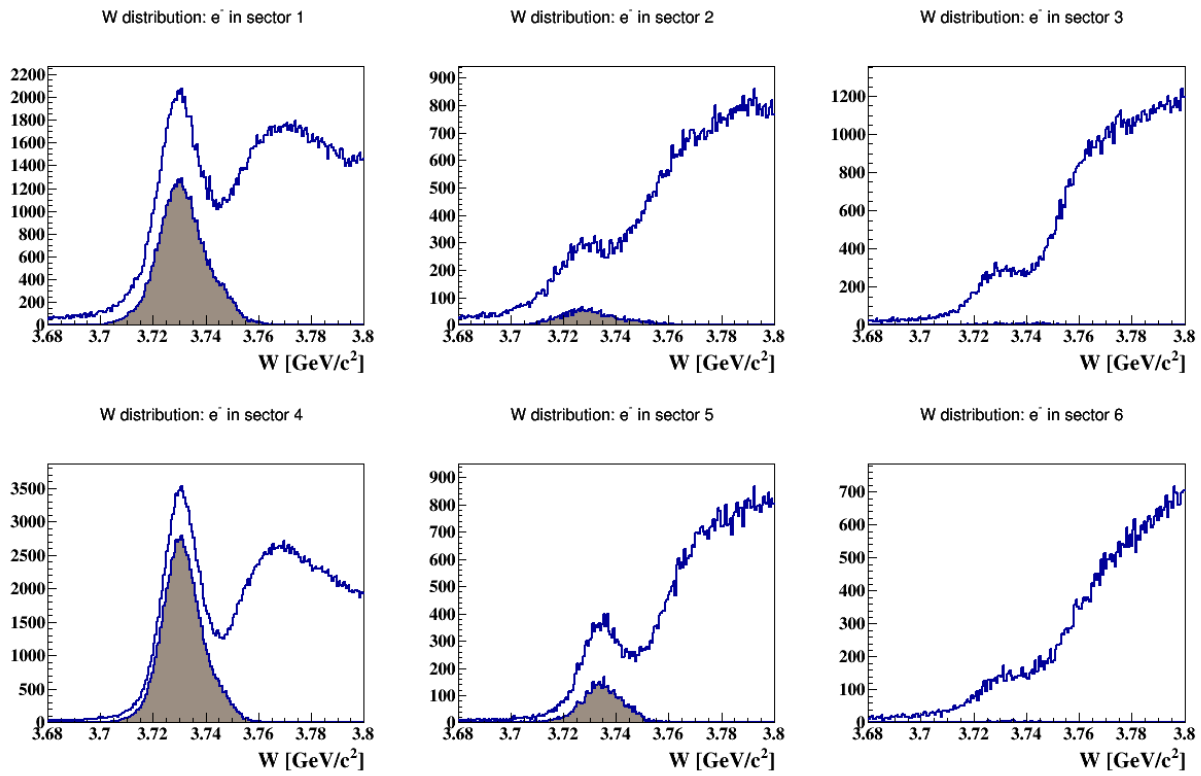

Figure 6: W distributions for the identified good tracks (in blue) and elastic events (in shaded brown) where the electron scattered in the different sectors of CLAS.

- 2.2.2 2nd paragraph: Due to the varying B(z) and therefore the varying Lorentz angle, the drift path is NOT the same for all electrons at all z. (Corrected in the 3rd paragraph.) More importantly, all times are given in TDC units instead of μs- we must know the conversion factor and the offset! (Is it the same for all TDC channels?)
1 TDC = 114 ns, the time offset is TDCmin (= 15 TDCs) and is the same for all the readout channels.

13) Fig. 2.19: I can't figure out what exactly is plotted here (in particular on the z-axis). If I understand Eq. 2.8 correctly, then R is simply deduce from TDC for the real data - so no surprise to see a straight line. How is this then linked to the simulated track?
Here R is from simulation and TDC is from real data. This figure is indeed here only to illustrate the Eq 2.8 and allows to associate simulated hits with measured ones. The text is modified to

clarify this point.

14) Figs. 2.20-22: Again, more detail needed to understand what's plotted and how it is calculated. Why is Delta-phi not zero for TDC = 15 (which corresponds to the outer radius of the drift region)?- Eq. 2.9: A (brief) derivation would help a lot here.
$\Delta\phi$ at the anode (TDC = 15) is not equal to zero because there is a drift in ϕ between the anode (the first GEM layer at radial distance equal to 60 mm) and the readout pads (at radial distance equal to 69mm). Regarding the derivation, figure 7 shows a simple drawing explaining how Eq. 2.9 can be derived.

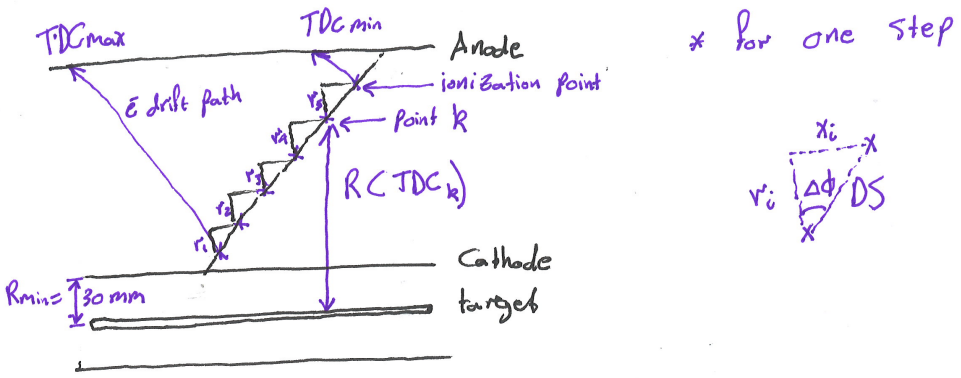

Figure 7: Schematic drawing shows how the radius of emmision (R) at each ionization point is calculated from the drift paths ($\Delta\phi$) and the drift speed (DS).

In figure 7, the radial distance of the ionization point k, $R(TDC_k)$, is equal to to the radial distance from the target to the cathode, R_{Min}, plus the radial distances ($\sum r_i$) that are caused by the drift from the first point of ionization at TDC_{max} to the point k. In each TDC bin, the radial drift distance (r_i) is calculated as:

$$r_i = \sqrt{DS^2 - r_{i-1}\left(\frac{\partial\Delta\phi}{\partial TDC}(TDC_i)\right)^2} \tag{2}$$

Adding all the terms, $R(TDC_k)$ is formulated as:

$$R(TDC_k) = R_{min} + \sum_{i=TDC_{Max}}^{TDC_k} r_i \tag{3}$$

15) 2.2.4: Eq. 2.12 is differential, while Eq. 2.14 is integrated over the whole track. Do you integrate Eq. 2.12? Otherwise, it probably doesn't work all that well. Maybe this is the reason why the bands visible in Fig. 2.29 are not well represented by the superimposed curves? BTW, what is the vertical scale on Fig. 2.29?
Eq. 2.14 represents the average energy loss per unit of length in the track, *vtl* being the visible track length. Assuming the energy loss in the drift region small, the two can be easily compared. Indeed at the lowest energy this assumption is not true anymore. But the difference between instantaneous and average $\frac{dE}{dx}$ is expected to be small compared to our resolution except very

close to threshold (see right panel of Figure 12).
In Fig. 2.29 the lines are just there to guide the eye. Since the vertical scale has never been carefully calibrated, we always present it in arbitrary units. To have a feeling of the units, we have extracted an over all conversions from comparing real data to simulation, where 1 ADC is equal to 17 eV (21 eV) deposited in the left (right) module of the RTPC.

16) p. 29, 2nd to last paragraph: I THINK I understand the Landau fit (over many tracks, no?) for each channel. But I don't understand the last step - why is it needed? What does it accomplish? For sure more details (and a plot) are needed.
Yes, the gain ratio of each readout pad is calculated from comparing all the experimental elastic tracks to their corresponding tracks obtained from simulation. These ratios give us a first gain for each readout pad. However, we noticed that some pads record lower ADCs than expected (issue shown in figure 2.28) and sometime noise. For these reasons, we wanted to make sure that the recorded ADCs by a given pad are similar to the recorded ADCs recorded by another pad in the same track. In figure 8, one can see improvements obtained by using this method to fine tune the gains obtained previously.

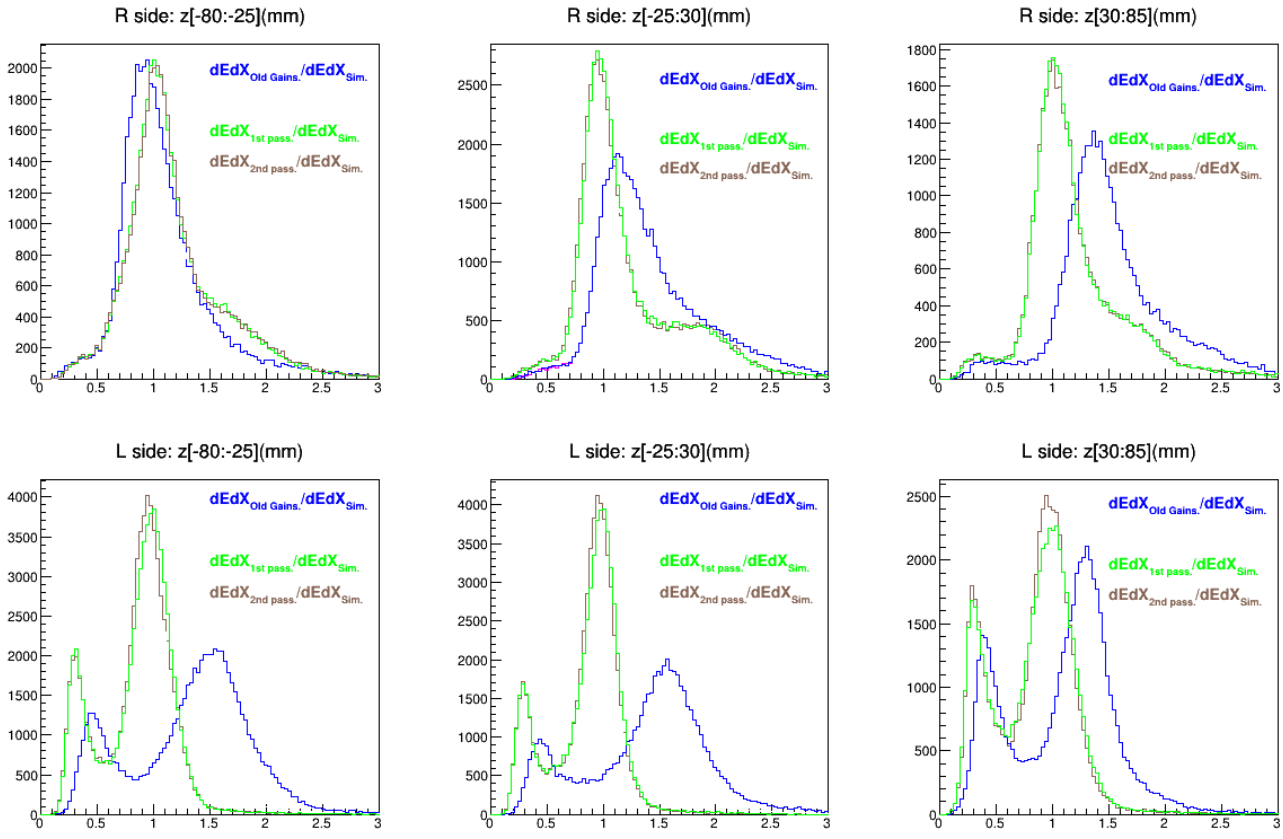

Figure 8: The ratio between the experimental dEdx and the simulated ones for different regions along z of the RTPC. The blue lines are using the first method of extracting the gains (comparing the experimental recorded dEdx to the expected values calculated from the Bethe-Block formula), the green lines are using the 1st pass of the second method (comparing simulation to data only) with all the elastic event sample and the brown lines are using the gains extracted from the second method (both steps).

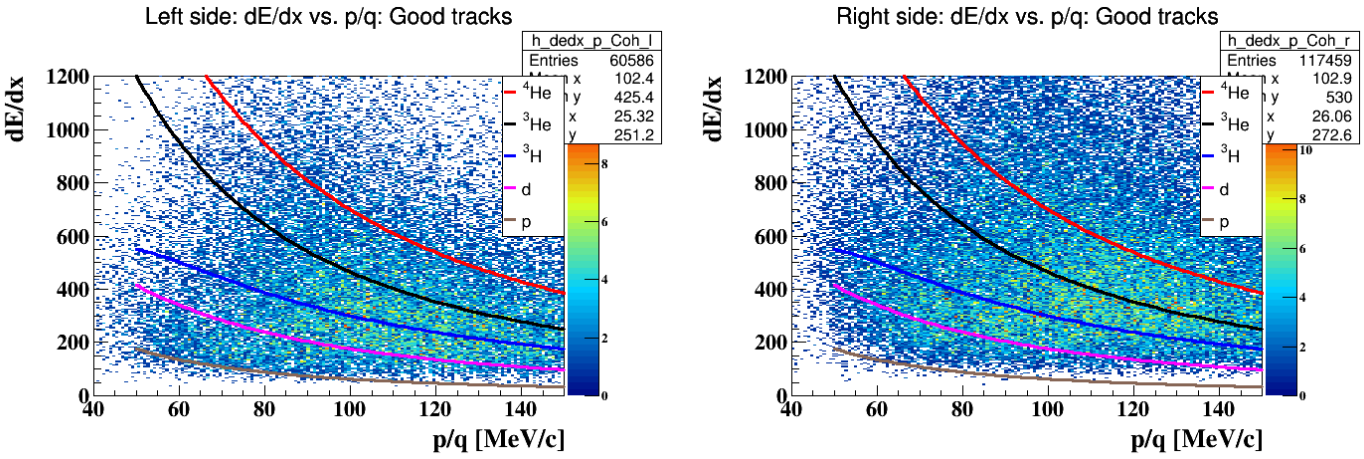

Figure 9: dEdx verus p/q distribution for the good tracks collected at 6 GeV beam energy.

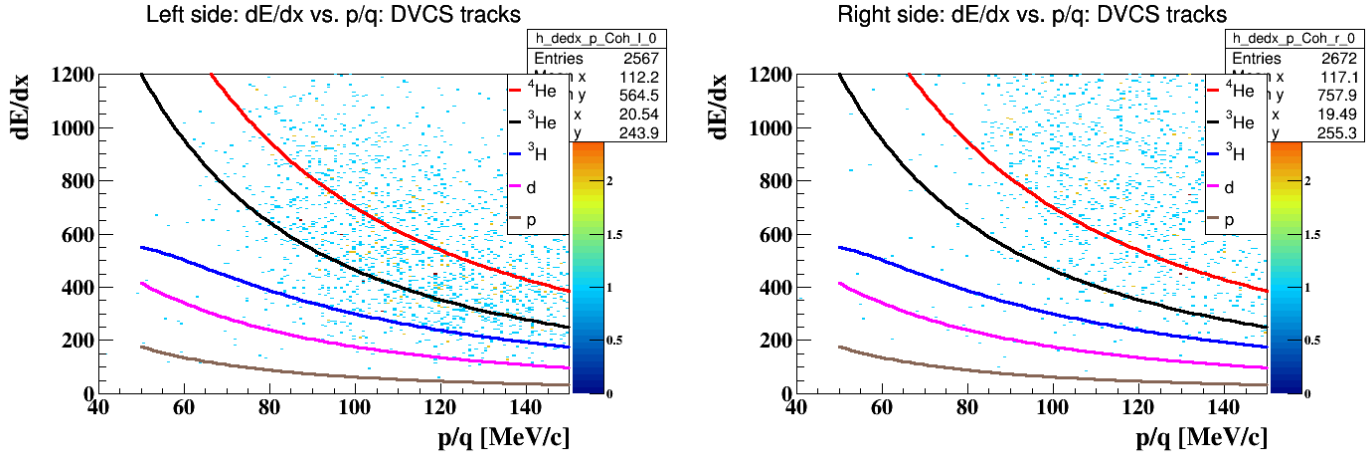

Figure 10: dEdx verus p/q distribution for the identified He4 DVCS nuclei at 6 GeV beam energy.

17) p.31, last paragraph: Could it be that the low-signal tracks are due to protons (maybe elastically scattered out of the Kapton target enclosure)? There could be some beam halo interacting with the straw tube. Last sentence (top p.32): HOW are 'events from the low-region' excluded from the analysis (for NON-elastic events)? Do you use a cut on dE/dx? Describe the cut! (It's not mention in Section 3.1.4 - but why bother with gain calibration if you don't use the ADC values?)

More work is needed to understand the nature of these low-signal tracks, but they cannot be protons as their dedx would be much smaller, and they are only present in one half of the RTPC. We looked hard but found no correlation between these tracks and any other experimental quantities. A possible explanation is that the gain might have been periodically lowered by high rates of events. For this DVCS analysis we do not use $\frac{dE}{dx}$ to select ^{4}He, instead we only use the DVCS exclusivity cuts. Figure 9 shows dEdx as a function of p/q for the good tracks from 6 GeV beam energy runs, while Figure 10 shows the same for identified coherent DVCS He-4 nuclei. One can see that the selected He4 nuclei have on average high dEdx trend that matches with the theoretical line, but the band seem too wide to apply a significative cut.

18) 2.2.5: 3rd line, the claim is made that elastic 4He produce too small a signal because of

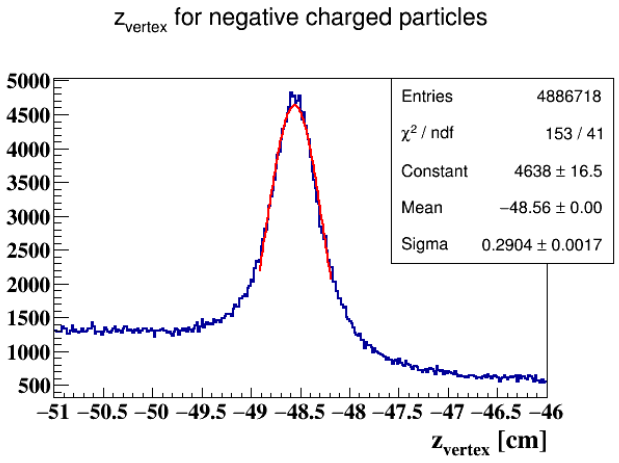

Figure 11: z-vertex of scattered electrons at 6 GeV beam energy from the downstream window of the target. The z-vetex resolution of CLAS here is about 3 mm.

their small Tkin. This is strange, since low Tkin actually means LOTS of energy LOSS - which is also born out by Fig. 2.29. Overall, it would be good to get a quantitative feeling for the amplitude of the noise (in mV and in equivalent dE/dx relative to good 4He tracks). It would be even better if we had any inkling about the source of the noise (electronics malfunction? cross-talk? antenna pick-up?), but of course that's not a requirement for the analysis to be approved.
The statement about too small Tkin is misleading and has been changed. The fact is that readout thresholds were set low to avoid efficiency problems, with the effect of recording more electronic noise. We do not know where the noise is coming from, only speculation. As for getting a feeling of the amplitude of the noise, one option is to compare Figures 2.30 with 2.25 and/or 2.28 top. This shows that the amplitude of the oscillatory noise is not much smaller than the typical hits from a ^{4}He track.

19) Fig. 2.30: What is plotted on the z-axis? (Occupancy?) Is this plot integrated over all 'good tracks', or only for tracks that actually traversed the selected pad (or a nearby pad)? If the former, what does a signal for a good track that crosses this pad look like?
The color scale on the z-axis is a hit yield. The hits included are only those recorded by one example noisy pad and only when those hits were used in a good track.

20) 2.3: 5th line p. 37: No, the z-vertex resolution for an extended target in the presence of the DVCS solenoid is a lot worse than 1 mm - see Fig. 3.1 So in fact the z-resolution of the RTPC is not that bad.
Indeed the indicated value is without solenoid. In the presence of the solenoid, the z-vertex resolution of CLAS is about 3 mm, which we measured from the downstream target window, as can be seen from figure 11.

21) Fig. 2.37: Clearly, momenta are shifted 10% lower on average. This is not surprising, since at low momentum, energy loss will reduce the reconstructed radius of the helix. However, since the 4He momentum enters various cuts, we need a better understanding of Deltap/p as a function of p and theta, e.g. through 2D plots like Figs. 2.11-2.13. Of course it would be even better to CORRECT p for energy loss and other effects - but Section 3.3 doesn't mention any

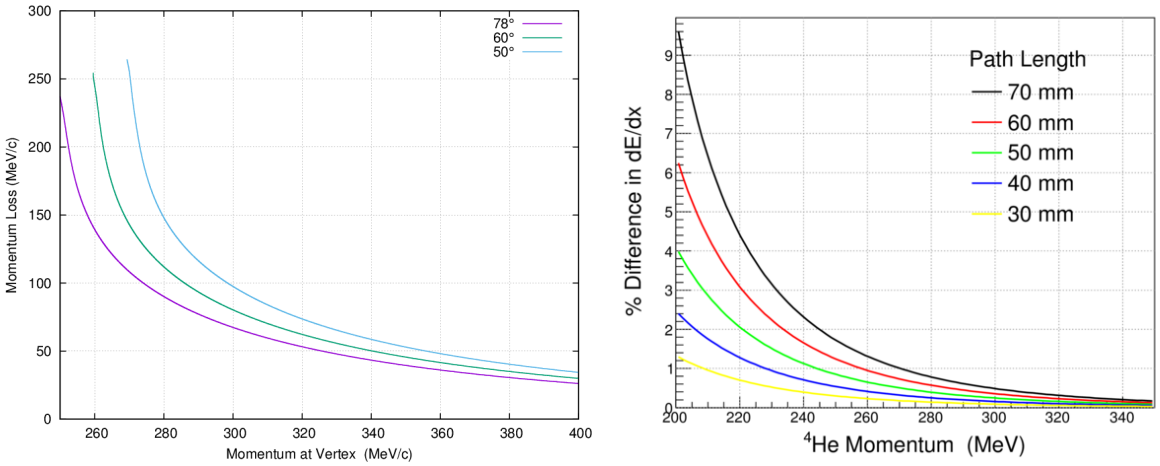

Figure 12: On the left is the energy loss correction (in terms of momentum) derived from full simulation for ^{4}He and a few relevant polar angles, where the x-axis is momentum at the primary vertex. On the right is the relative difference between the instantaneous ^{4}He $\frac{dE}{dx}$ at the midpoint of the drift region and averaged over the drift region, where the x-axis is the average momentum in the drift region. The maximum path length at 40° is about 50 mm.

kinematic corrections for 4He. (I don't insist on this, but the effect on the 'true exclusivity' of the final cuts should be discussed.
We do in fact correct for energy loss. The correction is calculated from energy loss in GEANT between the primary electron vertex and the midpoint of the drift region. This correction was parameterized in terms of (p, θ) and particle type, it was validated by hand-integrating Bethe-Bloch formula. The left panel of Figure 12 shows our energy correction for a few polar angles. The following plots, 13 and 14, show that the momentum shift after the energy correction as a function of the measured momentum is still present. One could deduce that our energy loss correction is not strong enough however no correlation is observed with the measured polar angle, which should be expected if the mismatch was due to energy loss. Different unidentified issues are probably at the origin of this problem.
We decided to test corrections based on the z-dependence shown in figure 15. Figure 16 shows the difference between the elastic 4He momentum and its calculated value from the electron scattering angle. A second test was performed by doubling the energy loss, which gives correct momentum. When applied on He4 DVCS, as shown in figure 17, we see a deterioration of the missing transverse momentum. We conclude that the momentum shift comes from more complicated effects linked to angles and possibly other experimental conditions and cannot be simply corrected by a scale factor.

22) Section 3.1: p. 40, 1st bullet: In DIS and SIDIS, the pe cut is supposed to remove events with large radiative effects due to photon radiation followed by elastic scattering. Here, this is actually part of the signal (interference of BH and DVCS). So, the cut should instead be chosen to lie just above the hardware trigger threshold of the EC, to avoid fluctuating values for this threshold to influence the electron sample.
The explanation in the note is wrong. This cut is applied to eliminate low momentum electrons because during the data acquisition, the EC threshold was set to 200 mV corresponding to electrons having a minimum momentum of about 0.7 GeV/c. In this analysis, we applied a conservative cut of 0.8 GeV/c to be above this threshold.

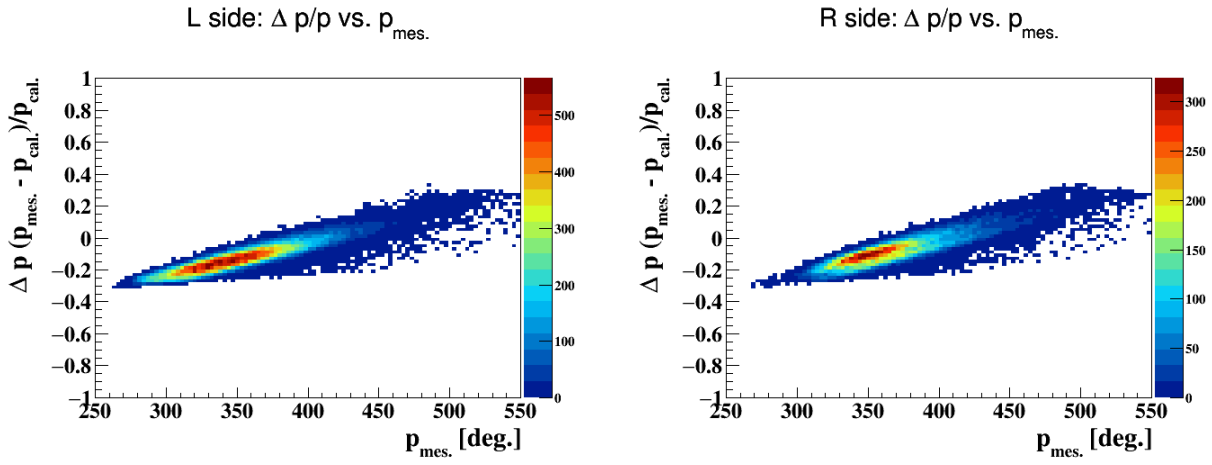

Figure 13: Δp/p as a function of the p for the identified elastic He4 at 1.2 GeV electron beam.

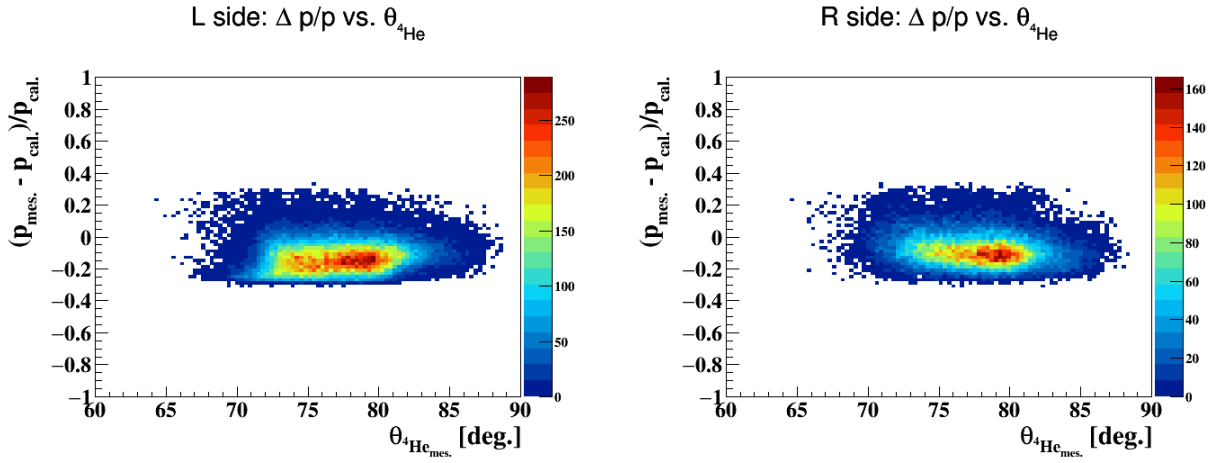

Figure 14: Δp/p as a function of θ for the identified elastic He4.

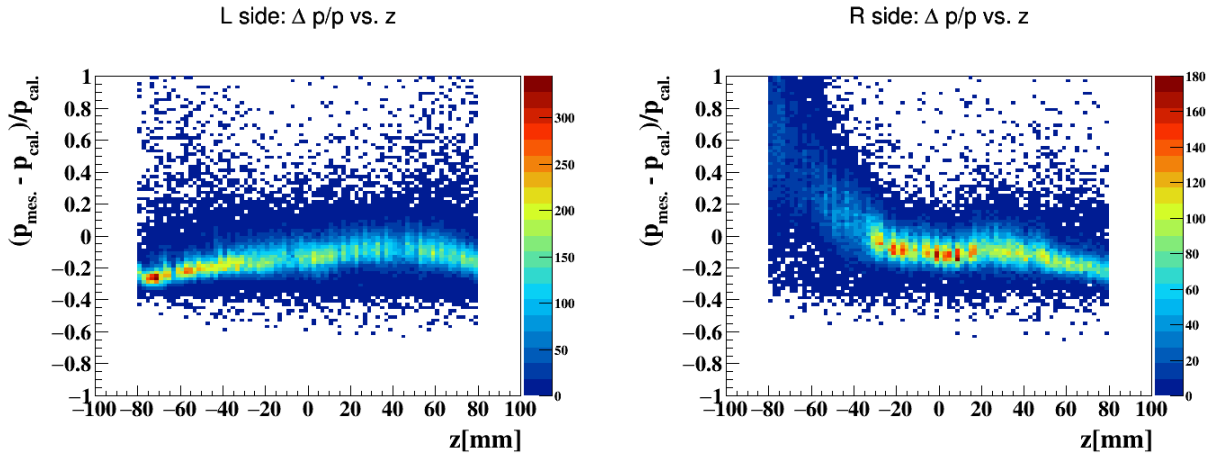

Figure 15: Δp/p as a function of z-vertex for the identified elastic He4.

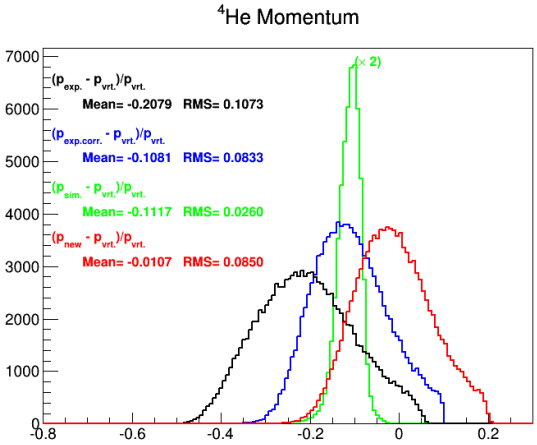

Figure 16: $\Delta p/p$ without any corrections (in black), after energy loss corrections (in blue), from simulation (in green), and after the corrections extracted based on the z-dependence (in red) on top of the energy loss corrections.

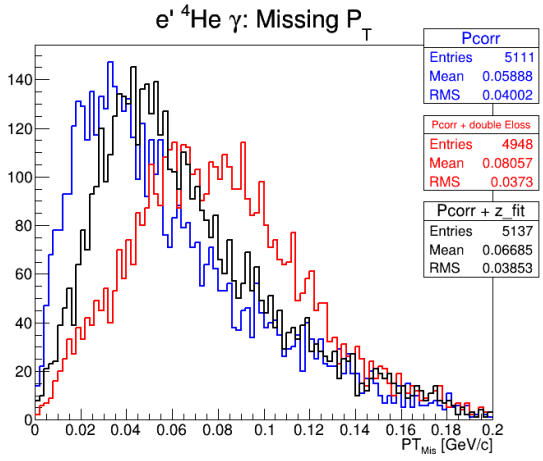

Figure 17: The missing transverse momentum for the identified coherent DVCS events, after applying only the energy loss corrections (in blue), doubling the energy loss corrections (in black), and after applaying the extracted momentum correction form the z-dependence.

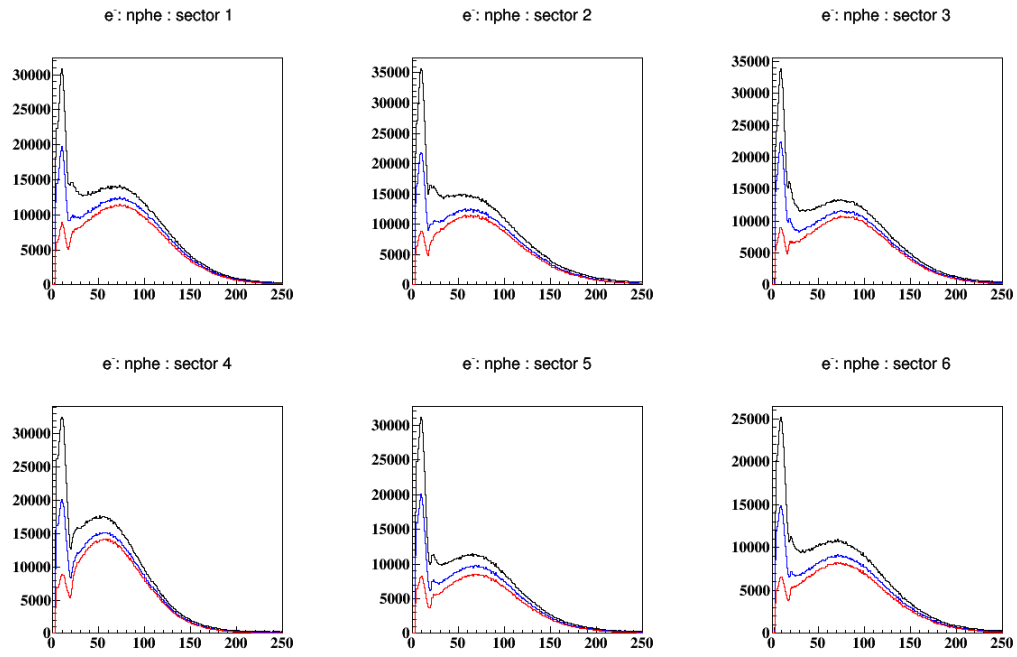

Figure 18: Distribution of nphe emitted by electrons in the six sector of CLAS.

23) Fig. 3.8: Any explanation for the second 'bump' right above 2 nphe? Similarly, the 'green curve' which is really red shows a steep edge, again at nphe=2. Are there any other cuts applied before this plot, e.g. exclusivity or Osipenko?
The "peak" visible in Figure 18 above 2 nphe is the tail of the single photo-electron peak. The supression at 1.5 nphe is just an effect of the trigger and creates the artificial appearance of a peak just above 2 nphe when only loose cuts are applied.

24) Fig. 3.9: Seems superfluous - it doesn't show anything new and doesn't contain all the fiducial cuts.
Removed.

25) p. 45 bottom: Are there any fiducial cuts to remove dead regions? Why not?
They are not implemented in this analysis as we deemed them insignificant for this low statistics asymmetry measurement.

26) Fig. 3.15: This may be my ignorance, but it looks like there is a secondary 'bump' between beta =0.9 and 1. What could it be? If it's neutrons, wouldn't that contribute to your background?
We seem to disagree there is a significant bump. However, if there are some neutrons, they will be highly suppressed by the DVCS exclusivity requirements. In particular we want to point out the energy of the neutral particle is always greater than 2 GeV. At such energies the time of flight measurement from the EC is not good enough to separate neutrons from photons anyway (see Fig. 41 and 42).

27) Bottom p.47: Indicate that the threshold on IC discris towards TDC has been too high to be useful and/or the flight path is too short to apply a beta cut as in EC.

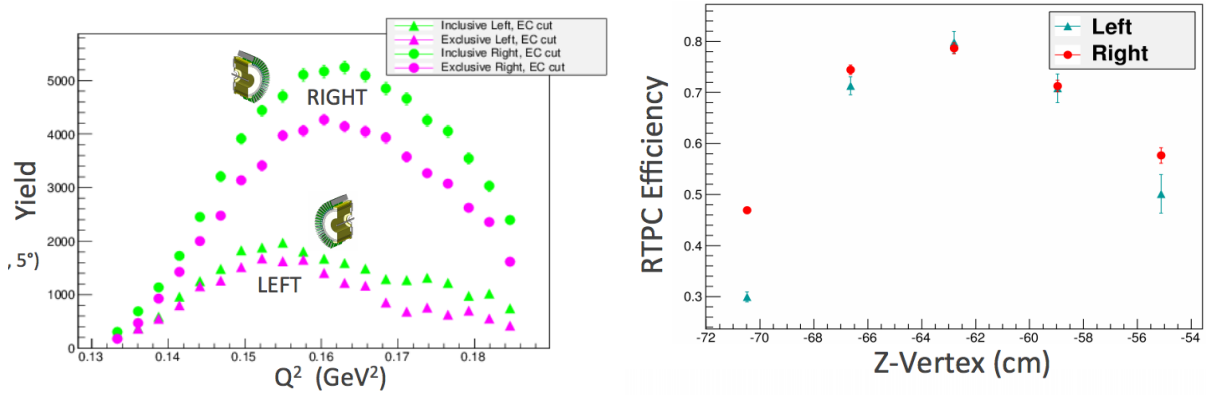

Figure 19: On left is the inclusive and exclusive elastic yields separated into the two RTPC halves (LEFT/RIGHT). Here the inclusive yields are the number of electrons in the elastic W-peak (e.g. Fig. 6) whose corresponding elastically scattered ^{4}He would have been in the acceptance of the RTPC, and the exclusive yields require the additional detection of the ^{4}He. The large LEFT/RIGHT differences in CLAS acceptance for elastic kinematics are clear in the inclusive yields. On right is the RTPC ^{4}He efficiency calculated from the ratio of exclusive and inclusive elastic yields. (Here LEFT/RIGHT is from the beam's perspective, i.e. beam-LEFT/beam-RIGHT)

The timing of the IC is not functionning properly for certain channels. Therefore, applying a timing cut would add inefficient regions in the detector that we wanted to avoid. Moreover, the comment from previous answer applies as well, such a cut would be very little help to reduce backgrounds at such high particle energies.

28) Fig. 3.19: The lhs of the RTPC apparently has only 1/2 the efficiency of the rhs. Is there any good explanation (at least qualitatively)? This could potentially distort *phi*-distributions, no?
This difference in the yield should not be linked to a different performance of the RTPC. They are due to the complicated convolution of CLAS and the RTPC acceptance. We measured the efficiency of RTPC using elastic scattering, and found that the left/right halves have similar efficiencies except near the upstream and downstream ends, as shown in Figure 19.

29) bulleted list p. 48-49, Bullet 2: Would be nice to see a distribution of number of active pads vs. p (but not necessary).
It is added and shown here in Fig. 20 as well.

30) As asked before: Why is there no PID cut at all? (E.g. Signal height vs. p)
We claim that kinematic exclusivity cuts are sufficient to cleanly select coherent ^{4}He DVCS events without the need for $\frac{dE}{dx}$ cuts. We performed few checks regarding applying a PID cut, where the full data was analyzed in the following three sets:
1. Processing all the reconstructed tracks in each event with the exclusivity cuts.
2. Processing events with only one good track in the RTPC being reconstructed.
3. Processing events with only one track that passes a dedx cut.
The results are shown in figure 21 in terms of the exclusive variables for the identified coherent DVCS events. One can see that applying a PID cut would only change the statistics and not the width of distributions. On the other hand, figure 22 shows a comparison between the reconstructed beam-spin asymmetries with and without applying a PID cut. The two sets of asymmetries are compatible within the given statistical error bars. From these two observations,

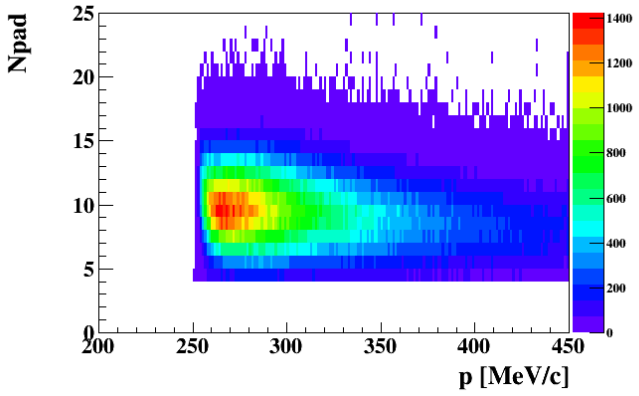

Figure 20: The number of active pads versus the measured p for the good tracks collected using 6 GeV electron beam.

we deduce that a PID cut on the Helium would not reduce any background contribution.

31) Also asked before: What coincidence time window do the *edist* and *sdist* cuts translate into? This is relevant for accidental coincidences. Fig. 3.23 indicates clearly that there is an uncorrelated (in z) background from those! Yet, there seems to be no discussion of accidental coincidences at all.
For *edist* and *sdist* part, it is answered previously in comment 6.

Regarding the background, figure 23 shows Δz distributions of the identified Coherent DVCS events after applying the exclusivity cuts without any initial constrain on Δz. This guides us to correct for these accidentals in our asymmetries in the form: $A_{LU\ \ corr.} = \frac{1}{1-contamination} A_{LU}$, with a 4.1% global accidental contamination.

Number of coherent DVCS events		
Δz [mm]	Left module	Right module
[-50:-30]	42	77
[-20:20]	2741	2856
[30:50]	34	78
Contamination percentage	2.7%	5.4%

Table 1: The numbers of the identified coherent DVCS events in the different regions in Δz for the two modules of the RTPC.

32) 3.2: Does the generator contain any kind of implementation for the spectral function ('Fermi motion') of the proton in 4He?
Yes, the Fermi motion is implemented based on the parameterization of C. Ciofi degli Atti and S. Simula (PRC 53 (1996) 1689). Figure 24 shows the proton initial momentum we used. We cut the high-momentum tail at 300 MeV/c, higher momentum should not contribute to the final sample because of our exclusivity cuts.

33) You mention, in 3.2.5, that the RTPC is not implemented in GSIM. Does this include the

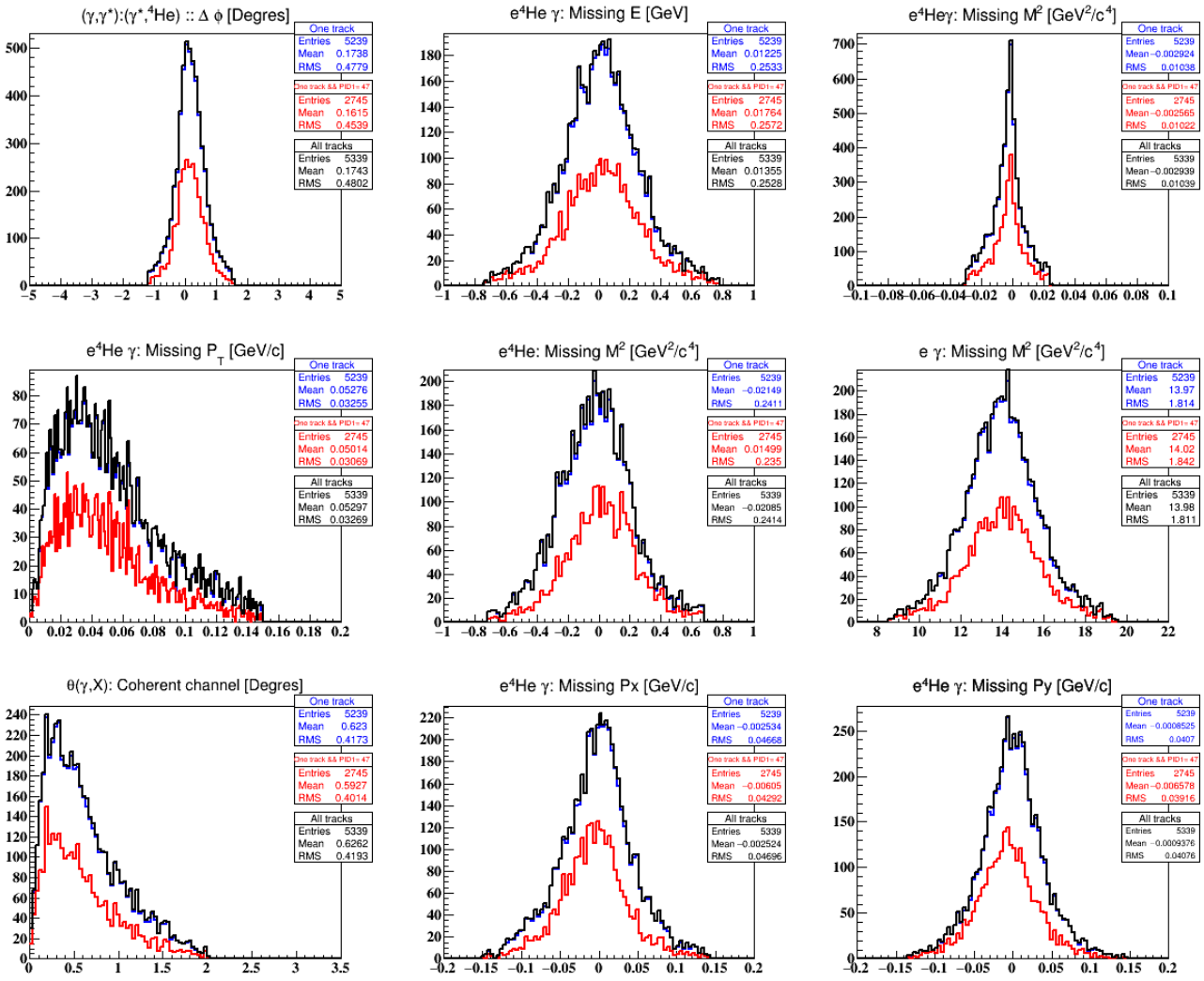

Figure 21: Distributions of the exclusive variable for the identified DVCS events with only one track in the RTPC (blue), one track and PID1 is equal to 47 (red), and processing all the tracks in each event with the exclusivity variables (black).

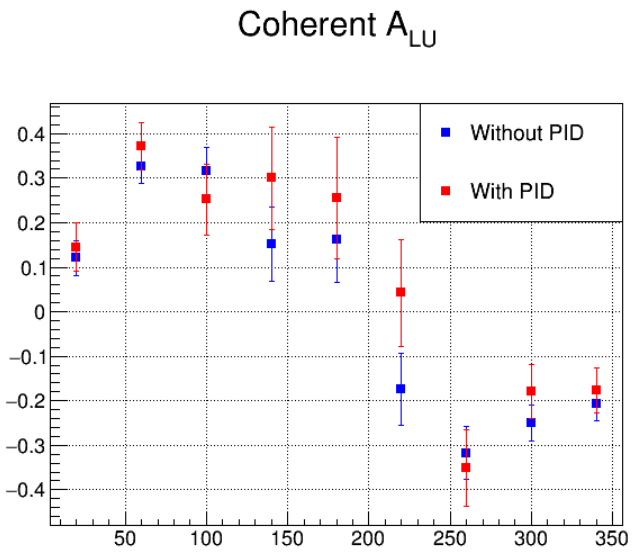

Figure 22: The integrated coherent beam-spin asymmetries as a function of ϕ with (red) and without (blue) applying a PID cut on Helium tracks.

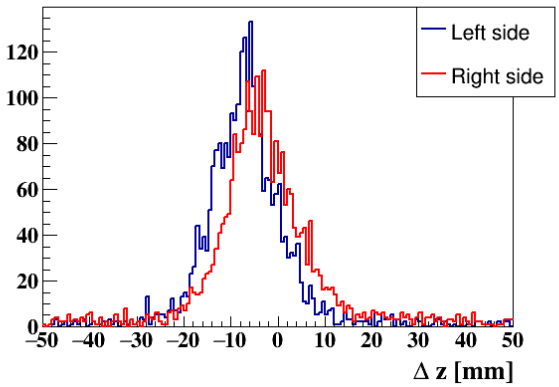

Figure 23: The z-vertex correspondence between the scattered electron and the recoil He4 for the identified coherent DVCS events after the exclusivity cuts in the two modules of the RTPC separately without any initial constrains on z-vertices of the individual particles. Table 1 summarizes the cut numerically.

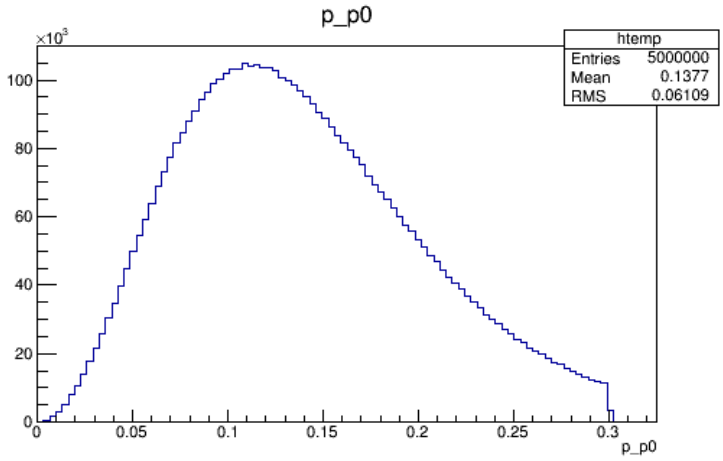

Figure 24: Fermi momentum distribution for nucleons inside ^{4}He in GeV/c.

materials as well? If those are not in GSIM, you might underestimate multiple scattering and energy loss of electrons and, particularly, outgoing protons.
No the material of the RTPC is implemented in GSIM, however it is only considered as dead material and the detection simulation is not implemented. The description is clarified in the note.

34) Also in 3.2.5, I would like a little more detail on the fastmc: How does it calculate the energy loss of the 4He? Is multiple scattering included? Could you show comparisons between measured and simulated distributions?
We do not specifically apply energy loss and multiple scattering in our fastmc, but we apply resolution effects based on experimental data that include both effects. The plots in Fig. 25 show the comparison between data and simulation in terms of theta, *phi* and momentum of the He-4 DVCS nuclei.

35) 3.3.: The kinematic corrections you mention are based on simulation only and mostly take care of energy loss by the protons. Most other CLAS analyses require additional, EMPIRICAL kinematic corrections (see, e.g. the BONuS experiment). Can you give a justification for leaving them out? It may be obvious, but you don't show or say it: Are the corrections explained in 3.3.1-3.3.3 applied to the real data as well?
For electrons and protons, the presented corrections in sections 3.3.1 and 3.3.2, respectively, are applied for experimental data and simulation. We did not find the need for additional kinematic corrections on protons and electron as we found good enough match already. In the case of the energy of the IC photons, the corrections for data and for simulation are different and presented in the following two sections, sections 3.3.3 and 3.3.4. In the latter case these where empirical corrections. Additional corrections are not pursued for the data since data and simulation already agree reasonably well regarding the quantities that are involved in event selection and asymmetry extraction.

36) 3.3.4: The 3 corrections you describe for IC photons are somewhat correlated, since they all are checked by optimizing m_{π^0}. Did you try a simultaneous fit of all parameters (or at least several ones) that enter the various corrections?
The position correction (3.3.4.2) is derived based on minimizing z-dependence of m_{π^0}, and is highly uncorrelated with energy corrections. The run-dependence (3.3.4.1) is also uncorrelated

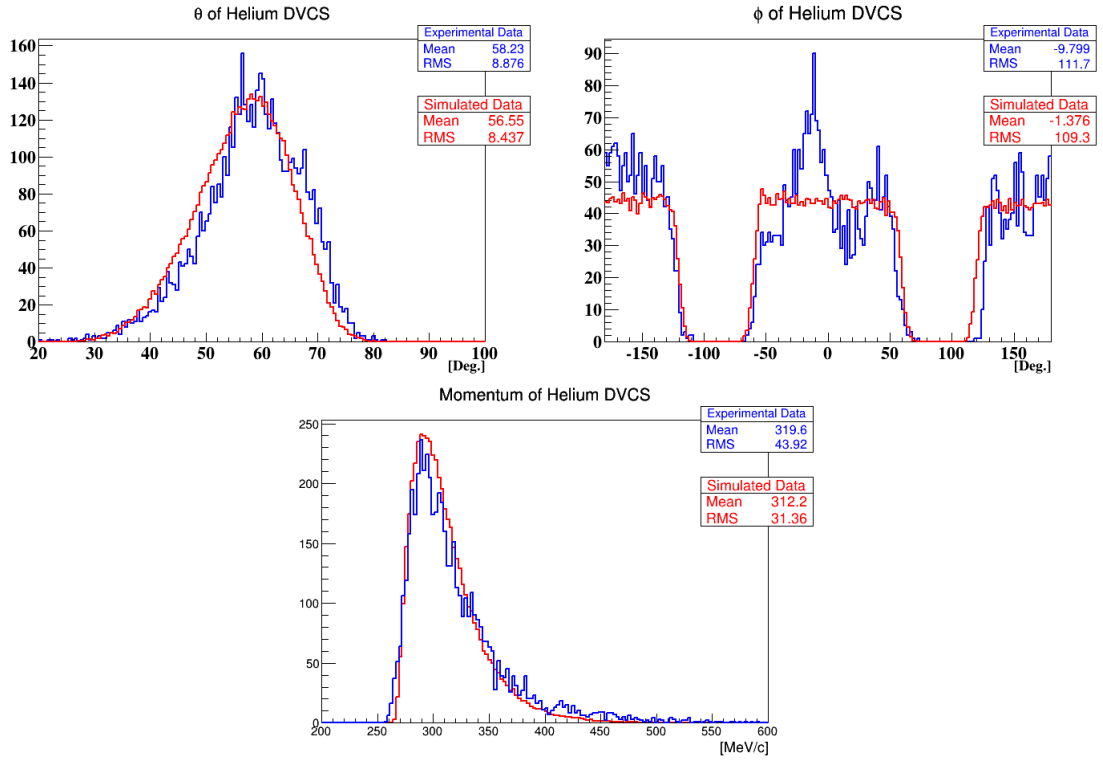

Figure 25: Comparison between experimental and simulated DVCS ^{4}He nuclei in terms of polar angle, azimuthal angle and momentum.

with energy, as can be seen in the top panel of Fig 3.35, but is primarily a run-dependent global scale factor on energy. Finally the radial- and energy- dependent energy correction (3.3.4.3) are indeed correlated and therefore treated multidimensionally (R, E).

37) Fig. 3.39, I am a bit troubled by the huge shift in missing energy - on average several 100 MeV - after applying the corrections. This contrasts to Figs. 3.34-3.38, where most deviations from the true pi0 mass appear to be less than a couple %.
Most π^0 are found at low energy, while the correction affects 2 to 6.0 GeV photons. This is the reason the correction has such an important impact. See later reply to question 31 ii from reviewer 2 for more details.

38) Sec.4.1, Fig. 4.1 and 4.2, Fig. 4.5: In addition to looking at He4/e and p/e, why don't you also look at e/FC to eliminate unstable runs?
We did not use the Faraday cup reading in the analysis. We feel it is an unecessary cut for an assymetry measurement.

Do we have an idea why the RTPC lost nearly 50% of its efficiency over the course of the experiment?
This is mainly related to experimental changes in the RTPC. In particular, we had leaks in our gas system that appeared during the run. This probably caused gas contamination, changing the properties of the detector.

39) Eq. 4.1: It would be nice to know the typical value (or range) for tmin.
We show in figure 26, for both DVCS channels, t_{min} distributions for our DVCS events.

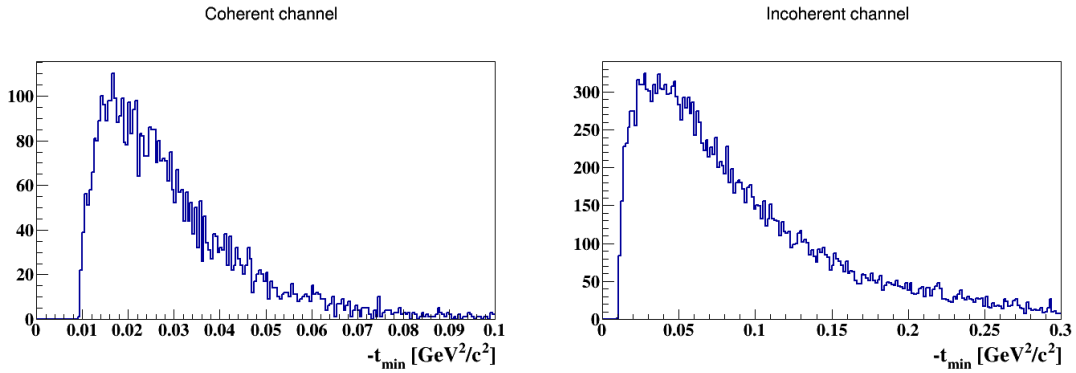

Figure 26: Coherent (left) and incoherent (right) tmin distributions calculated for the experimentally selected DVCS events. We use the experimental Q^2 and x_B of the individual events.

40) Fig. 4.2: I'm bothered by the wide distribution in Emiss (top middle), and don't understand why you use such wide cuts. Surely, anything above Emiss = 0.4 must have additional particles in it, and even if not, why not cut this tail? Note that the same tail is absent for the p (FIg. 4.6) where you use indeed a tighter cut, although you don't even account for the proton's initial momentum.
We applied 3σ based on the comparison between data and simulation, see figure 4.4 in the note. In the following, figure 27, we performed bins in the missing energy distribution and we watch the reconstructed beam-spin asymmetries. As a conclusion, we see that the reconstructed asymmetries are compatible within the given error bars.

41) Fig. 4.6: Here you could cut deeper on the ep missing mass. Why is it so lopsided? Didn't you correct the IC photons to avoid that?
We can always cut deeper. We choose not to cut by eye, but using 3 σ in order to avoid biassed choices. Moreover, most contamination eventually remaining is pi0 and is treated by a specific correction. We do not understand how IC correction can possibly affect the epX system.

42) Fig. 4.8: Again, the missing energy from epgamma is lopsided, as is the missing egamma mass. Looks like Egamma is still not properly calibrated; but then why are the corresponding plots for the coherent channel spot-on?
The assymetry effects are due to the background of the pi0 contributing only on one side of distributions. The peaks are indeed all slightly shifted, this is probably due to a complex mix of misalinements and miscalibrations. Any attempt to correct with a simple function for one variable makes the other worse. In particular, we want to point out that both epX and eγX missing mass are slightly off but epγ missing mass is peaked at 0. These problem do not appear for the coherent channel because of the larger mass term that reduce the relative impact of some of the measurement errors. Equation 4 shows that the precision on the calculated missing mass squared of $e\gamma X$ depends on the mass of the initial state hadron in each DVCS channel.

$$\frac{\partial MM^2_{e\gamma X}}{\partial E_\gamma} = 2 * (E_{\gamma^*} - M_{target} - E_\gamma) \tag{4}$$

43) 4.5: You discuss the pi0 background. Am I correct to assume that Eq. 4.11 is applied separately for each beam helicity? (I assume you use the same R, but of course the reconstructed

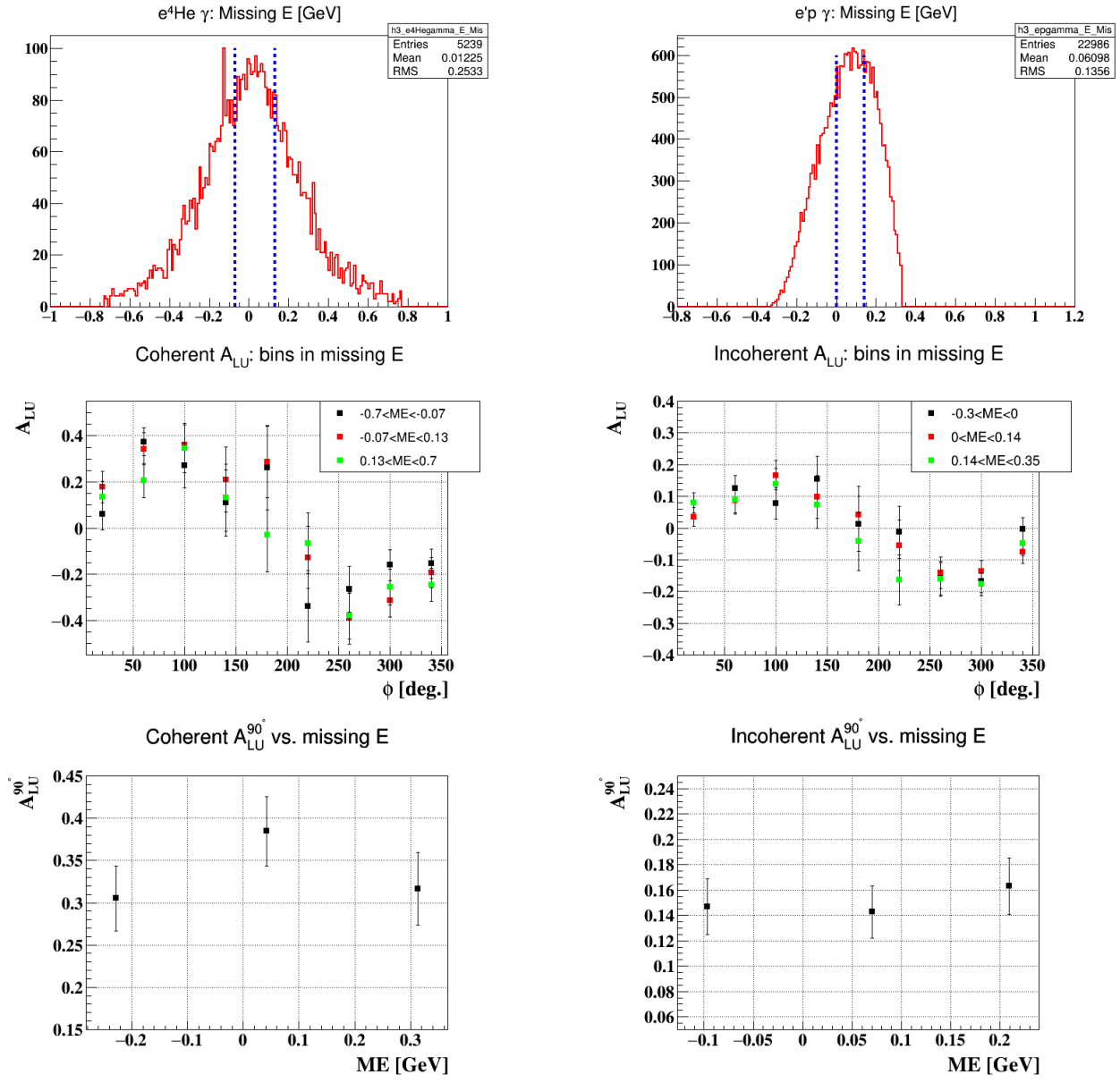

Figure 27: Coherent (left) and incoherent (right) missing energy distributions (top), the reconstructed beam-spin asymmetries as a function of ϕ (middle), and the extracted asymmetry at $\phi = 90^\circ$ from fitting the asymmetries as a function of the missing energy in each bin.

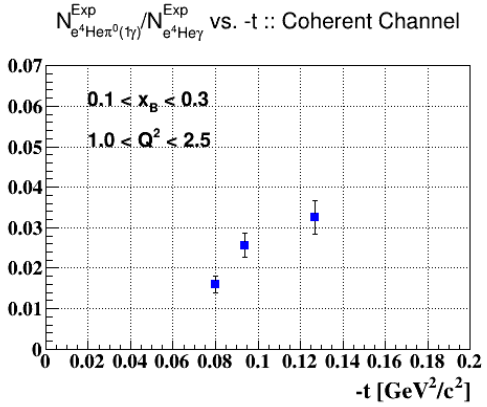

Figure 28: The coherent *pi*0-background yield.

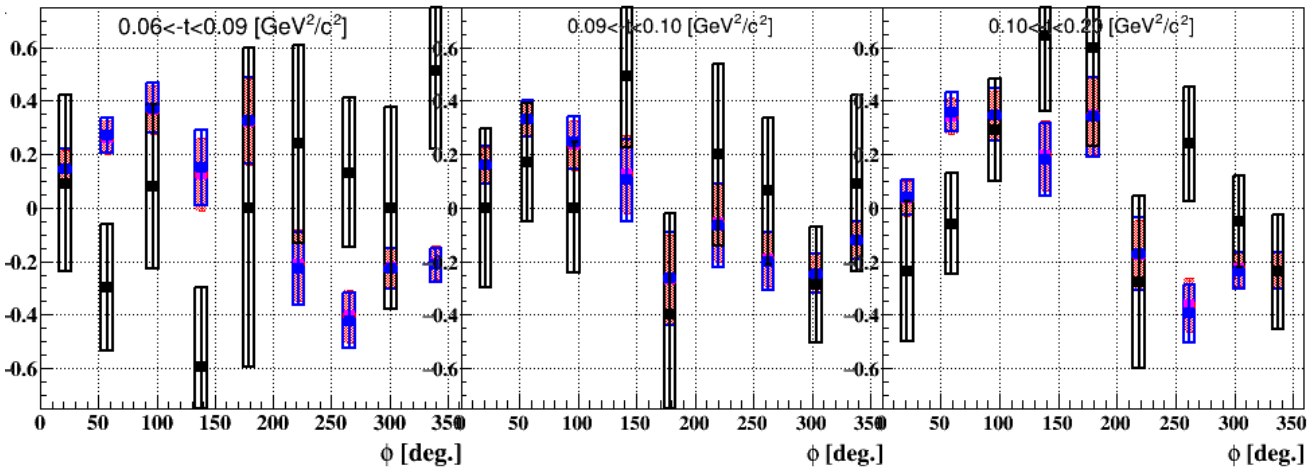

Figure 29: In black, measured coherent π^0 asymmetries. In blue, the coherent DVCS asymmetries without background subtraction. In red: the coherent DVCS asymmetries after the background subtraction.

pi0 events could - probably will - have an asymmetry).
Yes, the subtraction is done separately for each helicity direction. We modified the text to include that information. As can be seen from figure 28, the π^0-background yield with respect to the coherent DVCS events is around 2-4%.
Figure 29 shows the reconstructed coherent asymmetries in t-bins as a function of *phi*, where the red shaded point are the DVCS asymmetries after the background subtraction, the blue points are the DVCS raw asymmetries without background subtraction and the black points are the π^0-asymmetries ($e^4He\pi^0$ events).
This leads us to conclude that:
- The π^0-asymmetries are consistent with zero.
- 2-4% background yield does not affect much our DVCS asymmetries.
Therefore, assuming that the two helicity configuration have the same acceptance ratio R is a good approximation.

44)Unfortunately, no other backgrounds are discussed (not even dismissed): scattering from other target components (Kapton? windows?), events with more particles in the final state (especially since you allow such a large Emiss), and accidental coincidences (particular for the coherent channel), plus perhaps photon misidentification. The various strange 'bumps' I've pointed out along the way show that those backgrounds may not be totally negligible.
The procedure follows the same guidelines as for DVCS analysis on the nucleon. The neutral pion production occurs "without threshold" as seen from the $eHe\gamma$ sample, meaning that the contamination from $eHe\pi^0$ with one photon lost is distributed all the way down to the DVCS, in the limit where the second photon energy becomes negligible in the lab. Single charged pion production occurs with a small threshold but is inconsistent with the already detected particles (e and He). Two pion production is entirely cleaned up by the exclusivity cuts. Scattering from the windows is excluded by the vertex cuts. As far as accidental, we correct for that as presented in comment #31 from the first reviewer. For discussions of other background sources see also the answers to:
- Comment 46, figure 30, from the first reviewer.
- Comment 7, figure 47, from the third reviewer.
- comment 14, figure 52, from the third reviewer.

45) Fig. 4.11: For the final correction, do you produce the *phi*-dependence of R for each of the individual bins in xB, Q2 or t that you use?
Yes we do.

46) 4.7: I admit to being biased and a pain in the butt about this, but I NEVER understand why more or less arbitrarily varying a cut (and, in this case, even a rather meaningless cut in my mind) gives you a QUANTITATIVE estimate of background uncertainties. For one, you are mixing systematic effects from the tails with statistics (since you change the sample size). Plus, how do you know that there isn't even sizable background for your smallest (2.0 sigma) variation? I'd much rather see a sequential, quantitative discussion of possible background sources and direct estimates of their magnitude INSIDE all cuts (e.g., by selecting background events on purpose and looking at their distribution in the variables that you cut on). See above for a list of such backgrounds.
Cuts are arbitrary, we could choose 2.32 sigma or 2.74 and there is no strong argument for either. It is therefore necessary to associate an error with this choice. The chosen variable (missing mass of epγ) is neither meaningless nor arbitrary, it is the one with the larger tails even after applying all other cuts. From these, it seems clear that such a study indicates a clear source of systematic errors linked to background. It can of course be argued that this test does not account for the full background error, but we never claimed this, so we are unsure what is the source of the critic. In fact, we claim the opposite since we treat π^0 background independently and associate another systematic error to it.

Regarding the windows effect inside the exclusive distributions, the data has been processed with NO constraints on the z-vertex of the electron nor the ^{4}He. Figure 30 shows the exclusive variables as a function of z-vertex of the electron for the identified coherent DVCS events. The target extends from -74 cm to -54 cm with respect to the center of CLAS. As a conclusion, our vertex cut, shown in figure 3.1 in the note, remove most of the windows effect. For the remaining contamination, we correct for it as presented in comment 44 from the first reviewer.

47) p. 80: I believe that one-loop corrections aren't a big worry. However, one contribution I

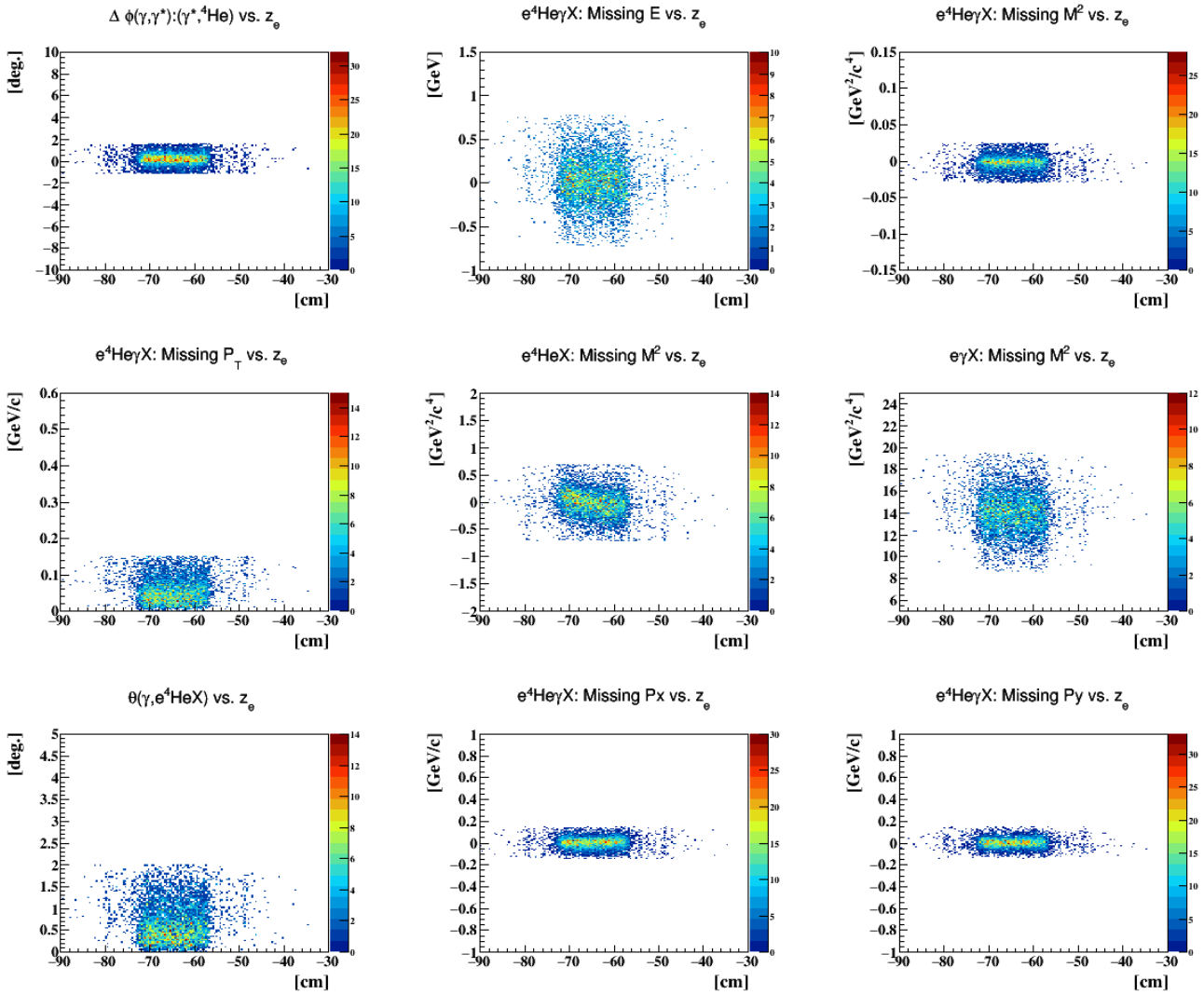

Figure 30: The distributions of the exclusive variables as a function of z-vertex of the scattered electron after applying all the exclusivity cuts without any initial constrains on Δz nor the z-vertices of the individual particles.

can think of is the radiation of a second photon, e.g. right before the actual DVCS event (and not connected to a pi0). It's not clear to me that this is a priori a small effect, again especially given the wide Emiss cuts.
It has been shown that such effects are small for asymmetries on free proton and we see no argument to claim otherwise. Actually reviewer 2 in its question 41 is supporting this point.

48) Fig. 5.2: 'red error bars' aren't visible - use shaded bands instead. To do, unbinned fit and separate the systematic errors.
In figures 31 and 32 we show the coherent and the incoherent beam-spin asymmetries respectively. In blue the statistical and the systematic errors are added quadratically, in green the statistical errors and brown bands present the full systematic uncertainties. The red lines are fits to the data and presented in chapter 5 of the note.

49) Fig. 5.3: Why the weird vertical ticks and tick labels? At least 0 should be clearly marked. Also, indicate the averages of the 2 other variables in the same way in the 3 plots, indicating that it is an average?
It is corrected in the second version of the analysis note, see figures 5.2 and 5.4.

50) Fig. 5.5: Are the curves integrated over the experimental acceptance? Again, showing averages for all 3 variables (preferably for each data point) would help interpret the applicability of the curves. - No matter what, you must supply tables for all your ALU(90deg) results with averages of all kinematic variables for each data point - after all, there aren't so many.
The theoretical curves are not integrated over the experimental acceptance. For example, they are calculated at fixed xb, Q2 and *phi* when looking to the dependence on t. Tables for all the two dimensional bins are added to the note for both the coherent and the incoherent channel as well as at the end of this document in tables 2 to 7.

51) Fig. 5.6: It would be nice to superimpose the incoherent p results from 4He on the same graphs.
Figures 5.4 and 5.6 are superimposed in figure 33

52) Fig. 5.7: I'm confused why Im(HA) is rising with Q2 but falling with xB. These 2 are pretty tightly correlated! Any explanation?
The new extraction of the GPDs show almost the same trend in Q^2 and x_B, where the data is fitted with a form in which the real and the imaginaries parts of the CFF H_A are the free parameters. The previous observation might come for the neglecting some parts of the full formula that we thought would be negligible.

53) 5.4: 3rd paragraph: Be careful not to over interpret the meaning of your results. For one, your xB is more closely related to xi, not x in DIS. Also, there are other possibilities to explain the smaller asymmetries for bound protons than the EMC effect - e.g., FSI.
We are not sure what you are referring to. We clarified a little the paragraph in order to alleviate any issues.
Regarding the FSI effect, this can be investigated by construction bins in missing transverse momentum. Figure 34 shows the extracted A_{LU} at 90° from fitting the asymmetry signals for different p_t bins. As a conclusion one can see that the incoherent asymmetries are consistent and so the FSI seem to have no big effects on the measured asymmetries. This question of course is to be discussed in more detail in the paper, rather than in the analysis note.

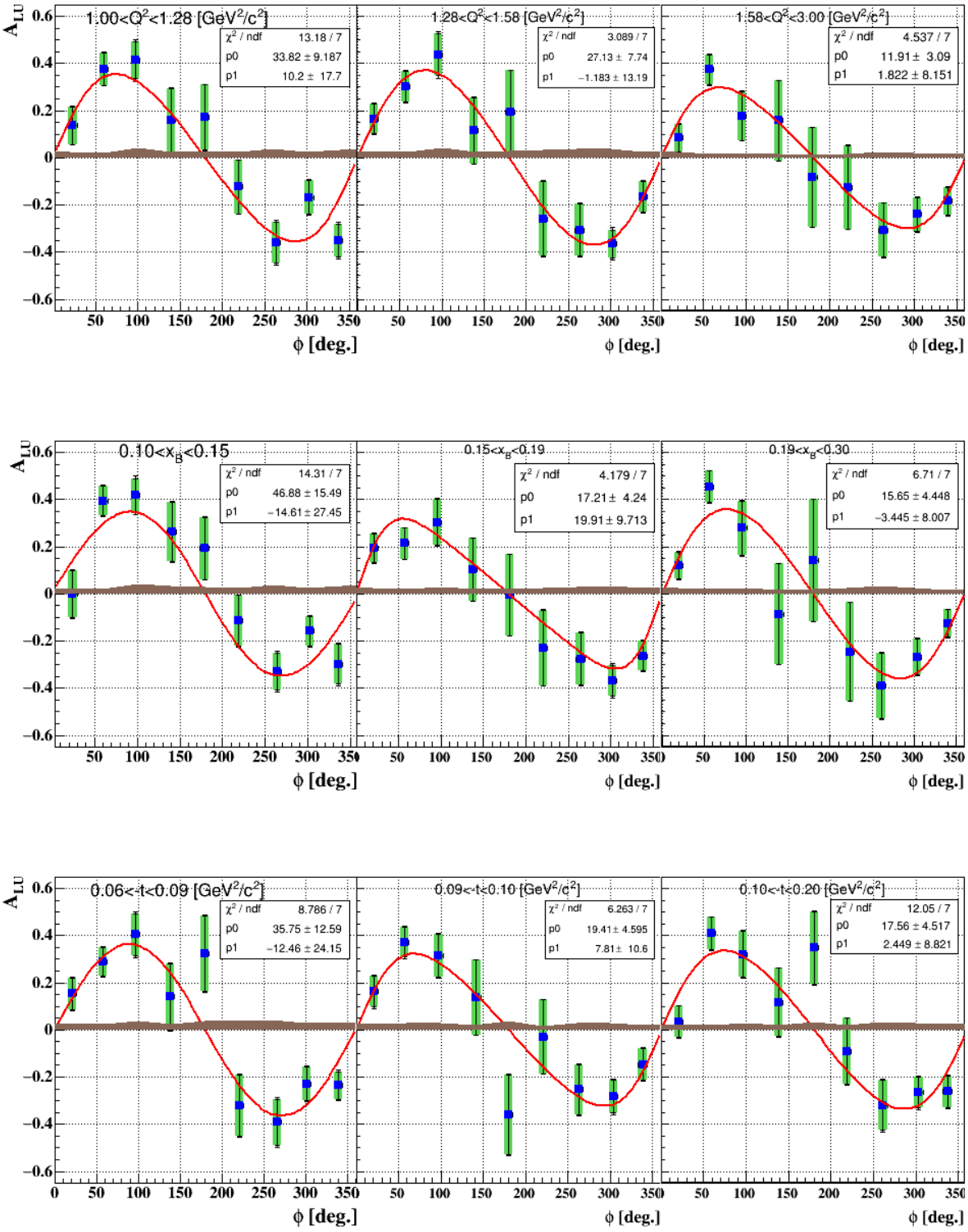

Figure 31: Coherent beam-spin asymmetries

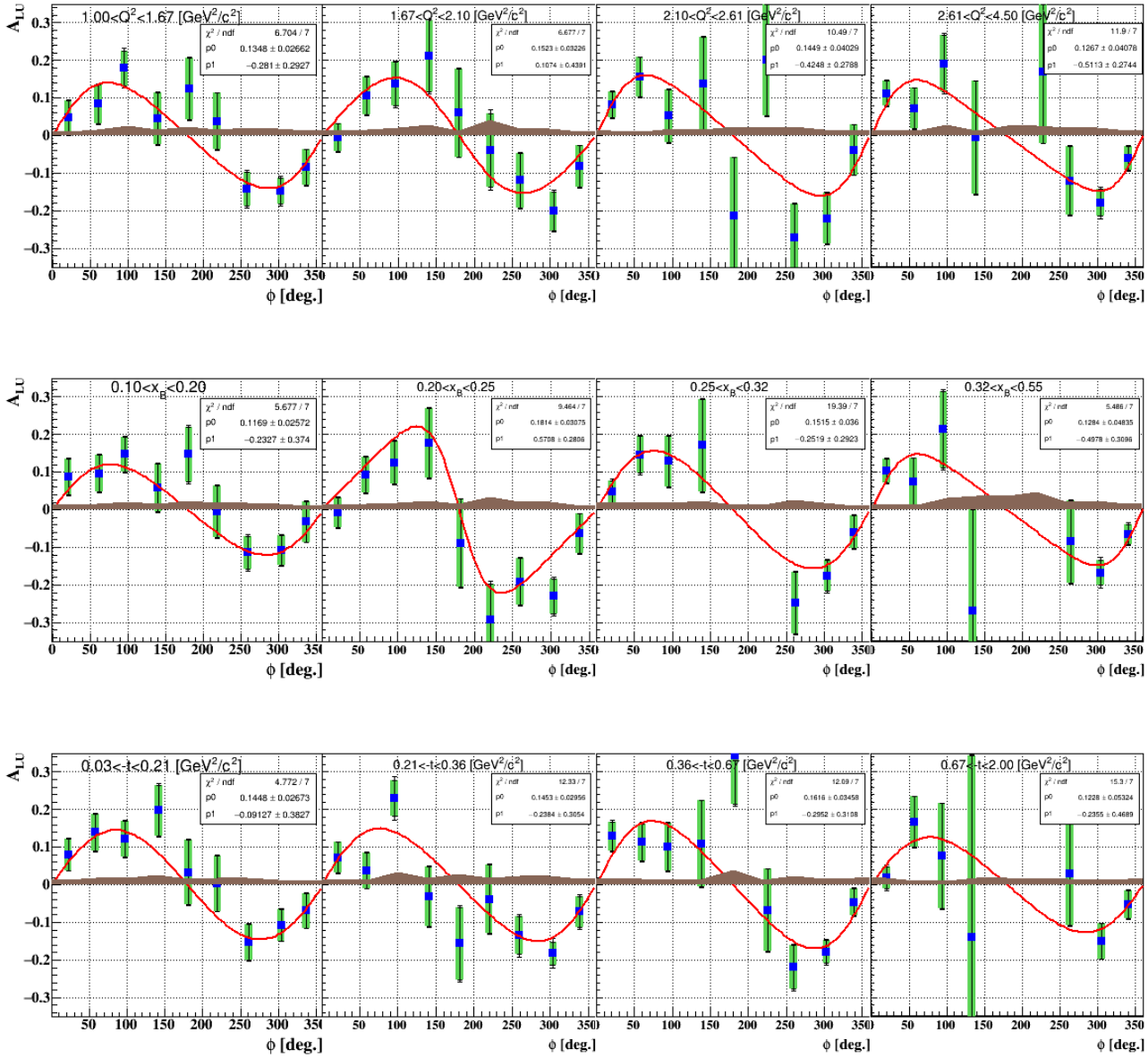

Figure 32: Incoherent beam-spin asymmetries

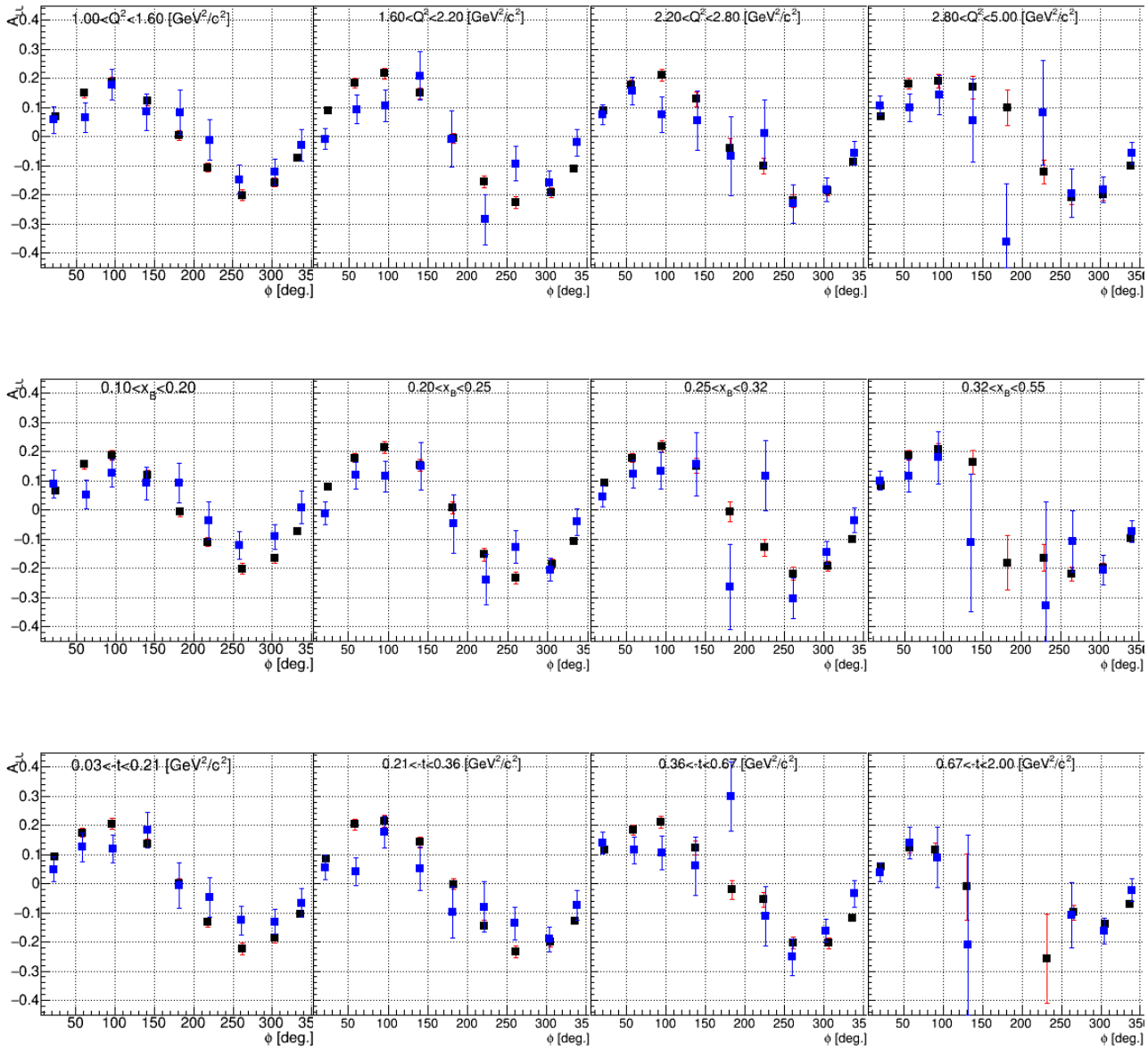

Figure 33: The blue (black) points are the incoherent (free) proton A_{LU} as a function of ϕ in Q^2, x_B and $-t$ bins.

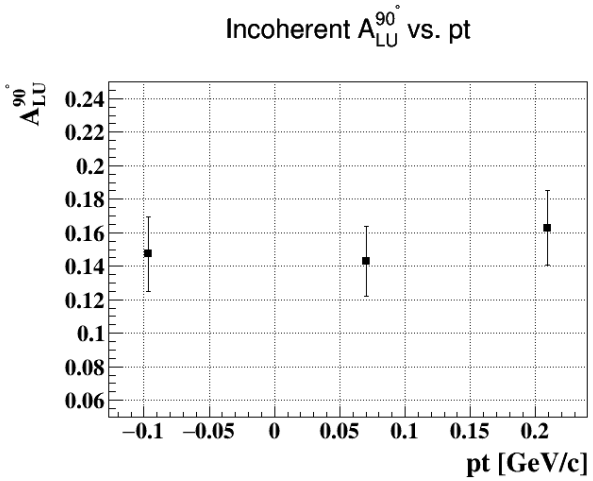

Figure 34: The incoherent beam-spin asymmetries at $\phi = 90^\circ$, from fitting the signals, as a function of the missing pt.

54) 4th paragraph: I am not sure what you are saying with 'in the same coherent domains of ...'. Can you specify exactly which range in x, t and Q2 either data set is integrated over?
We modified the text to include that information.

55) Fig. 5.9: Certainly interesting, but maybe careful with the interpretation. Once again, I don't understand the very different behavior with xB and with Q2. Also, the x-dependence might be affected by the very different SHAPE of the coherent results vs. *phi* - indicating that the denominator may play a role. Of course, there is no expectation that coherent 4He should agree with free p - for one, all the nucleons are moving inside, and there are neutrons as well as protons. Your disagreement with HERMES is also interesting - any comment on the possible source? Did they also use their own free p data? Of course, they have much less stringent cuts, in particular on exclusivity ...
HERMES data are selected for very small $-t$ and then assumed to be in the coherent regime from this cut. The large difference between the measurement shows that the detection of the recoil has a strong impact on the final result. However, we do not want to comment more than necessary on the quality of HERMES result, it is not the place.

2^{nd} reviewer

1) p. 5-6: define ksi and t and indicate how they will be calculated in this analysis.
Experimentally, only ξ and t are measurable in the DVCS reaction. At twist-2 order, ξ can be calculated as $xB/(2-xB)$, where xB is the Bjorken variable $(= Q^2/(2M_N(E-E')$ where Q^2 is the vertuality of the exchanged photon, M_N is the mass of the nucleon and $E(E')$ is the energy of the incident (scattered) electron. The squared momentum transfer t is equal to $(p'-p)^2$, where $p'(p)$ is the nergy momentum four-vector of the final-state (initial) hadron target.

2) Eq. 1.7: define ξ_A and ξ_N in function of measured quantities.
$\xi_A = x_A/(2-x_A)$ and $\xi_N = xB/(2-xB)$.

3) Eq. 1.11: not of any consequence for the CAN, but should be corrected: this is taken from Eq. 29 of ref. 2, but there, it is zeta, and not ξ. The relation between the 2 variables is in their Eq. 3d.
Done.

4) p. 11: 'The exclusivity of the selected DVCS events WAS APPROXIMATELY insured by a cut ... egX (resolution on this variable = ... GeV)'.
Done.

5) Need to insert a short chapter (1 to 2 pages) before the one on RTPC with all running conditions and analysis conditions: very short description of set-up, positioning of RTPC, solenoid and IC wrt to CLAS center, beam intensity and polarization (including the Moller measurements), current in solenoid, magnetic field intensity and direction in solenoid, current in torus, inbending ... Date of data taking. Then cooking pass number and date (for reference in case another one is made in the future), and for each calibration, name of person in charge.
Done.

6) p. 14: I am confused by the description of the second gap, which does not correspond with the indications on Figs 2.2 and 2.5. Fig. 2.2 indicates it is filled with He, while the text says it is with the drift gas.
This gap is filled with the drift gas. I used different colors in figure 2.2 to indicate different gases. The ^4He label in figures 2.2 and 2.5 is for the green line representing a track not for the gas.

7) p. 11: Is the overall gain really 10^6 (100 per layer)? Any experimental indication?
The gain of such TPC has been studied by CERN's Gas Detector Development Group (Fabio Sauli, Progress with the Gas Electron Multiplier, 2nd Workshop on Advanced Transition Radiation Detectors for Accelerator and Space Applications (Bari, Sept. 4-7, 2003), Nucl. Instr. and Meth. A522(2004)93). The results shown in figure 35 demonstrate that one should not simply add gains to each other for multilayer GEM amplifications. We did not evaluate precisely the overall gain in our chamber, so we do not have a value for the eg6 RTPC at this point.

8) p. 16 track fitting: is it really a 5-parameter fit? why not imposing that the circle goes through x=y=0; that would be a 4-parameter fit. In fact Eq. 2.2 further down indicates that there are indeed 4 degrees of freedom. x0, y0, R, slope and constant !!!!!.
See answer to question #5 of reviewer 1 about the use of the beam position in the fit. However, this is not used as an absolut constrain so the number of degrees of freedom remains 5. Eq. 2.2 has a -4 factor only because of the accounting for the beam position information ($N_{dof} = N_{pts} + 1 - 5$).

9) p. 17-18 + fig. 2.7 caption: r_0 is the radius of curvature, not the curvature. Also the He4 travels in a clockwise direction if one looks into the beam, not in the direction of the beam (if B is in the direction of the beam).
Corrected.

10) p. 18: I suppose the resolutions mentioned 2 lines below Eq. 2.2 come from the vertical widths of graphs such as Figs 2.21 and 2.22. I can read also the resolutions in *phi* and z in section 2.3. Correct?

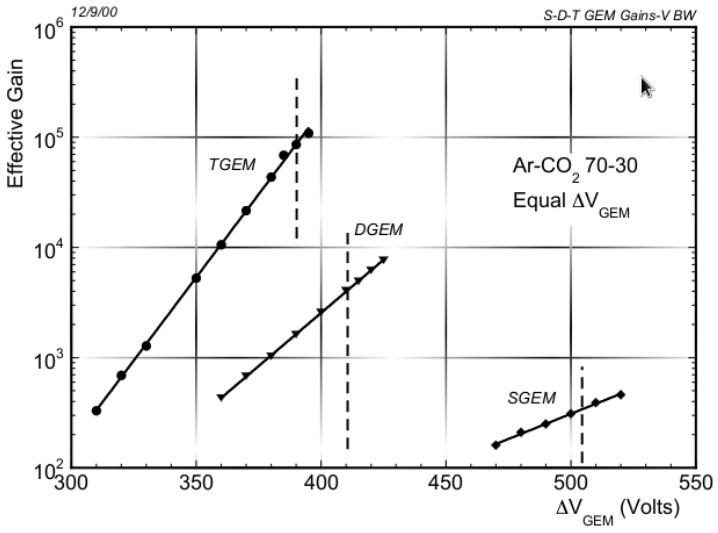

Figure 35: The effective gain as a function of the voltage across the GEM foils of Single-GEM (SGEM), Double-GEM (DGEM) and Triple-GEM configurations.

Answered in comment 5 from the first reviewer.

All this should be mentioned here. No variations observed (or expected from simulation) depending on He4 energies and angles? Also may be worth adding at the end of the first line after Eq. 2.2: 'each hit 'i', determined from the TDC information as described in Section 2.2.3'.
- Regarding the dependence on the azimuthal angle (ϕ), the drift paths were extracted for each half of the RTPC and as a result we have seen the two sets of drift paths overlap with no variations. For the dependence on the momentum and the polar angle, we used the identified elastic events for our calibration where the domains of the momentum and θ are limited. However, we do not expect any dependence on these two variables.
- The sentence is added.

11) Fig. 2.10: why not centered at 0 like *sdist*?
Answered previously in comment 7 of the first reviewer.

12) Fig. 2.11 2.12 and 2.13: did you check for any dependence of Delta-z and other Delta's on CLAS sector? If yes, should be mentioned and described. If not, would like to see it.
In figures 36, 37 and 38, we show the corresponding distributions in the different sectors of CLAS for the identified good tracks at 1.2 GeV beam energy.

13) Are Figs 2.6 to 2.11 for elastic He4 or for coherent DVCS events? any difference between the distributions for these two types of events?
The figures are for the good tracks collected during the 1.2 GeV runs. Yes, one can see different level of performance of the RTPC during the experimental data taking period is due to some known experimental setting changes, indicated in figure 4.1.
In comment 7 of the first reviewer, we have shown the sdist and edist distributions for the identified elastic events without applying any requirements on sdist and edist. Figure 39 shows the equivalent distributions of the identified coherent 4He DVCS nuclei using the cuts based on the first version of the note. Following your comments, we now tighten these and use: -3 mm <

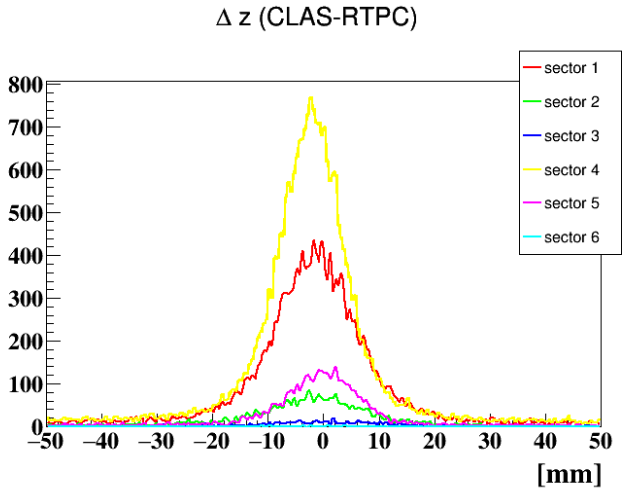

Figure 36: Δz distributions between the scattered electron in the different sectors of CLAS and the recoil particle in the RTPC for the identified good tracks at 1.2 GeV beam energy.

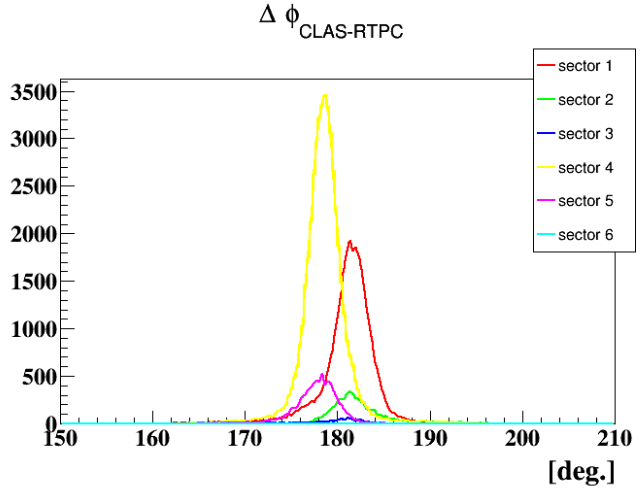

Figure 37: $\Delta\phi$ between the scattered electron in the different sectors of CLAS and the recoil particle in the RTPC for the identified good tracks at 1.2 GeV beam energy.

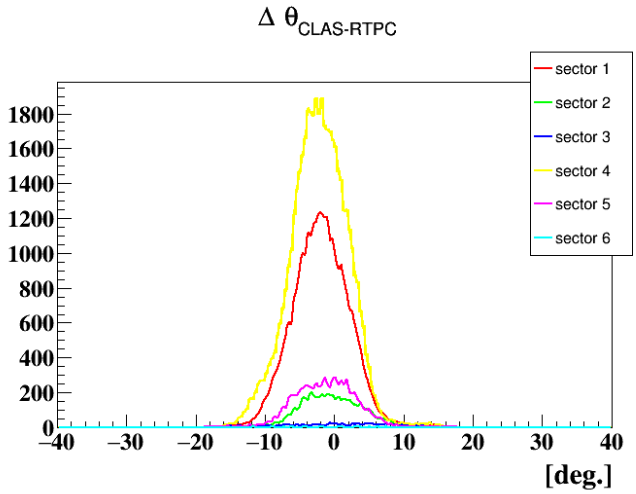

Figure 38: Δ*theta* distributions between the scattered electron in the different sectors of CLAS and the recoil particle in the RTPC for the identified good tracks at 1.2 GeV beam energy.

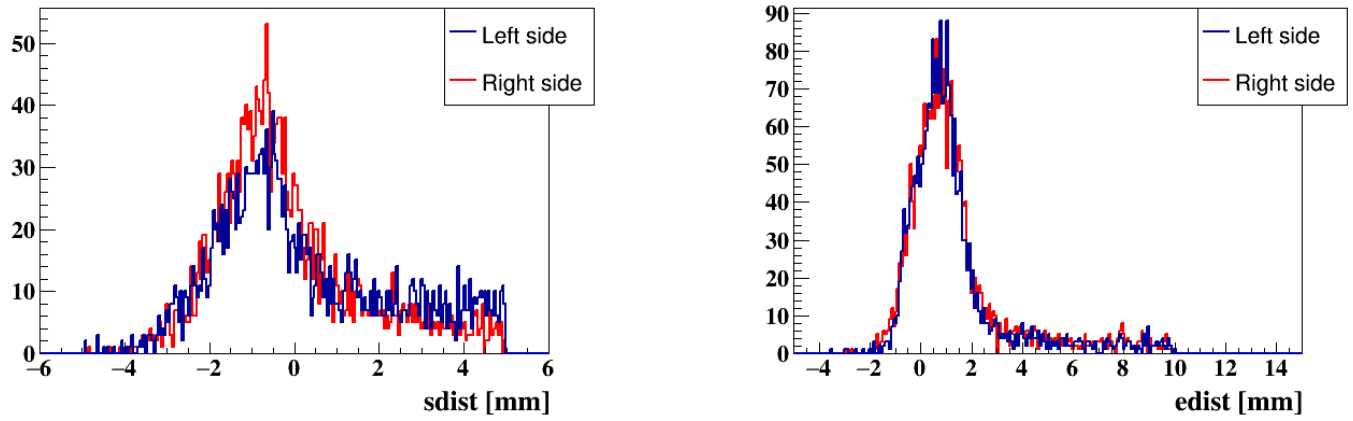

Figure 39: sdist (left) and edist (right) of the identified 4He DVCS nuclei via the exclusivity cuts.

sdist < 2 mm and -2mm < edist < 3 mm are for the second round of the analysis.

14) p. 23, 2nd paragraph: you write TDCmax = DPL/DS. Is not it (TDCmax - 15)*114 ns = DPL/DS?
We show it in this form to simplify the correlation between these variables. Indeed it is TDCmax-15 without the conversion unit as our drift speed is in TDC units.

15) p. 23: can you show the dependence of TDCmax/2 on z for a given run?
The figure in p.24 (figure 2.16) is for a single experimental run.

16) 'Figure 2.18 ALSO shows the percentage increase in good tracks (GT) ...'
Added.

17) Eq. 2.8: is not it TDCmax instead of a fixed 75?

Typically, it has to be TDCmax instead of 75, while this change has no effects on the final extracted drift paths as it comes as a selection cut in the first pass to get an initial set of the paths. In the second pass, all the hits are processed and R is calculated more precisely from the drift paths (equation 2.9 in the analysis note). More checks were performed using TDCmax and as a result, the previously extracted drift paths overlap on the new ones.

18) Eq. 2.9 does not have the right dimensions. Should not the second term be multiplied by 114 ns?
Corrected. The sum is multiplied by a TDC unit.

19) p. 29, 3rd paragraph: remove 'The results are shown in figure 2.26' as the method should be described first, the figure appears later and the results are commented at the bottom of the page.
Done.

20) p. 32 bottom: 'large' -> 'wide'. More importantly, give in conclusion in which data sets the ADC information will be used, since it is not so clear later that it is used for elastic events selection, but not for DVCS events selection.
Done.

21) p. 37: 'The CLAS detector NOMINALLY provides electron detection ...'. Also in Table 1 caption, add '(neglecting the contributions from the CLAS resolutions).'
Done.

22) Chapter 3 intro: should prepare (for the publication) an argumentation to neglect other possible source of background (e.g. e He4 pi0 gamma).
Answered previously in comments 44 and 46 of the first reviewer.

23) Chapter 3: the effect of some of the early pid cuts should be looked at after exclusivity cuts (for both samples of coherent and incoherent events). Ideally without the pid cut in question, but if this is not practical, with this cut included. For example, the z-vertex of Fig. 3.1, if looked at with the DVCS exclusivity cuts, could persuade us that there are no window contributions there, especially in the incoherent channel. If the z-cut cannot be removed in this exercise, it is still useful to see if there is or not an increase towards the ends of the cut. So I am thinking not only of fig. 3.1, but also fig. 3.8.
Answered previously in comments 44 and 46 of the first reviewer.

24) p. 42: section??
Removed.

25) p. 48, 2nd line of 3.1.4: chapter and section numbers to be fixed. Same p. 55 in 3.2.5.
Done.

26) Figs 3.21 and 3.22: would (part of) the tails of these distributions be attributed to random coincidences? If yes, what about a subtraction?
Yes, this is true and discussed in comment 7 from the first reviewer and comment 13 of the second reviewer.

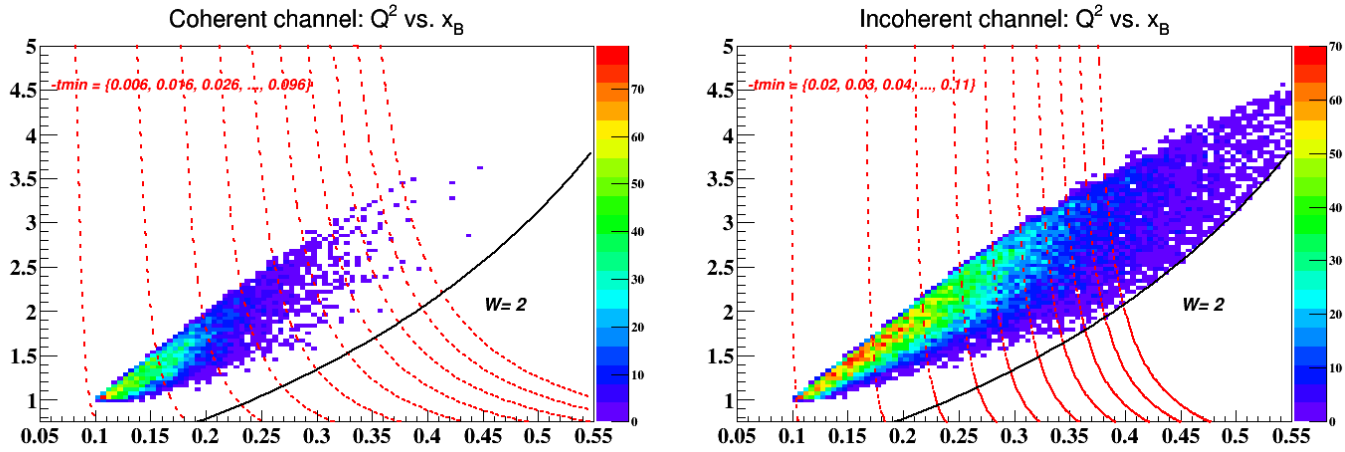

Figure 40: The coherent (left) and incoherent (right) Q^2 versus x_B distributions of the identified DVCS events, with W and -tmin cuts, at different values, in the Q^2-x_B plane.

27) Fig. 3.39: More than a factor 2 gain in statistics between pass1 and pass2 in eHe4g events or are these arbitrary subsets of the total sample? More worrisome, why a 40% loss in statistics between pass1 and pass2 in epg events or are these arbitrary subsets of the total sample?
The full data set was included in pass1 and pass2 distributions. The 35% loss in the incoherent DVCS events is because we were not seeing real indications about the peaks in the exclusivity distributions. So the 3 sigma cuts were very wide to adapt to very broad distributions.

28) p.65: (optional addition) Since I noticed many people do not have a good sense of (the kinematical dependences of) tmin, it would be instructive to add 2 plots of lines of constant tmin in the Q2-xB plane within the acceptance locus limited by beam energy and W cut, both for He4 and for proton.
The plots in figure 40 show the Q^2 as a function of x_B for the identified coherent and the incoherent DVCS events, with $Q^2(x_B)$ at fixed -tmin values and the W cut.

29) p.65: Eg cut: should add that the simulation indicates that no DVCS events are expected (in IC) with photon energy less than 2 GeV.
Added. Figures 41 and 42 show the energy of the simulated coherent and incoherent DVCS photons, respectively.

30) p. 67: specify/explain what is an equivalent set of DVCS exclusivity cuts or the simulated events.
We apply similar exclusivity cuts as presented for the experimental coherent DVCS events. That is each exclusive distribution is fitted by a Gaussian and a 3σ cut is applied. So the cut are not identical, but obtained with the same method. This is done to avoid issues on variables where the peak is not in the exact same place in simulation and in data.

31) Fig. 4.8:
i) the experimental widths are similar to the simulated ones: can we conclude from this that the Fermi motion has negligible effects (which I am ready to believe considering the beam energy).
Not actually, because the simulation also includes the Fermi motion effect as shown previously. See the answer to comment 32 of the first reviewer.

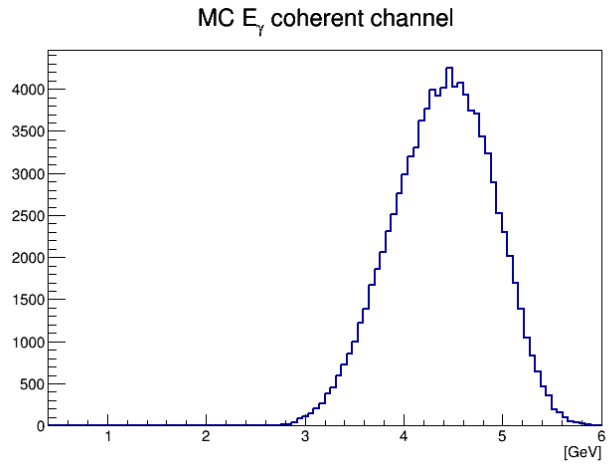

Figure 41: The energy of the simulated coherent DVCS photons

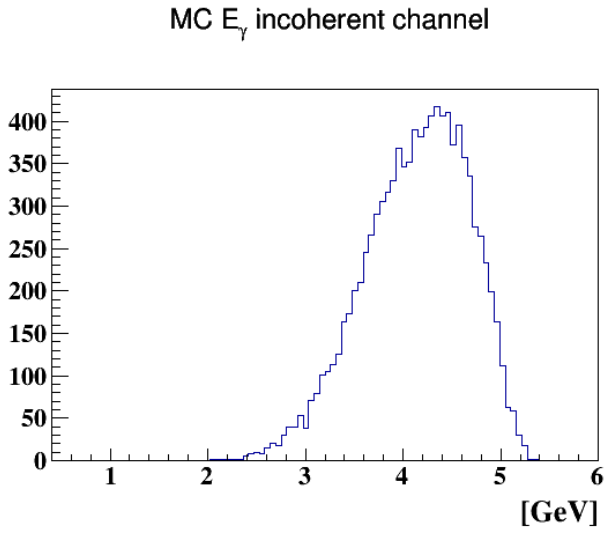

Figure 42: The energy of the simulated incoherent DVCS photons.

ii) any comment on the significant shifts in 2 of the distributions?
The large shift in missing energy is due to the correction in 3.3.4.3. That correction is measured in the range of E_γ available in the IC from $\pi^0 \rightarrow \gamma\gamma$ decays, which is about 0.8 to 2.5 GeV. The correction takes the form of Equation 3.14, which contains a linear scale factor on the energy and an offset, both parameterized as a function of radius as shown in Figure 3.38. To apply the correction on a photon, its radius is used to get the linear energy dependence, and then that is extrapolated to the measured energy of the photon. For DVCS, this goes well above the measured range of photon energies used to derive this correction. It should be noted that previously accepted corrections for photon energies included parameterizing a similar, but 1-dimensional, radial-dependent energy scaling based on the reaction of physical interest (DVCS), effectively to fix the missing mass or energy in DVCS to the zero just by adjusting the photon energy. Here we derive the photon energy correction based on an independent decay (π^0) and assume an extrapolation to the energies of interest. Figure 43 illustrates the size of the correction at high energy and its effect on DVCS. This relates to question #37 from the first reviewer also.

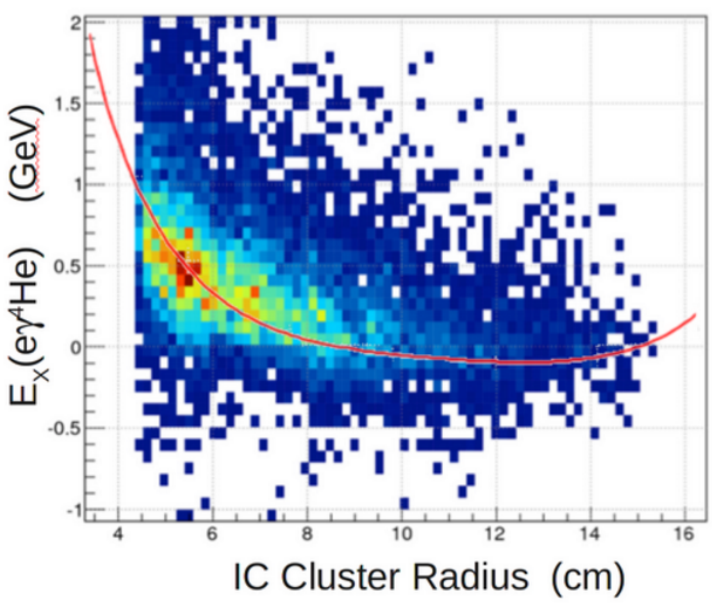

Figure 43: The histogram is the coherent DVCS event selection before the photon energy corrections in 3.3.4.3. The red curve is the correction of 3.3.4.3 for 4 GeV photons, our average DVCS photon energy.

32) p.73: remove 'in figure??'
Corrected. Figure 4.7 in the place of ??

33) p.74: remove ', as expressed in equation??,' and refer to eqs 1.4 to 1.6 for ALU.
Done.

34) Conclude section 4.4 by a table of bin values for all variables in the two topologies.
See tables 2 to 7 at the end of this document.

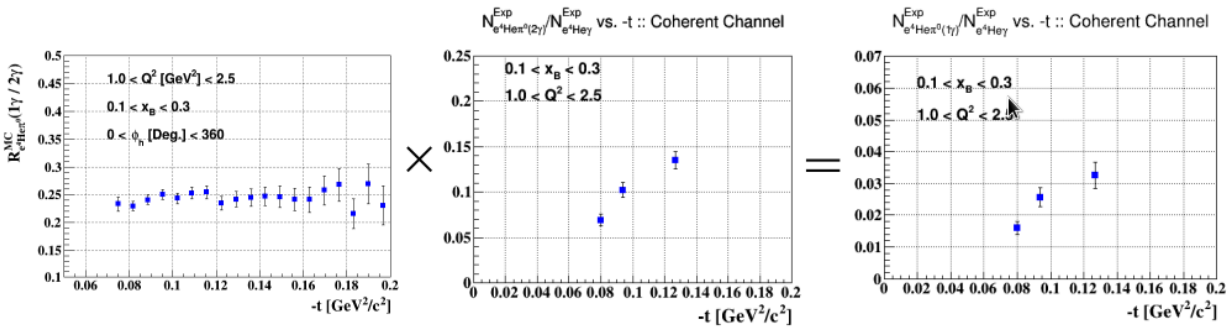

Figure 44: In -t bins; the coherent acceptance ratio (left) is multiplied by the coherent yield of π^0 production (middle) resulting in the backgroud yield (right).

35) Section 4.5: I have a potential issue with the way you use the acceptance ratio. Since, even after integration, one can see some kinematical dependences, I would expect that a 2D subtraction using an integrated R is not rigorous. Mathematically, if I call ijkl the bin indices of the 4 variables: N(ij) = sum(over kl) [Nexp(ijkl) - R(ijkl)NexpPi0(ijkl)] is what you want and is different from sum(over kl)[Nexp(ijkl)] - sum(over kl)[NexpPi0(ijkl)] which you are using. In the end, the difference might be small, but maybe not negligible compared to systematic uncertainties.
You probably forgot a R term in the second formula. Rewriting the formulas: The 4-dimensional background subtraction takes this form:

$$N^{true}_{DVCS}(Q^2, x_B, t, \phi) = N^{Exp.}_{DVCS}(Q^2, x_B, t, \phi) - R^{Sim.}(Q^2, x_B, t, \phi) * N^{Exp.}_{\pi^0}(Q^2, x_B, t, \phi) \quad (5)$$

In order to get the 2-dimensional binning, for instance the $Q^2 - \phi$, we integrate over the other two variable, here are x_B and t like:

$$N^{true}_{DVCS}(Q^2, \phi) = \sum_{x_B,t} N^{Exp.}_{DVCS}(Q^2, \phi) - \sum_{x_B,t}(R^{Sim.}(Q^2, x_B, t, \phi) * N^{Exp.}_{\pi^0}(Q^2, x_B, t, \phi)) \quad (6)$$

What we do in our analysis is:

$$N^{true}_{DVCS}(Q^2, \phi) = \sum_{x_B,t} N^{Exp.}_{DVCS}(Q^2, \phi) - \sum_{x_B,t} R^{Sim.}(Q^2, x_B, t, \phi) * \sum_{x_B,t} N^{Exp.}_{\pi^0}(Q^2, x_B, t, \phi) \quad (7)$$

We carried out our analysis in this way and we assume that it is a good approximation based on:
- Figure 44 shows that the background yield is really very small.
- R is alomst constant in $Q2$, x_B and t. See the one-dimensional dependences of R in section 4.5.1.
- In any case, in the 2D correction, we are indeed dependent on the reproduction of the integrated variables. The figures 4.3, 4.4, 4.7 and 4.8 are here to show that we have a good reproduction of the variables and should not be sensitive to such problems.
- We carry out a full procedures to add the slight deviations in R that comes from this assumption as a systematic uncertainty on the reconstructed asymmetries. See section 4.7 in the analysis note.

36) Section 4.7: should distinguish from the start in the text down to Table 4.1 between overall normalization error (beam polarization) and bin to bin systematic errors.
All the systematic errors are added bin by bin except the beam polarization, which is added to the value of the asymmetry at 90° after fitting the signal.

37) p. 77 last sentence: it is ALU(90°) here and you should mention that it is extracted from the ALU(phi) distribution from a fit to be discussed in section 5.1.
Yes, it is ALU(90°) from the fit. The text is modified to detail this information.

38) p. 77: When you change the missing mass cut, do you do a similar change in the numerator of R?
We used the same acceptance R. The analysis is refined using different acceptance R. The details with the new results can be found in the answers to comments 20 of the third reviewer.

I read on Fig. 4.13 Coherent ALU(3sigma) - ALU(2sigma) = 0.02; for a mean value of .32, that makes 6.2%, not 4. Incoherent OK.
Indeed it is 0.018 resulting in 5.7%. Corrected.

39) Fig. 4.13 coherent again: I worry that ALU increases with a tighter cut. For an asymmetry, a tight cut might be closer to the real value. Comment? Do you see this on all bins? Is this figure integrated on all bins?
This came from applying the same acceptance R. See the answer to comment 20 from the third reviewer, where the analysis is refined and the results are flat within the error bars. And, yes the figure is integrated over all the bins.

40) p. 79: change 83.67% to 0.8367 to distinguish from the following percentage value 3.5% which is really a ratio DeltaP/P.
Done.

41) Radiative corrections: the conclusion could be that we neglect this effect in the end result and table. By the way, I am not aware of any asymmetry for any exclusive channel (elastic, DVCS,...) where the radiative effects are not negligible. If you know a counter example, please let me know.
Indeed, all the previous studies have concluded that the radiative corrections have no sizeable effect to the asymmetry ratios comparing to the other systematic sources.

42) p. 83: Belitsky and Muller (PRD 79 014017) updated earlier DVCS calculations, getting rid of some approximations in their formulae. I know that it makes a difference in the case of a spin 1/2 target (indeed Hall A is using the new formulae from PRD 82 while some CLAS publications still refer to the old ones), but what about a scalar target? Could you please check from this PRD 79 if you have to change the expressions of your α_i's?
We now use the refined parameterization (http://arxiv.org/pdf/0809.2890.pdf) in opposition to the old parameterization (http://arxiv.org/pdf/hep-ph/0302007v2.pdf). Using only the twist-2 terms, we note that:
- The coefficients of the squared DVCS amplitude remain the same. However, in our preliminary CFF extraction, we assumed the pure DVCS to be negligible.
- The interference coefficients change.
- The squared BH amplitude is the same in both calculations.
For instance the following plot, 45 shows the α_0 as a function of ϕ using the two models of calculation. We updated all fits in the note with the most recent formulas.

43) Eqs 5.2 to 5.5: should not they be the same as A.18 to A.21?
They are actually the same, only notations vary. In any case, we will include all the terms in the

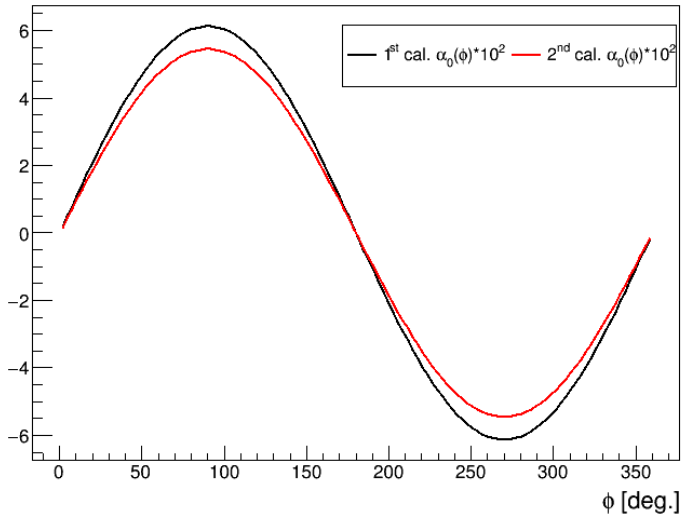

Figure 45: α_0 as a function of ϕ using the old (black) and the new (red) KM parametrizations.

second version of the analysis note with the refined parametrization. The fitting form for the asymmetries will be changed such that the real and the imaginary parts of the CFF H_A will be the free parameters in the fit.

44) p. 84: the last paragraph of section 5.1 is confusing. I would altogether replace it by : 'This two-parameter fit allows us to extract ALU(90 °) already used in Section 4.7 and hereafter in this chapter for comparison with the HERMES data and with model calculations. We checked that adding a cos(2phi) term in the denominator does not change the extracted values of ALU(90°), within the quoted statistical uncertainties. Furthermore, alpha and beta are linear functions of the imaginary part and real parts of the Compton form factors (single He4 CFF in the coherent case, proton CFF's in the incoherent case). Then, in the coherent case, this two-parameter fit can equivalently be replaced by a fit in function of Im(HA) and Re(HA) treated as free parameters, see Section 5.3.'
The paragraph is changed.

45) When adding the systematic and statistical uncertainties in quadrature, should not include the error on beam polarization.
This is what we do, we add the beam polarization error as a normalization to the extracted asymmetries from fitting the signals.

46) It seems your *phi* values are at the middle of each phi-bin. The phi values in each bin should be event weighted (in the same way as Q2, xB, t). Once you do that, you'll have to redo all your fits.
It is not the middle, it is the mean value of *phi* in each phi bin.

47) Fig. 5.2 top left: value of <-t> missing. Added. Section 5.2.1: the drop at high t is 'suggested', not 'observed' by HERMES.
Corrected.

48) Fig 5.5 caption: 'top left' -> 'top'; 'top right' -> 'middle';

Changed.
The kinematics of the CLAS results are not the same as on the figures. The ones in figure 5.4 are showing the mean Q2, xB and -t for each bin. In Figure 5.5, we show the mean values over the full data. For example, in the Q2 dependence plot, xB= 0.267 and -t =0.506 are the mean values over all the bins.

49) Section 5.2.3: in order to convince us (and others) that the proton BSA you analyzed are compatible with the published results, could you reproduce figure 4 of ref 34 (ask FX if need be) and place on it the results from your fits of Fig. 5.6 (the kinematics will differ slightly, but the closest match for each point)
We will use the published results to construct the asymmetry ratios.

50) Section 5.3: do you really get Im(HA) and Re(HA) from alpha and beta or do you redo the fit? I would favor the latter.
The fitting function is now changed and is function of Im(HA) and Re(HA) only.

Also at this stage, it does not cost you anything to put the whole expression 5.1 in the fit, including the cos(2phi) term in c2BH and the apha3 term, since all the coefficients are known and it does not add any parameter. The end result might not be significantly different, but it is a more convincing procedure.
Done.

51) Overall, the physics discussion of the results may not be up to the level of a publication, but this is beyond the scope of the present review. It is not enough to say that we agree or disagree with a given calculation, one may want to give tentative explanations. The most significant deviation from model expectations is R_{incoh} at small xB. Are we then at too small Q2 for validity of leading-twist approximation (but the sin(phi) dominance is what is expected from leading twist)? If we suppose leading twist OK, what would that mean for the bound proton? Etc ... Physics discussion will be developed in the paper.

52) p. 97: 3.23 -> 2.11
Corrected.

3rd reviewer

1) Page 5, 2nd paragraph '..., such as confinement size of the bound nucleons ...' - '..., the quark confinement size of the bound nucleons ...'
Changed.

2) Page 6, in Figure 1.2 it looks like beta = b+b' rather than b-b'.
The figure is corrected.

3) Page 9, Fig caption 1.5, last sentence '...-t,0.2 and 0.4 2 GeV^2/c^2 ...'. Is -t= 0.42?
It is -t= 0.4 GeV^2/c^2. Corrected.

4) Page 10, A strange introduction into the need of an RTPC, section 2.1. No logical conclusion about the lack of exclusivity in the HERMES results, for example, to justify the RTPC. First

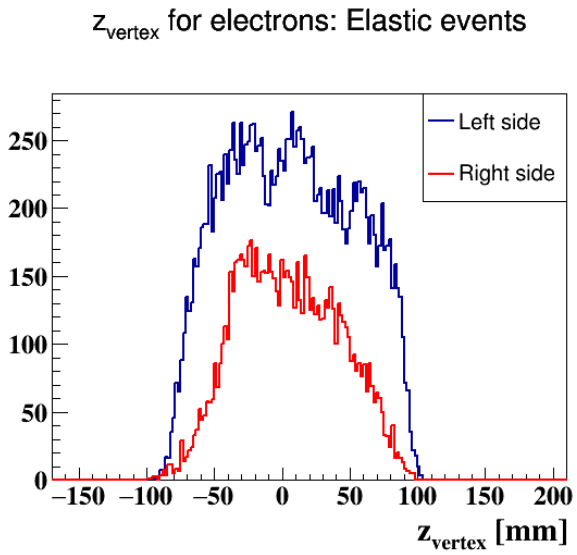

Figure 46: z-vertex distribution for the electrons of the identified elastic events in the two modules of the RTPC.

paragraph talks directly about the momentum per charge of the He4 needing an RTPC.
We have added a longer and hopefully clearer introduction.

5) Page 13, Chapter 2, 2.1 , 'mechanical' in Fig. 2.2 is misspelled in the mechanical support (green boxes). Corrected.

6) 2.2.1.1 Why not choose a region that is relatively flat in the vertex cuts. I understand we lose events but why not choose a region with less steep variations for example, -50,+50mm for z_{RTPC} and then as part of the systematic studies see what effects if any are introduced by the upstream and downstream regions to recover more statistics. See also reviewer 2 request to see this distribution after exclusivity cuts: this may be a clearer way to look in the end regions.

7) Page 17, 2.2.1.1 RTPC good track requirements, bullet 2, I understand that the z cut of -80,+80 mm is well within the physical dimension of the RTPC, however the z acceptance of the RTPC is changing rapidly between -80 to -50 and +50 to +80, therefore why not have a tighter cut first. It can be opened later to increase the statistics when it is shown that there are no systematic effects of the edge regions.
Both 6+7: Regarding the calibration, the z cut is meaningless since we make the calibration in z bins anyway. If we want calibration for the outer z as well we need to keep it. Regarding the data analysis, for the elastic events at 1.2 GeV data, if we remove both z-vertex cuts and apply the other quality cuts on selecting the electron and the recoiled 4He, we obtain figure 46 for the z-vertex distributions of the elastic events: (where both vertices are taken with respect to the center of the RTPC). As a conclusion, the [-80:+80] mm cuts on the helium z-vertex appear to be the suitable cuts to ensure that the reconstructed tracks are within the physical volume of the RTPC.

8) 2.1.3, 1st paragraph, 3rd sentence'... spatial reconstructing ...' should be '... spatial reconstruction ...'
Done.

9) Page 17, 2.2.1.1 RTPC good track requirements, bullet 5, why is *sdist* (-2.0,2.0 mm) with better number of digits compared to *edist* (-1,5 mm). Is there a resolution difference?
This is answered in our answer to question #7 from the 1st reviewer.

10) Page 19, in Figures 2.7, 2.8, 2.9 and 2.10 when comparing the left and right RTPC modules the total number of events is similar even though the shapes are not the same . However, when elastic tracks are used the left and right samples are dramatically different in size. Is this due to electron efficiencies in the CLAS detector between left side and right side? This difference is again seen later in Fig. 3.19 for example and 3.23.
Answered previously in comment 12 of the 1st reviewer.

11) Page 24, Figure 2.16, do we understand why at z=0 $TDC_{max}/2$ is the largest.
Because of the generated electromagnetic field where:
- One can see from figure 2.4 that the magnetic field at the sides of the RTPC is slightly deviated from the direction of the beam line and weaker.
- The generated electric field between the two cylinders (cathode and anode) produces small gradient components at the sides. We added field cages at both ends of the RTPC to adapt for these gradient components, but they were disconnected soon in the run because of HV trips. The electric field might therefore be significantly off on the sides.
However since the TDCmax are extracted directly from data, we are unable to assess which effect is stronger.

If there is a small region around the center that is most stable one should perhaps again analyze the data with a z cut that is narrower from what has been taken in the analysis to check systematic effects.
We performed an additional iteration of the analysis where the events with the scattered electrons being originate within 6 cm from the center of the RTPC, and compared it to the case where the full length of the RTPC is considered. The results are presented in figures 47 and 48 for the coherent and the incoherent channel respectively. As a conclusion, one can see that cutting in the flat region around the center of the RTPC has no direct impact on the exclusive distributions.

Is run 61510 typical?
Yes, it is one of the good runs.

It would be important to check systematic effects on the results as a function of groups of runs with roughly common position of the maximum of $TDC_{max}/2$.
Figure 49 presents the reconstructed coherent A_{LU} as a function of ϕ for different groups of run numbers. Within the given statistics, the asymmetries are compatible.

12) Page 24, in Fig. 2.18, it is not clear at what z the $TDC_{max}/2$ was plotted.
It is integrated over the full z range of the RTPC to show the variation with time during the experimental data taking period.

13) Page 44, figure 3.8 indicates a Cherenkov detector response of the sum of all sectors. It would be helpful to show the response per sector and how well the phototubes of each sector are calibrated with each other. The spectrum as shown seems to indicate an average performance with a mean of 7 to 8 photoelectrons. However, the shape on the low number of photoelectrons hints at a mismatch of performance between different sectors. The cut of the

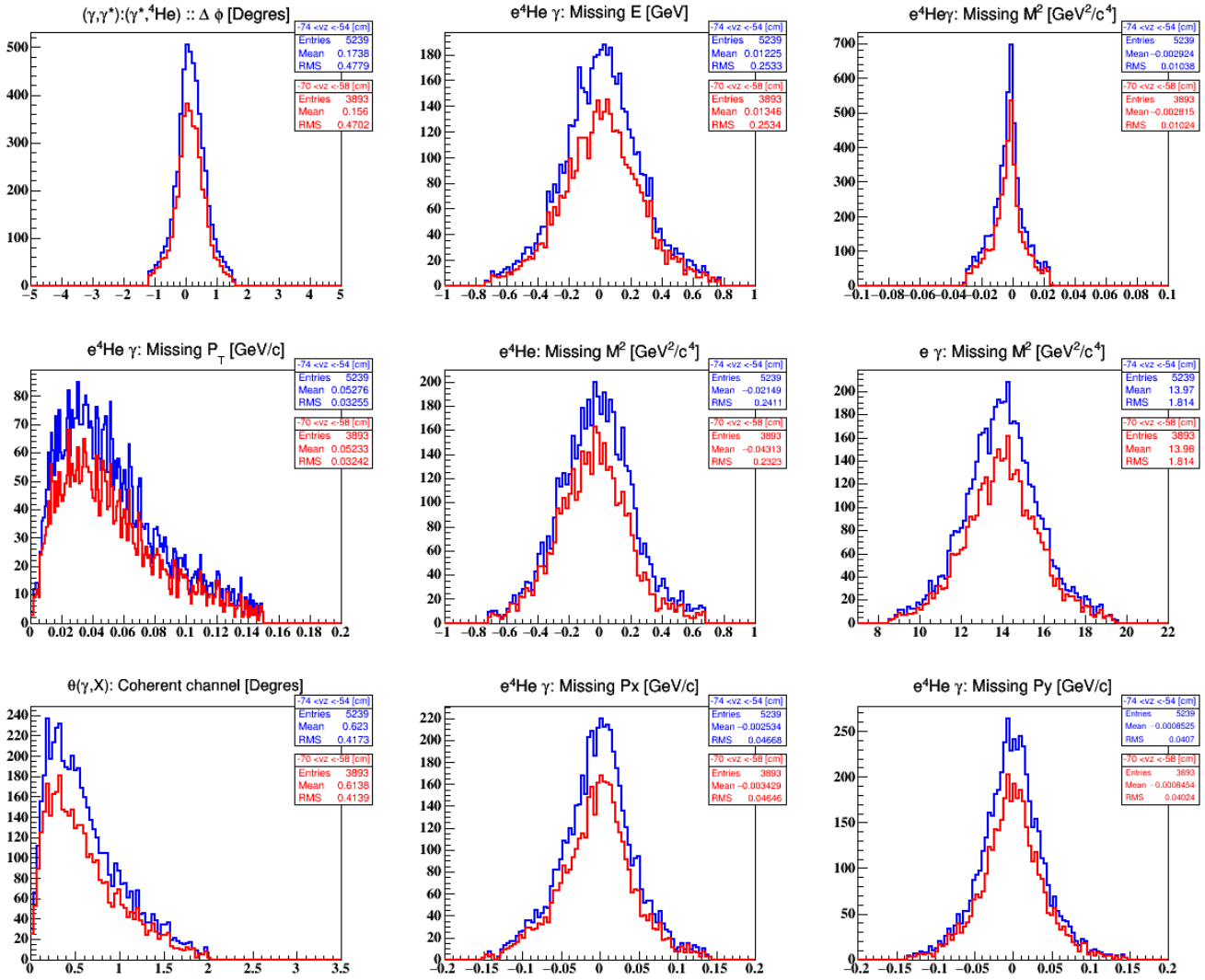

Figure 47: The coherent exclusive distributions for events originating from the full length of the RTPC (in blue) and for eventsoriginating within 6 cm from the center of the RTPC.

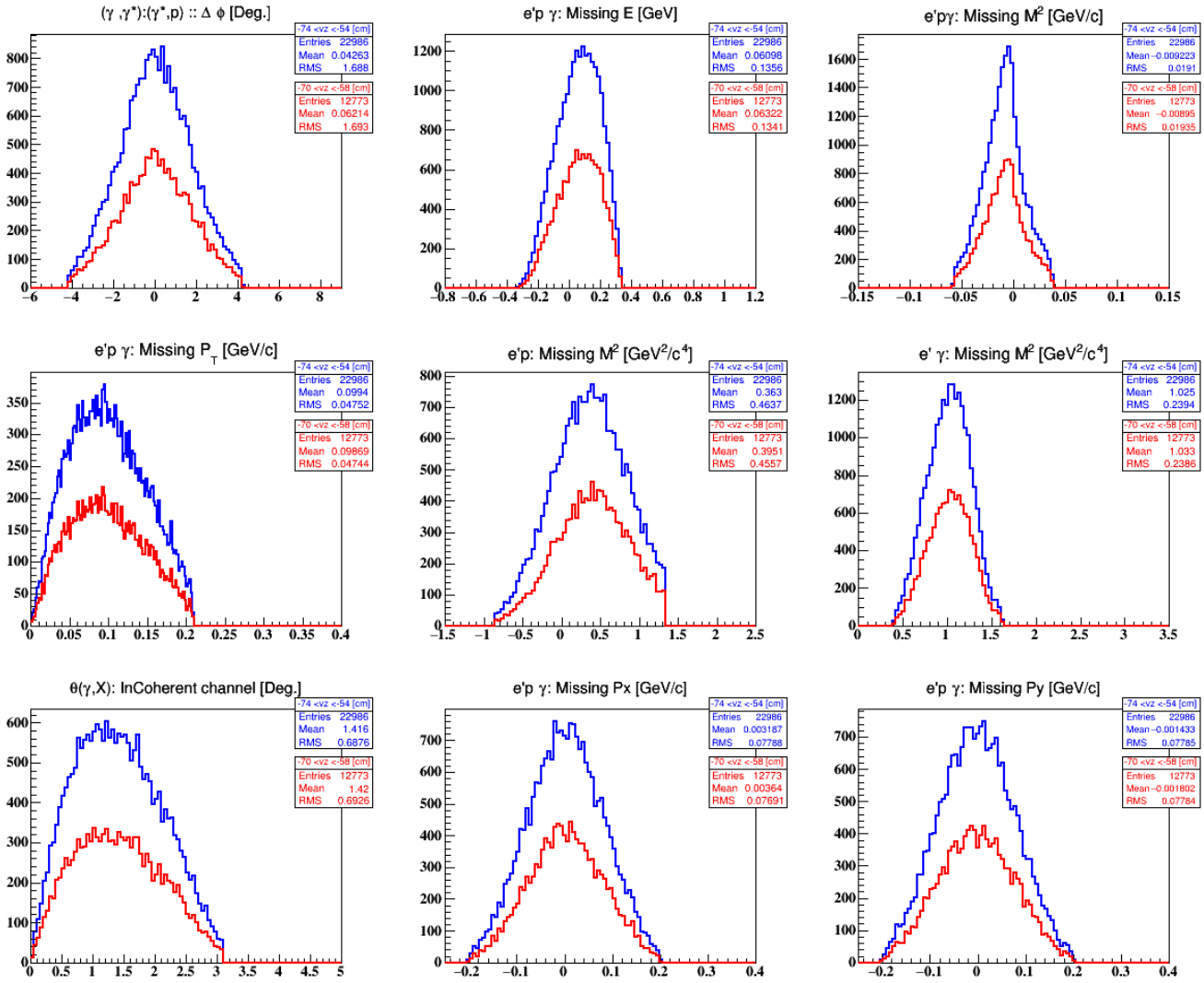

Figure 48: The incoherent exclusive distributions for events originating from the full length of the RTPC (in blue) and for eventsoriginating within 6 cm from the center of the RTPC.

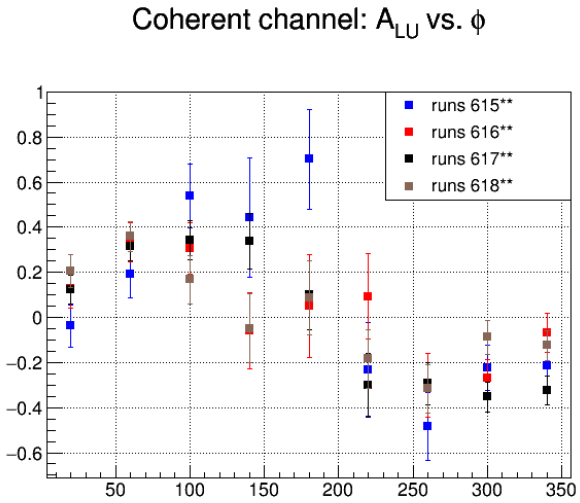

Figure 49: The reconstructed coherent beam-spin asymmetries as a function of ϕ for different groups of runs that exhibit similar trends in the drift speed based on figure 2.18 in the analysis note.

number of photoelectrons to define a good electron track could be optimized per sector and not on the total spectrum as shown. In the end, I would like to see this figure after exclusivity cuts. See the answer to comment 23 from the first reviewer. The sector-dependent distributions after the exclusivity cuts are shown in figures 50 and 51 for the coherent and the incoherent channels respectively without any initial cut on the number of photo-electrons. In figure 52 we show the integrated coherent and incoherent A_{LU} as a function of ϕ using nphe>20 and nphe>40 cuts. This leads us to conclude that the small contribution that remains from the single photo-electron peaks has no significant effect on the reconstructed asymmetries.

14) Page 49, the RTPC track requirement z_{RTPC} cut in Fig. 2.6 of page 19 is set to be within the RTPC volume according to 2.1.1.1 bullet number 2. Then in page 49, Fig. 3.19, when RTPC events are correlated with the electrons detected in CLAS, it is set all the way to the edges of the RTPC. Aren't the proponents worried about edges and inconsistencies with earlier cuts?

For the DVCS events, figure 53 shows the distribution of the He4 DVCS events after the exclusivity cuts without applying any PID cuts on the He4 selection. Following your observation, we set the cut at -80 and 80 as for elastics.

15) Page 50, figure 3.23 the left side is showing half as many events as the right side of the RTPC. Although a priori that should not affect the *phi* distributions of the results, like for instance in figure 4.10, page 74, I would like to see separate *phi* distributions of the He4 asymmetries for the two halves of the RTPC and check that they are compatible.
Figure 54 shows the integrated (over Q2, xB and t) beam-spin asymmetries for the two halves of the RTPC separately and the integrated asymmetries over the whole RTPC.

16) Page 68, figure 4.4, the experimental coplanarity angle is significantly shifted compared to the simulated one. Is this understood? Also, do you know why the experimental missing pT distribution looks much more smeared out than the simulated one for 4He but not for the proton. Is the He4 multiple scattering and fluctuations in energy loss taken in to account in the

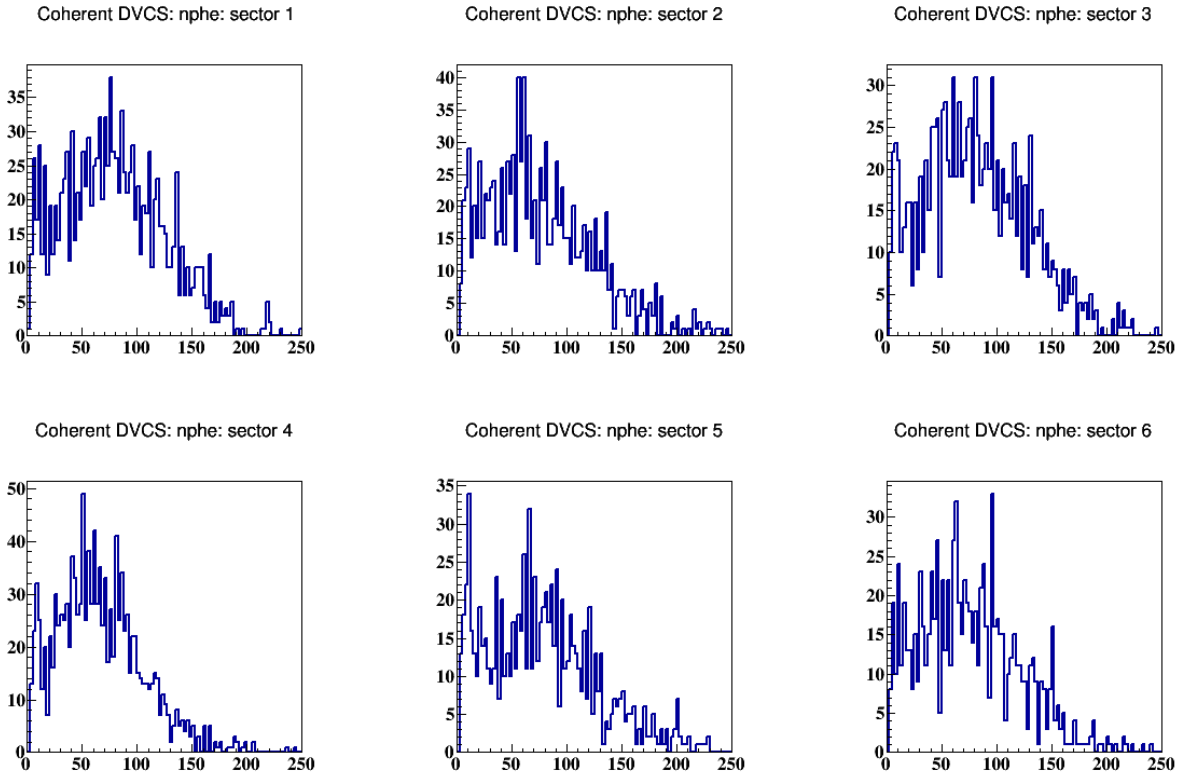

Figure 50: The sector-dependent distributions of the number of photoelectrons produced by the electrons of identified coherent DVCS events.

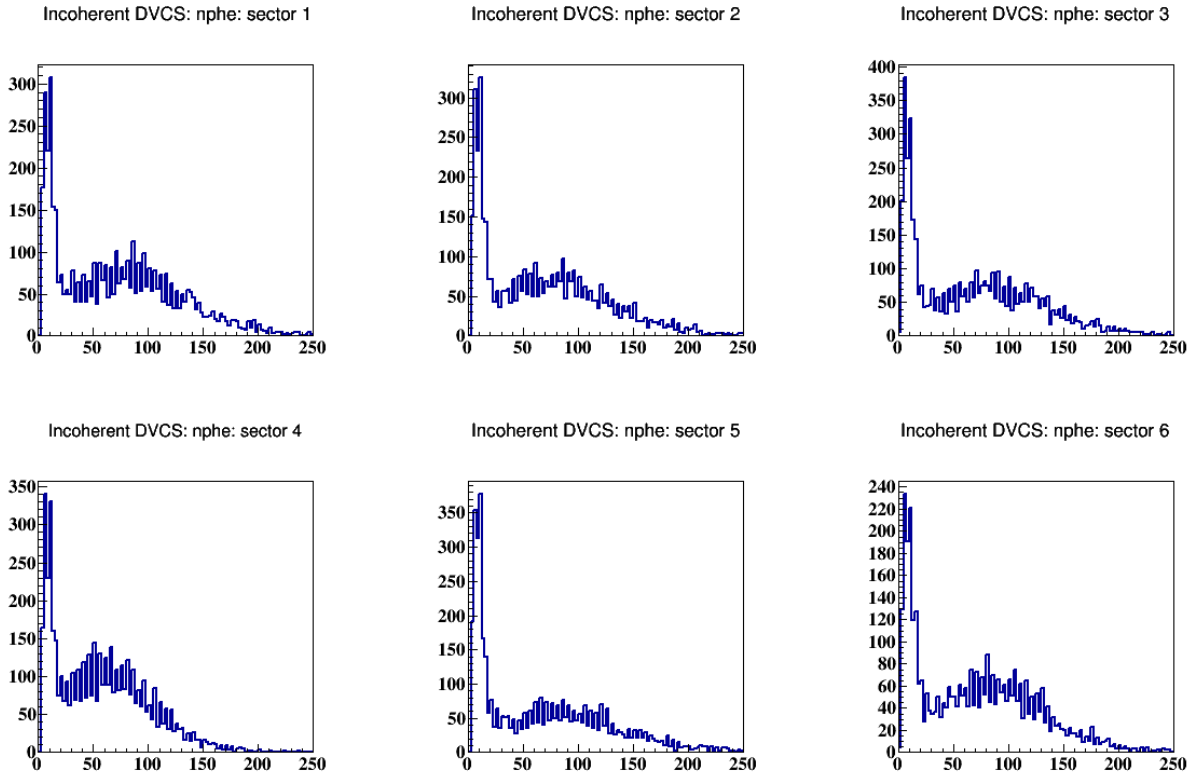

Figure 51: The sector-dependent distributions of the number of photoelectrons produced by the electrons of identified incoherent DVCS events.

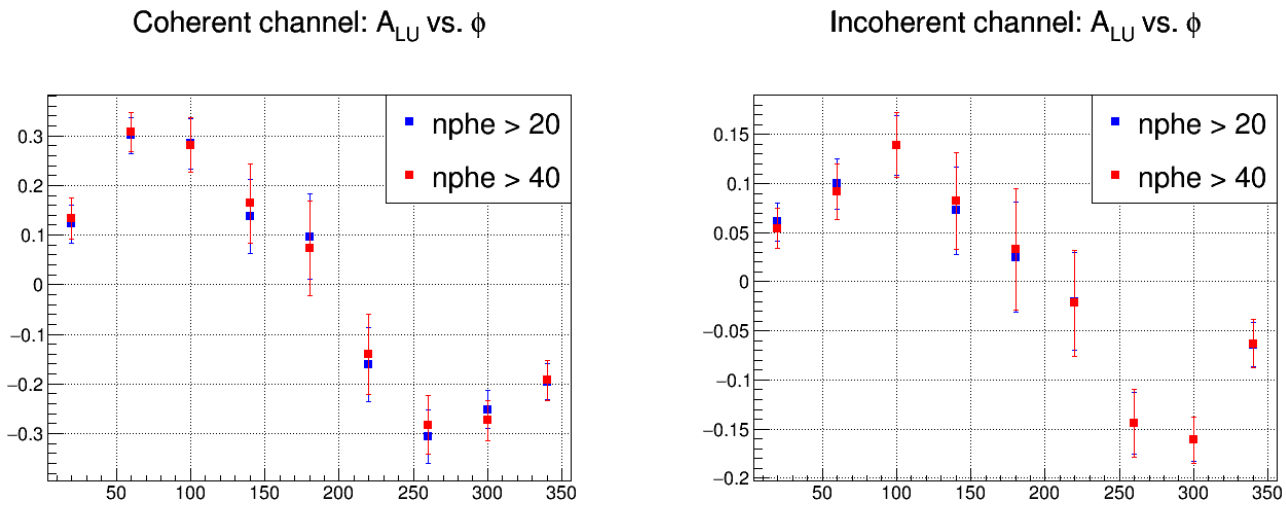

Figure 52: The Coherent (left) and incoherent (right) beam-spin asymmetries using the cuts nphe > 20 (blue) and nphe > 40 (red).

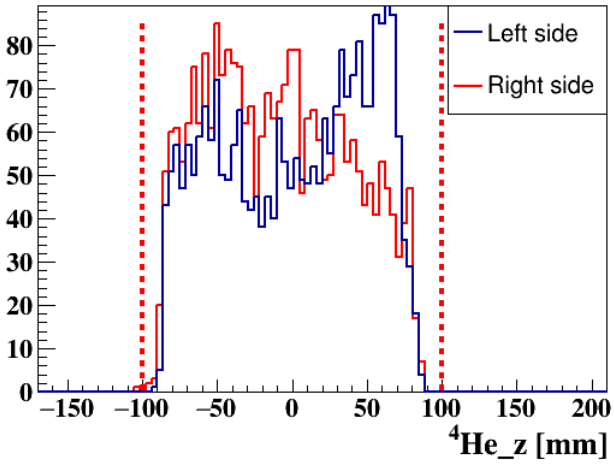

Figure 53: ^{4}He z-vertex distribution for the identified DVCS events in the two modules of the RTPC. The events are selected by applying the exclusivity cuts with no cut on the helium PID nor the z-vertex.

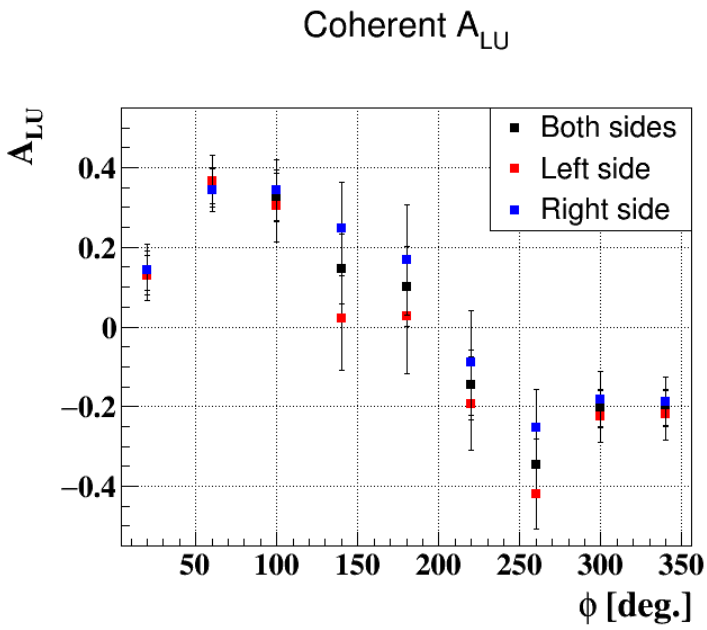

Figure 54: The reconstructed beam-spin asymmetries as a function of the hadronic angle ϕ in the two modules of the RTPC separately and the integrated signal over the whole RTPC.

simulation?
The difference in phi comes from the fact that experimentally there are some dead regions in the azimuthal range of the RTPC (the locations can be figured out from figure 2.27 in the analysis note). These dead regions are not implemented in the fastmc and might affect slightly efficencies. We consider that most of such acceptance issues cancel for the measurement of asymmetries. The incoherent missing-pT is highly smeared by Fermi motion, while the coherent one is not, and this is visible by comparing the two channels' missing-pT in the figures. This makes its agreement between experiment and simulation less sensitive to resolution for the incoherent channel, and probably related to the worse agreement for the coherent channel. However, this does not play a significant role in the asymmetry measurement, as can be seen in the asymmetry extracted for different missing-pT ranges shown in figure 34. Regarding the multiple scattering and the energy loss, we do not apply them individually, but we apply an overall smearing to the kinematics of the Helium nuclei based on the real data.

17) Page 69, first paragraph: Is the timing information between the electron and the proton included? Are there any timing cuts between the electron and proton?
We do apply a timing cut between the electron and the proton through $\Delta\beta$ cut which is defined in equation 3.4. There the t_{TOF} is the difference between the time at the vertex of the electron and the time of the proton.

18) Page 72, figure 4.8: Why is there such a big discrepancy between the experimental and simulated data for e'p gamma: missing E and e'gamma: missing M^2 in the case of the proton? There is no similar discrepancy in the coherent case for He4, see figure 4.4?
See the answer to comment #31 of the second reviewer.

19) Page 77-78, (Systematic: DVCS selection cuts): You are barely changing your statistics moving out from a 2 sigma cut. To truly show that your cuts are sufficient and don't influence the results, you should do something more drastic. It would be much more convincing if , for example, you would compare the results within a 1 sigma range (inner 66% of events) with the results between 1 sigma and 3 sigma (outer 33% of events).
Included in the answer of the next question.

20) Page 86:
a) It would be nice if you could give the chi2 and error on the fit.
b) Have you tried fitting the spectra including the cos(2phi) term? How strongly does the minimizer prefer using the simple 2-parameter form from equation 5.6?
Referring to comment 38 of the 2nd reviewer. We were taking the same acceptance R for the different cuts. In the following we show the corresponding R for each cut width, where similar changes in the cut width are applied in the dominator and the numerator of R. Regarding comment 19 of the 3rd reviewer, we take cuts from 1 to 5 σ. The cuts are shown in figure 55 and the corresponding acceptance ratios are shown in figure 56. We fit here our beam-spin asymmetry signals with the full expression ($\frac{\alpha sin(\phi)}{1+\beta cos(\phi)+\eta cos(2\phi)}$). Figure 57 shows the reconstructed bean-spin asymmetries as a function of ϕ integrated over Q2, xB , and -t for the coherent and the incoherent DVCS channels. In Figures 58, 59, 60, and 61 we show α, β, η, and χ^2 of the fits as a function of the cut width for the coherent and the incoherent channels. The beam-spin asymmetry at $\phi = 90^\circ$ ($= \frac{\alpha}{1-eta}$) is shown as a function of the cut size for both DVCS channels in figure 62.
c) How sensitive are the fit results to your binning? You could investigate by e.g., adding/removing a bin in *phi*, or by shifting the bin edges. (Or you could remove any bias

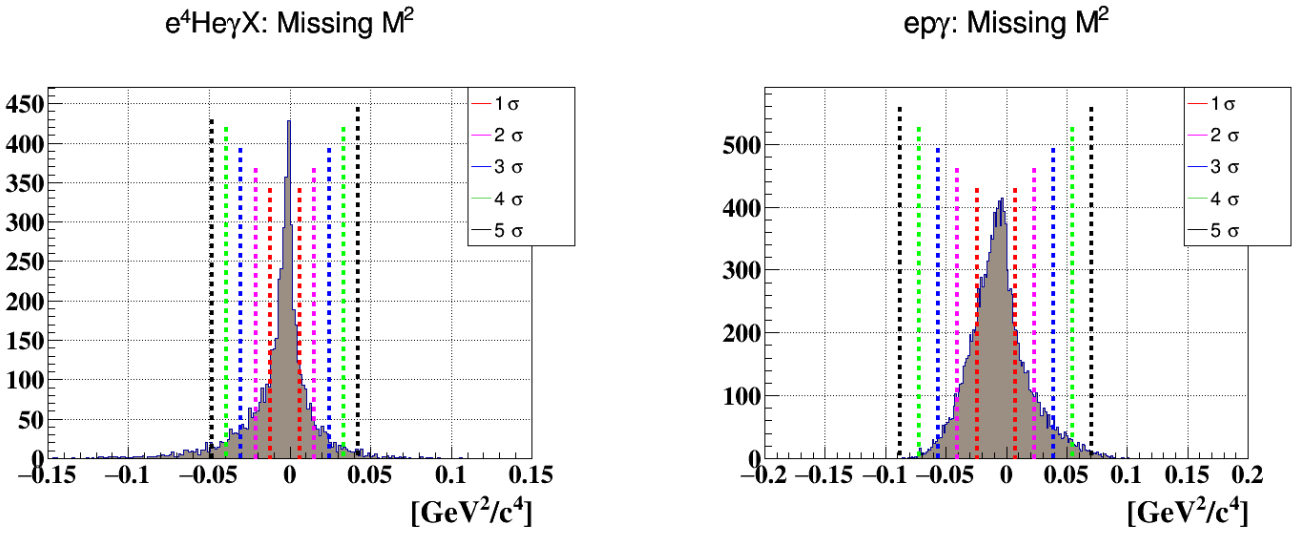

Figure 55: The cuts applied on the missing mass squared of the coherent (right) and the incoherent DVCS channels in order to estimate the systematic uncertainties stemming from the DVCS selection cuts.

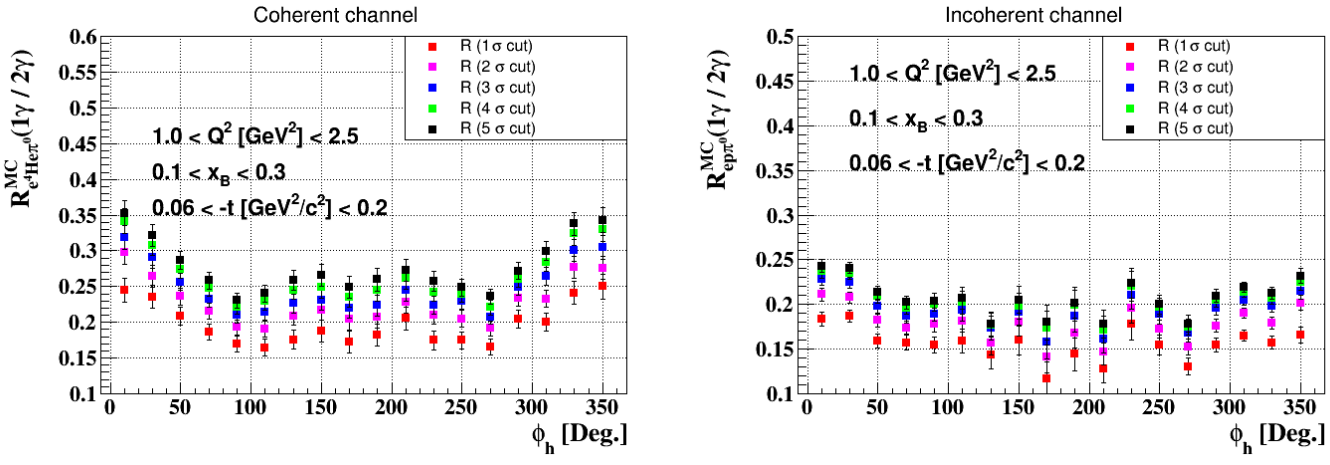

Figure 56: Coherent (right) and incoherent (left) acceptance ratios corresponding to the different cuts shown in figure 55.

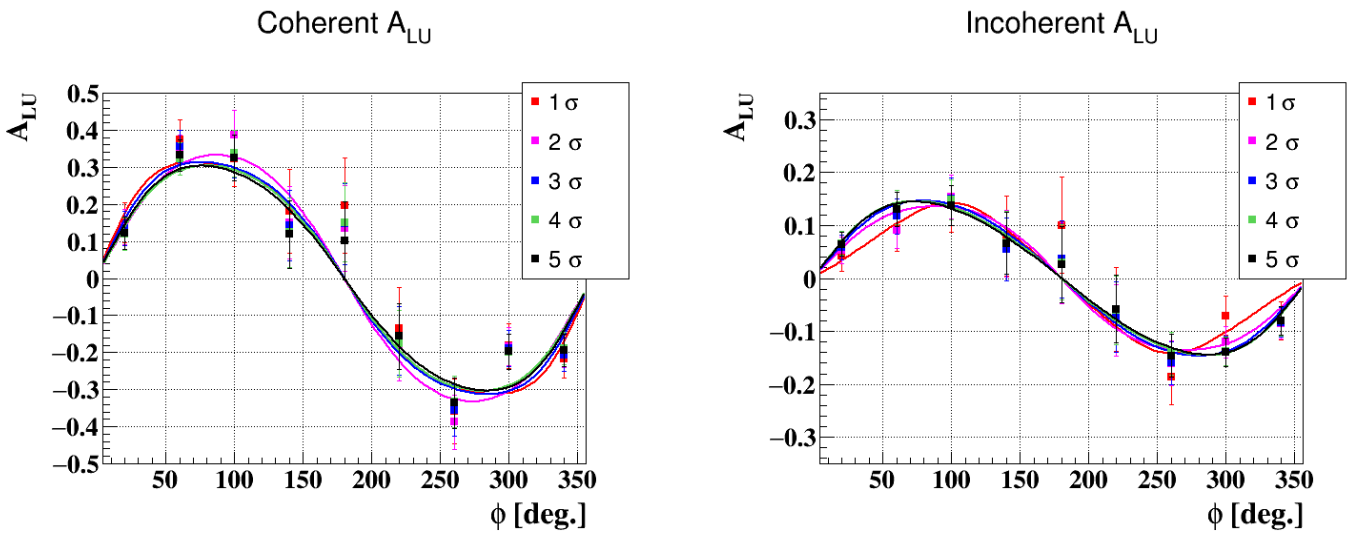

Figure 57: Integrated coherent (right) and incoherent (left) beam-spin asymmetry signals as a function of the angle ϕ. The different colored points indicate the different cuts shown in figure 55. The colored lines are fits to the data points of the form $\frac{\alpha sin(\phi)}{1+\beta cos(\phi)+\eta cos(2\phi)}$.

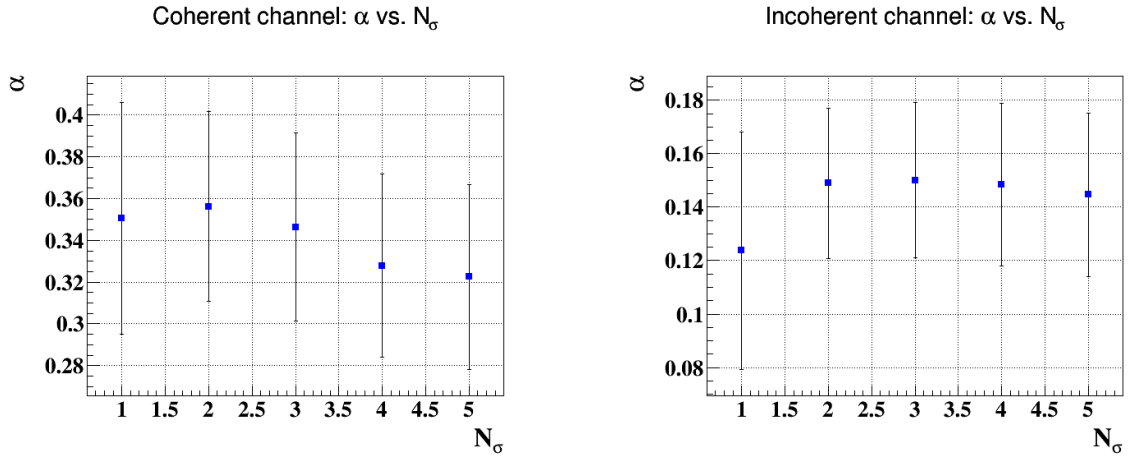

Figure 58: The coherent (left) and incoherent (right) α parameter of the fits as a function of cut width.

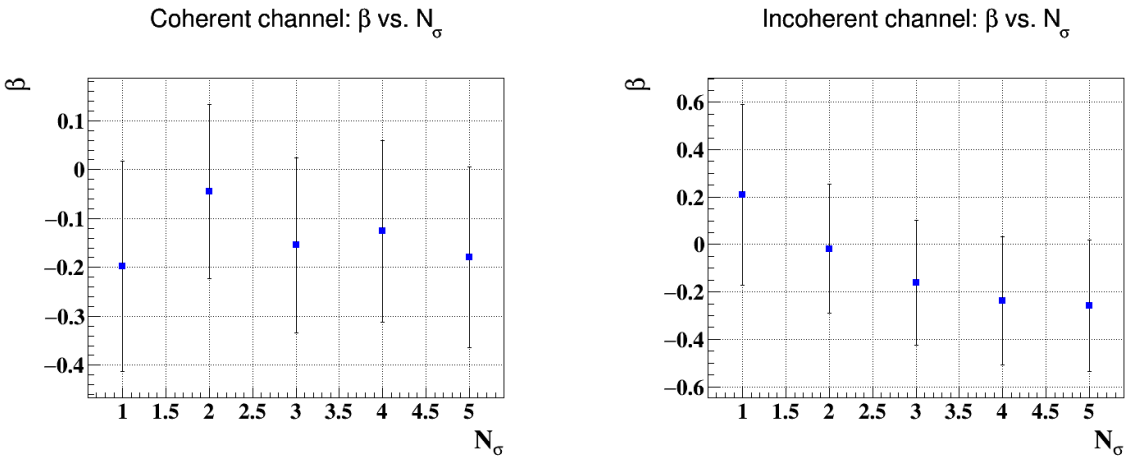

Figure 59: The coherent (left) and incoherent (right) β parameter of the fits as a function of cut width.

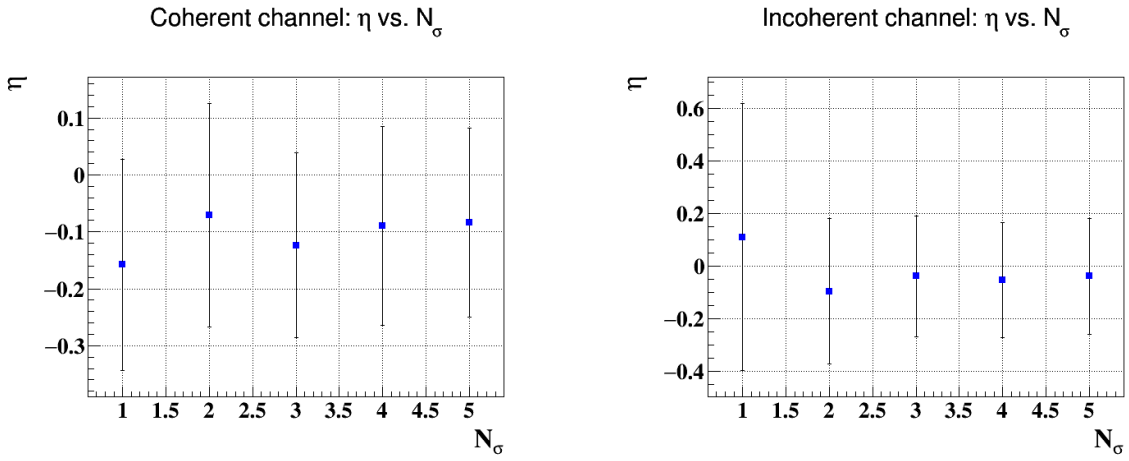

Figure 60: The coherent (left) and incoherent (right) η parameter of the fits as a function of cut width.

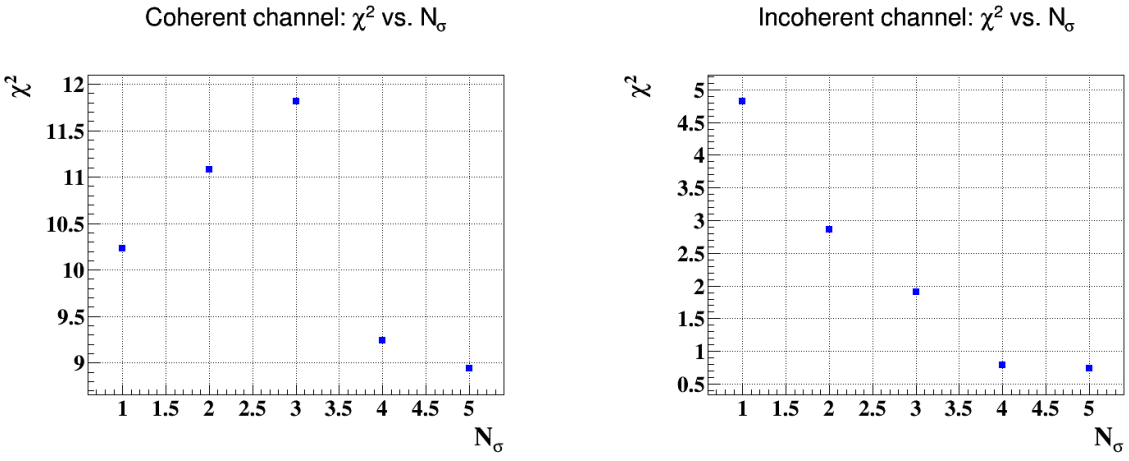

Figure 61: The coherent (left) and incoherent (right) χ^2 parameter of the fits as a function of cut width.

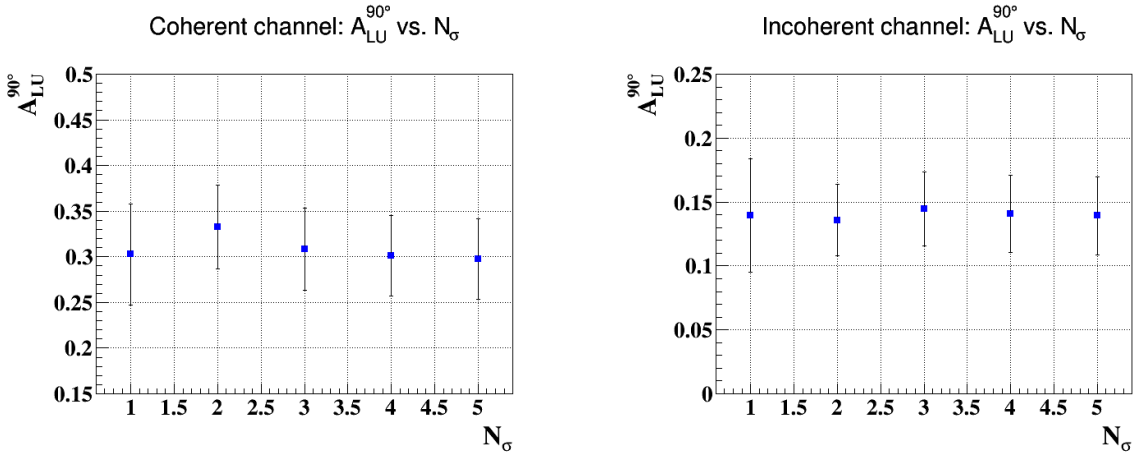

Figure 62: The coherent (left) and incoherent (right) beam-spin asymmetry at $\phi = 90°$.

introduced by the choice of binning by doing an unbinned fit...)
In order to evaluate this uncertainty we binned the data into 11 bins in phi and we compared the reconstructed asymmetries to the results from our old binning. Figure 63 shows the coherent reconstructed A_{LU} as a function of ϕ in Q^2, x_B and $-t$ bins. The coherent, figure 64, and the incoherent, figure 65, measured A_{LU} at $\phi = 90°$ are showing 5% to 10% systematic uncertainties, which will be added to our estimated uncertainties for the extracted asymmetries at $\phi = 90°$.

21) Page 91: you do need to quantify 'significant trends'. For example by showing how much better a fit with a simple A1 + A2*x works as compared to just a fit of a constant.
Physics discussion to be developed in the paper.

22) Page 92, third paragraph, last sentence: not true, within errors the values are compatible with each other!
Modified.

23) In summary, the analysis seems sound and clearly a lot of work has gone into it, but to be fully convincing more checks are needed in my opinion. The key observables presented here are beam spin asymmetries which are more forgiving given that many of the systematic errors cancel. However, I have yet to see solid systematic studies performed on the stability of the final results with respect to selection cuts and exclusivity cuts.

a) A systematic study of the *phi* dependence of the He4 asymmetry seen by the left side and the right side of the RTPC need to be carried out.
The reconstructed asymmetries in each module of the RTPC are shown in figure 54. In terms of the exclusivity distributions, see figure 66, the performance of the two sides of the RTPC are very similar.

b) A good justification of the cuts ranges used is not always provided. The rejection efficiency of the cuts is not determined systematically. Of course, the statistical and systematic errors will depend on these cuts and the change of the physics results needs to be tested against the range of these cuts.
Point raised and answered in Q47 of Reviewer 1.

c) The stability of the physics results needs to be tested more meaningfully (see above comment at page 77-78).

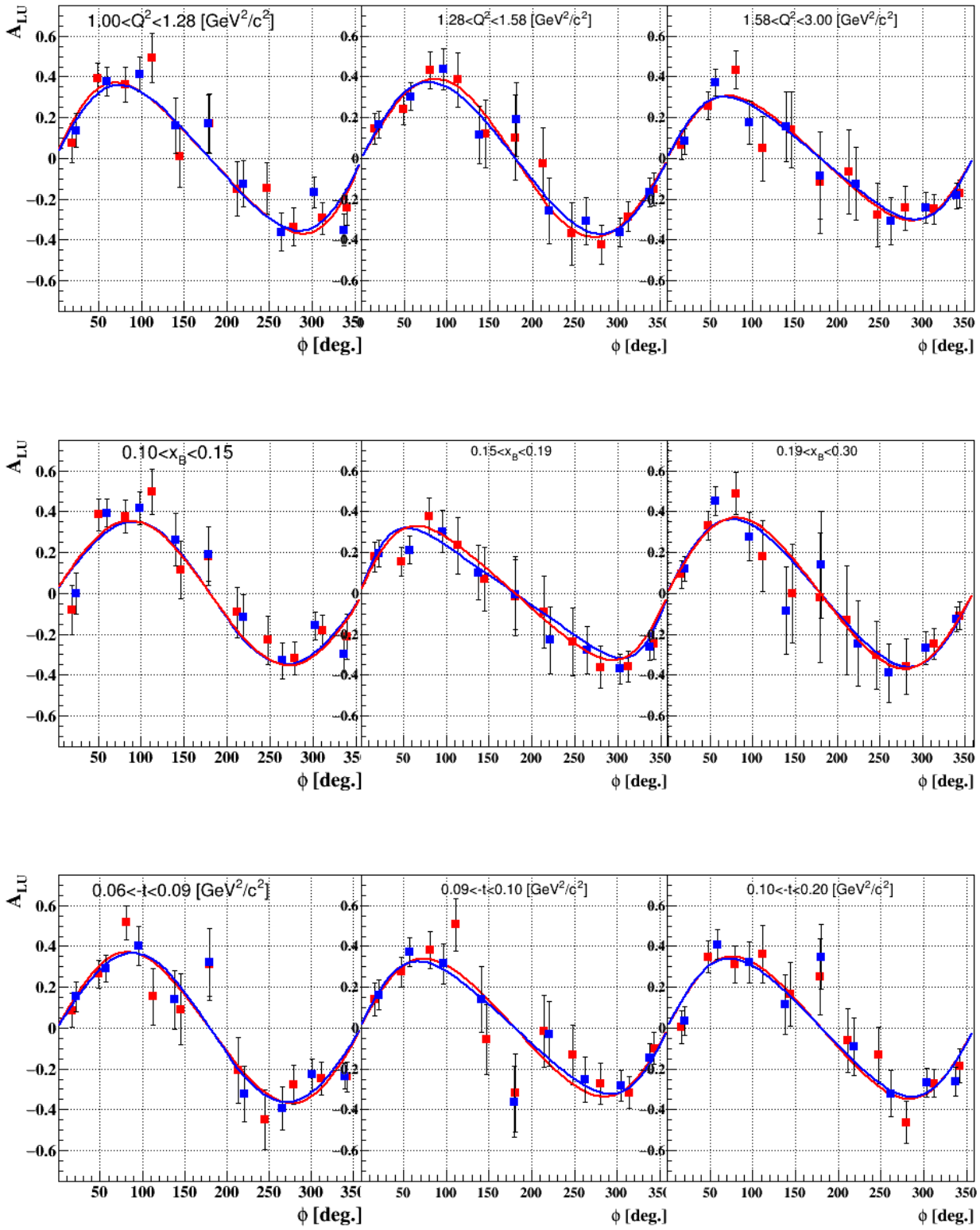

Figure 63: The measured coherent beam-spin asymmetry as a function of ϕ in Q^2, x_B and $-t$ bins, using two binning sets in ϕ: 9 bins (in blue) and 11 bins (in red).

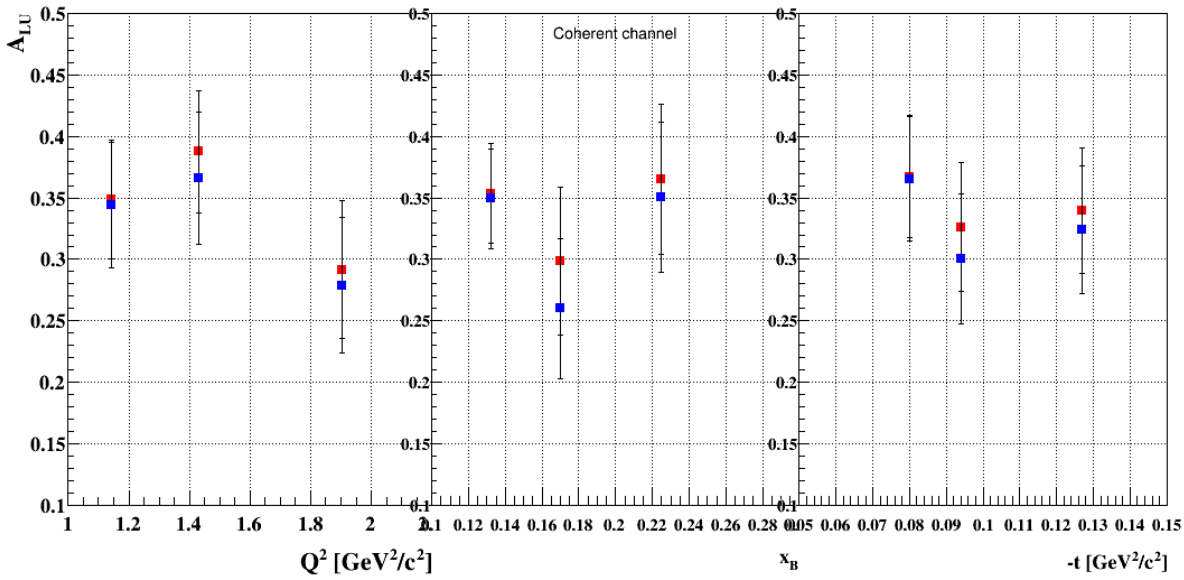

Figure 64: The coherent $A_{LU}(\phi = 90°)$, from the fit, as a function of Q^2, x_B and $-t$, using 9 (in blue) and 11 (in red) bins in ϕ.

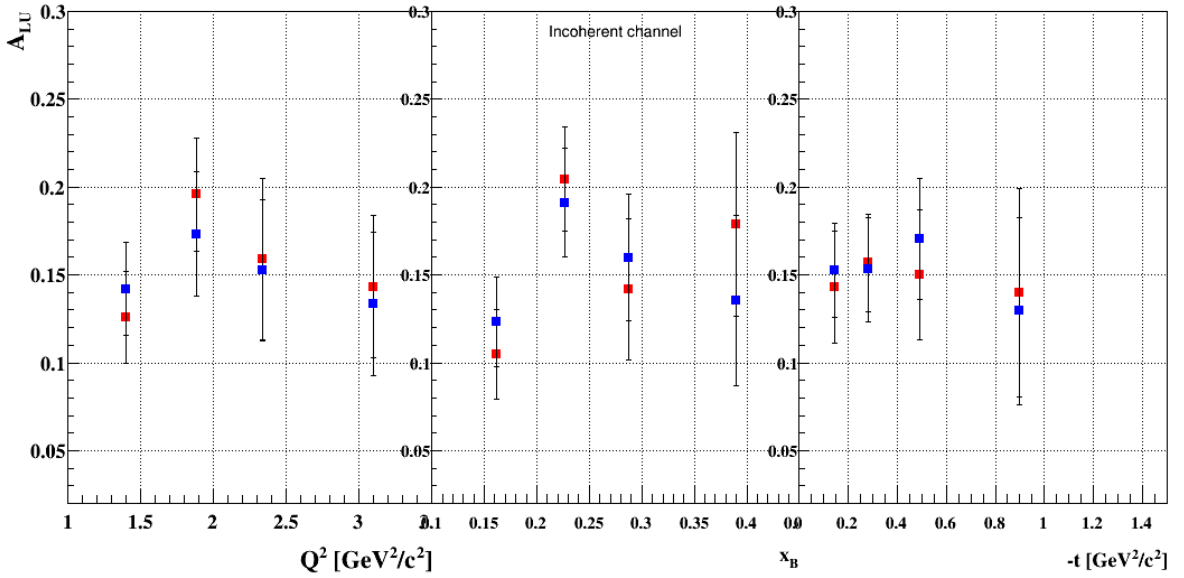

Figure 65: The incoherent $A_{LU}(\phi = 90°)$, from the fit, as a function of Q^2, x_B and $-t$, using 9 (in blue) and 11 (in red) bins in ϕ.

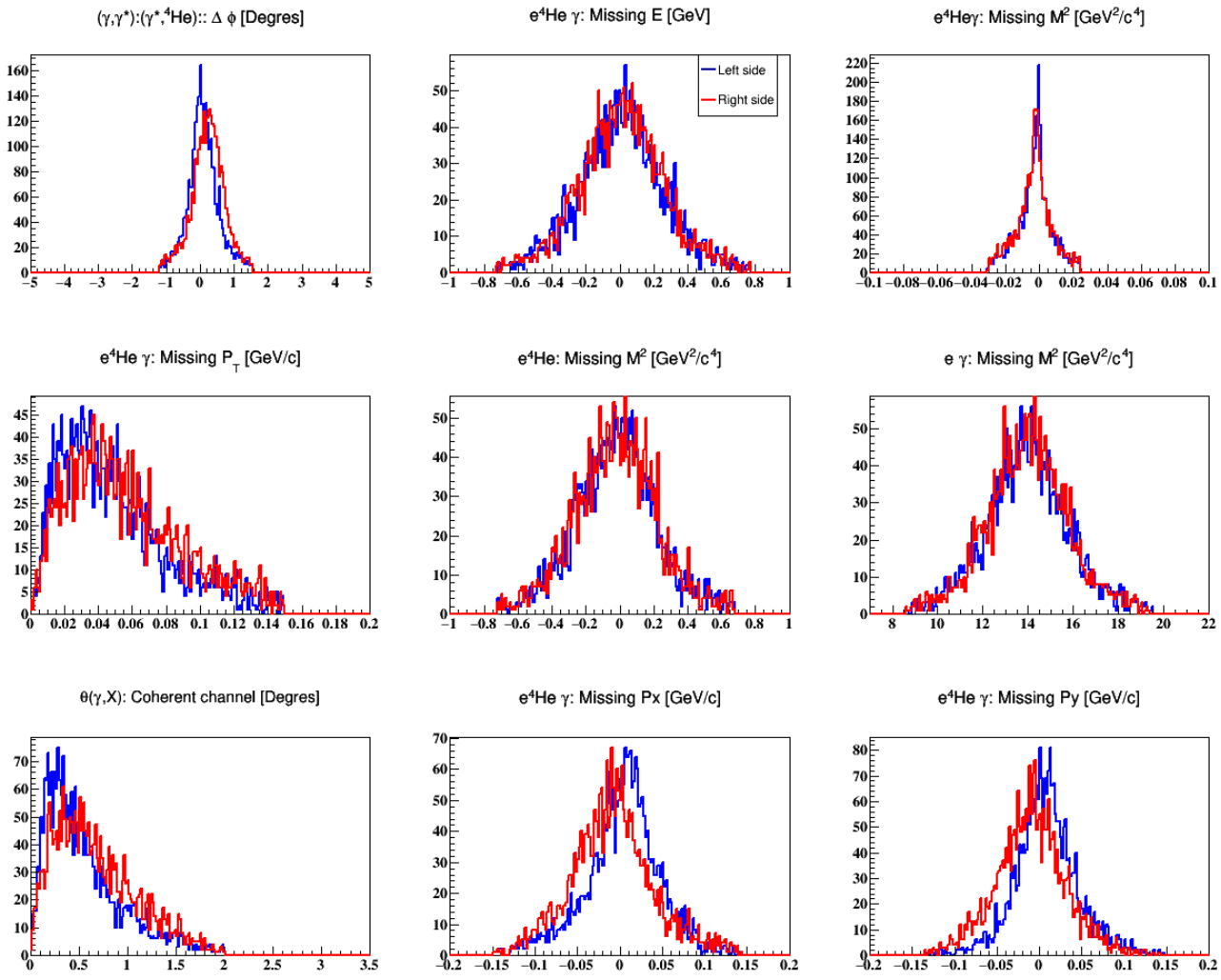

Figure 66: The distributions of the exclusive variables of the identified coherent DVCS events in the individual modules of the RTPC.

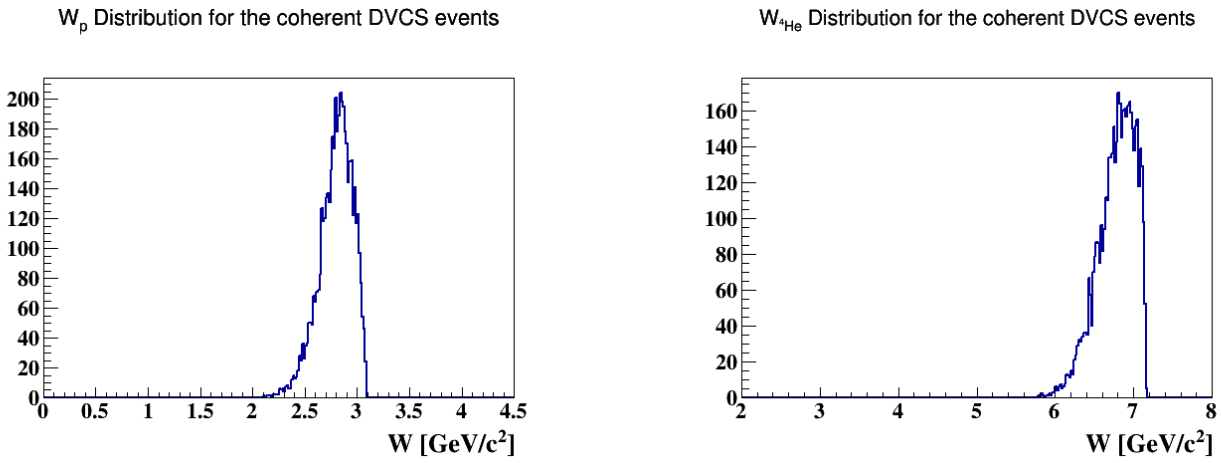

Figure 67: W distributions of the identified coherent DVCS events. On the left: W_p is calculated assuming the target is a nucleon. On the right $W_{^4He}$ is by using the real mass of He4.

Point raised and answered in Q19.

d) I have no comments on the physics interpretation discussed in this note until I am confident about the stability of the results.

- External question: what W > 2 $GeV^2$2 cut, where the target is assumed to be a nucleon, does for the case of the coherent channel?
To investigate this effect, we removed W cut and identify the coherent DVCS events via the exclusivity cuts presented in chapter 4 of the analysis note. The results are presented in figure 67. As a conclusion, this cut has no effect on the coherent channel and is removed.

ALU tables

$< Q^2 >$	$< x_B >$	$< -t >$	$< \phi >$	$A_{LU} \pm$ stat. $\pm$ syst.
1.143	0.136	0.096	23.32563	0.1370716 ± 0.08373948 ± 0.02571563
1.143	0.136	0.096	59.81847	0.3758095 ± 0.07101178 ± 0.01885969
1.143	0.136	0.096	97.78493	0.4125528 ± 0.08798407 ± 0.04038886
1.143	0.136	0.096	140.0018	0.159693 ± 0.1366452 ± 0.02678967
1.143	0.136	0.096	179.0882	0.1714253 ± 0.1398893 ± 0.02789155
1.143	0.136	0.096	219.1279	-0.1240822 ± 0.1156237 ± 0.02484531
1.143	0.136	0.096	263.7259	-0.3608519 ± 0.09411095 ± 0.03891253
1.143	0.136	0.096	302.9283	-0.1683747 ± 0.07604881 ± 0.02632836
1.143	0.136	0.096	337.3336	-0.3508557 ± 0.07680001 ± 0.03431105
1.423	0.172	0.099	19.94307	0.1650792 ± 0.067211 ± 0.02673700
1.423	0.172	0.099	57.17185	0.3028724 ± 0.068908 ± 0.02503328
1.423	0.172	0.099	95.77216	0.4372785 ± 0.099537 ± 0.04267748
1.423	0.172	0.099	137.9543	0.1147926 ± 0.142932 ± 0.02500644
1.423	0.172	0.099	180.9498	0.1924395 ± 0.1806951 ± 0.03026008
1.423	0.172	0.099	220.1671	-0.2589808 ± 0.1611112 ± 0.03447198
1.423	0.172	0.099	263.1496	-0.3065283 ± 0.1158366 ± 0.03663218
1.423	0.172	0.099	302.3187	-0.3646641 ± 0.069707 ± 0.03835156
1.423	0.172	0.099	338.0674	-0.1660148 ± 0.069482 ± 0.02613428
1.902	0.224	0.107	20.96588	0.0841330 ± 0.06370723 ± 0.02345626
1.902	0.224	0.107	56.59966	0.3739804 ± 0.06574343 ± 0.01851792
1.902	0.224	0.107	95.79632	0.1779531 ± 0.1058264 ± 0.0173685
1.902	0.224	0.107	139.5123	0.1574064 ± 0.1713567 ± 0.01702304
1.902	0.224	0.107	179.5613	-0.0837227 ± 0.2119008 ± 0.01265815
1.902	0.224	0.107	221.6768	-0.1251566 ± 0.1783256 ± 0.01528429
1.902	0.224	0.107	263.0872	-0.3069055 ± 0.1173135 ± 0.02602474
1.902	0.224	0.107	303.6431	-0.2404473 ± 0.07568278 ± 0.02071202
1.902	0.224	0.107	339.2973	-0.184311 ± 0.06150122 ± 0.01635832

Table 2: Coherent ALU in Q2 bins

$< Q^2 >$	$< x_B >$	$< -t >$	$< \phi >$	$A_{LU} \pm$ stat. $\pm$ syst.
1.164	0.132	0.095	24.70837	-0.0009864 ± 0.1023417 ± 0.02214862
1.164	0.132	0.095	60.38457	0.394491 ± 0.06742577 ± 0.01984295
1.164	0.132	0.095	98.05482	0.4169974 ± 0.0822727 ± 0.04084068
1.164	0.132	0.095	140.4849	0.2629772 ± 0.1287244 ± 0.03336946
1.164	0.132	0.095	178.7877	0.1917519 ± 0.133959 ± 0.02937379
1.164	0.132	0.095	218.4067	-0.1139352 ± 0.1099316 ± 0.02438166
1.164	0.132	0.095	263.7104	-0.3303477 ± 0.08687361 ± 0.0372357
1.164	0.132	0.095	302.0021	-0.158615 ± 0.06873616 ± 0.02598807
1.164	0.132	0.095	335.3734	-0.2978278 ± 0.09144179 ± 0.03198552
1.439	0.17	0.099	21.20114	0.1944966 ± 0.06481715 ± 0.023002136
1.439	0.17	0.099	57.05011	0.2135007 ± 0.0688628 ± 0.01959182
1.439	0.17	0.099	95.32827	0.3033697 ± 0.1028014 ± 0.0295878
1.439	0.17	0.099	137.6747	0.1027237 ± 0.134283 ± 0.01876947
1.439	0.17	0.099	180.8816	-0.0055032 ± 0.1730991 ± 0.0197908
1.439	0.17	0.099	220.8371	-0.2294214 ± 0.1615644 ± 0.0270881
1.439	0.17	0.099	264.4366	-0.2758285 ± 0.1156173 ± 0.02923329
1.439	0.17	0.099	302.6414	-0.3697083 ± 0.07362371 ± 0.03312501
1.439	0.17	0.099	337.925	-0.2626907 ± 0.06672689 ± 0.02543044
1.844	0.225	0.107	19.94412	0.1199148 ± 0.0610976 ± 0.024893846
1.844	0.225	0.107	56.1033	0.4535308 ± 0.07056983 ± 0.02240954
1.844	0.225	0.107	95.56723	0.2782661 ± 0.1178502 ± 0.02714954
1.844	0.225	0.107	139.3193	-0.0854730 ± 0.2144445 ± 0.01668931
1.844	0.225	0.107	180.6025	0.1409771 ± 0.2599303 ± 0.02044162
1.844	0.225	0.107	223.7917	-0.2456453 ± 0.2105987 ± 0.02706752
1.844	0.225	0.107	260.904	-0.3907139 ± 0.1417117 ± 0.03533464
1.844	0.225	0.107	304.3742	-0.2674945 ± 0.08101173 ± 0.02630272
1.844	0.225	0.107	340.0658	-0.125335 ± 0.06016415 ± 0.01755089

Table 3: Coherent ALU in xB bins

$< Q^2 >$	$< x_B >$	$< -t >$	$< \phi >$	$A_{LU} \pm$ stat. $\pm$ syst.
1.36	0.160	0.080	21.30242	0.1531553 ± 0.07225752 ± 0.026305318
1.36	0.160	0.080	57.11194	0.2900274 ± 0.06585235 ± 0.02439207
1.36	0.160	0.080	96.15277	0.4041914 ± 0.09641501 ± 0.03947151
1.36	0.160	0.080	137.9588	0.1402594 ± 0.1434757 ± 0.02522018
1.36	0.160	0.080	179.2052	0.3218006 ± 0.1641379 ± 0.03717874
1.36	0.160	0.080	221.4243	-0.3213178 ± 0.1356342 ± 0.03708316
1.36	0.160	0.080	265.92	-0.392002 ± 0.1066914 ± 0.04038161
1.36	0.160	0.080	301.3226	-0.2284983 ± 0.07726413 ± 0.02940459
1.36	0.160	0.080	339.661	-0.2348847 ± 0.06494273 ± 0.02810254
1.507	0.179	0.094	21.17746	0.1631617 ± 0.07120653 ± 0.026711914
1.507	0.179	0.094	56.92214	0.3715996 ± 0.06870001 ± 0.02842517
1.507	0.179	0.094	97.24788	0.3145243 ± 0.09659388 ± 0.03076673
1.507	0.179	0.094	141.6889	0.1388844 ± 0.1607593 ± 0.02150343
1.507	0.179	0.094	179.6762	-0.3612444 ± 0.1723714 ± 0.03603272
1.507	0.179	0.094	220.3783	-0.029479 ± 0.1576259 ± 0.01477838
1.507	0.179	0.094	262.64	-0.2524102 ± 0.1096333 ± 0.02830972
1.507	0.179	0.094	303.6787	-0.282367 ± 0.07599572 ± 0.02864878
1.507	0.179	0.094	338.2113	-0.1464348 ± 0.07113145 ± 0.02012911
1.610	0.193	0.127	21.08428	0.0341355 ± 0.07013161 ± 0.021403381
1.610	0.193	0.127	59.38832	0.4083206 ± 0.07247885 ± 0.02045513
1.610	0.193	0.127	96.08225	0.3209038 ± 0.1013991 ± 0.0313346
1.610	0.193	0.127	138.5581	0.1170443 ± 0.146122 ± 0.02038013
1.610	0.193	0.127	180.2608	0.3477719 ± 0.1581127 ± 0.0354366
1.610	0.193	0.127	218.4883	-0.091217 ± 0.142311 ± 0.01898904
1.610	0.193	0.127	261.3985	-0.320382 ± 0.1108918 ± 0.0327608
1.610	0.193	0.127	303.3648	-0.266328 ± 0.07080153 ± 0.02802882
1.610	0.193	0.127	337.2208	-0.261976 ± 0.07224138 ± 0.02615273

Table 4: Coherent ALU in -t bins

$< Q^2 >$	$< x_B >$	$< -t >$	$< \phi >$	A_{LU} ± stat. ± syst.
1.395	0.166	0.407	21.10406	0.04811468 ± 0.04658231 ± 0.012062557
1.395	0.166	0.407	61.33965	0.0836005 ± 0.0531715 ± 0.015623204
1.395	0.166	0.407	95.84617	0.1792438 ± 0.05315892 ± 0.02637904
1.395	0.166	0.407	140.0124	0.04524659 ± 0.07010027 ± 0.0158652
1.395	0.166	0.407	181.9726	0.1242038 ± 0.08510458 ± 0.02346724
1.395	0.166	0.407	219.0216	0.03828423 ± 0.07649991 ± 0.01509915
1.395	0.166	0.407	259.0493	-0.1422473 ± 0.0495869 ± 0.02266091
1.395	0.166	0.407	303.8597	-0.1478417 ± 0.03942399 ± 0.01968592
1.395	0.166	0.407	337.5399	-0.0844819 ± 0.04879445 ± 0.01425768
1.886	0.233	0.499	20.62881	-0.0058365 ± 0.03877985 ± 0.012482536
1.886	0.233	0.499	58.90961	0.1058029 ± 0.05262749 ± 0.016983385
1.886	0.233	0.499	95.93819	0.1373368 ± 0.06176916 ± 0.02021609
1.886	0.233	0.499	141.0758	0.2106814 ± 0.09877572 ± 0.02858216
1.886	0.233	0.499	179.8328	0.06009099 ± 0.1188988 ± 0.01464961
1.886	0.233	0.499	220.9095	-0.03806458 ± 0.1066278 ± 0.04304848
1.886	0.233	0.499	260.608	-0.1192977 ± 0.07428519 ± 0.01808374
1.886	0.233	0.499	304.2599	-0.2011292 ± 0.05552498 ± 0.0198082
1.886	0.233	0.499	338.4649	-0.0815212 ± 0.0567802 ± 0.01138369
2.338	0.29	0.521	20.72956	0.08229175 ± 0.03744839 ± 0.013506039
2.338	0.29	0.521	56.90895	0.155593 ± 0.05379751 ± 0.01010521
2.338	0.29	0.521	94.91647	0.05217237 ± 0.0715696 ± 0.017660975
2.338	0.29	0.521	141.1955	0.1371172 ± 0.1260972 ± 0.01618568
2.338	0.29	0.521	181.6533	-0.2127209 ± 0.1556657 ± 0.02363223
2.338	0.29	0.521	224.0629	0.2006703 ± 0.1501709 ± 0.02122811
2.338	0.29	0.521	261.0354	-0.2716077 ± 0.09343596 ± 0.02419026
2.338	0.29	0.521	303.8146	-0.2199163 ± 0.06880397 ± 0.01534961
2.338	0.29	0.521	339.3798	-0.0379564 ± 0.06803362 ± 0.014507918
3.098	0.379	0.65	20.11158	0.1124871 ± 0.03615842 ± 0.014743619
3.098	0.379	0.65	56.98647	0.0725830 ± 0.0555646 ± 0.014717011
3.098	0.379	0.65	95.74599	0.1911079 ± 0.07990027 ± 0.02811833
3.098	0.379	0.65	137.8186	-0.005798 ± 0.1509773 ± 0.01296021
3.098	0.379	0.65	179.3002	-0.605363 ± 0.2490573 ± 0.027008585
3.098	0.379	0.65	227.8571	0.1695245 ± 0.1915087 ± 0.02732611
3.098	0.379	0.65	263.4649	-0.120036 ± 0.09407594 ± 0.02149023
3.098	0.379	0.65	303.8994	-0.178453 ± 0.04217566 ± 0.02211641
3.098	0.379	0.65	340.4588	-0.059749 ± 0.03455414 ± 0.01412915

Table 5: Incoherent ALU in Q2 bins

$< Q^2 >$	$< x_B >$	$< -t >$	$< \phi >$	$A_{LU} \pm$ stat. $\pm$ syst.
1.425	0.162	0.397	21.03589	0.08658236 ± 0.04970597 ± 0.013707438
1.425	0.162	0.397	62.13969	0.09617981 ± 0.0520029 ± 0.016508612
1.425	0.162	0.397	95.88097	0.1468384 ± 0.05007717 ± 0.02161179
1.425	0.162	0.397	140.2158	0.05840751 ± 0.06522249 ± 0.0149864
1.425	0.162	0.397	181.147	0.1472116 ± 0.07694323 ± 0.02355567
1.425	0.162	0.397	218.8907	-0.0045843 ± 0.07180578 ± 0.01995755
1.425	0.162	0.397	259.1392	-0.1140192 ± 0.04807579 ± 0.01836548
1.425	0.162	0.397	303.893	-0.1078614 ± 0.04183492 ± 0.01540446
1.425	0.162	0.397	337.0219	-0.0313563 ± 0.05506042 ± 0.01052464
1.922	0.227	0.418	22.06063	-0.0071624 ± 0.04158333 ± 0.013118195
1.922	0.227	0.418	58.5659	0.09277118 ± 0.05070619 ± 0.016106517
1.922	0.227	0.418	96.23033	0.1248119 ± 0.05973952 ± 0.01838518
1.922	0.227	0.418	141.4482	0.1767175 ± 0.09500723 ± 0.0246086
1.922	0.227	0.418	181.8282	-0.0887164 ± 0.1180524 ± 0.01655364
1.922	0.227	0.418	221.2517	-0.2925814 ± 0.102211 ± 0.03431685
1.922	0.227	0.418	260.3485	-0.1909171 ± 0.06539497 ± 0.02278749
1.922	0.227	0.418	303.5284	-0.2302893 ± 0.05094602 ± 0.02067598
1.922	0.227	0.418	337.3474	-0.0637682 ± 0.05413252 ± 0.01008997
2.354	0.287	0.492	20.85891	0.04657884 ± 0.036766 ± 0.01988718
2.354	0.287	0.492	57.91331	0.1459641 ± 0.0526584 ± 0.019557668
2.354	0.287	0.492	94.69206	0.128379 ± 0.07104001 ± 0.01884086
2.354	0.287	0.492	139.8528	0.1707919 ± 0.1258279 ± 0.02424851
2.354	0.287	0.492	179.8321	-0.3851509 ± 0.1628791 ± 0.014502416
2.354	0.287	0.492	225.9931	0.359824 ± 0.1375561 ± 0.014015373
2.354	0.287	0.492	261.519	-0.2473872 ± 0.08518201 ± 0.02723866
2.354	0.287	0.492	304.2744	-0.1756475 ± 0.04527543 ± 0.01784578
2.354	0.287	0.492	338.8707	-0.0591266 ± 0.04527858 ± 0.01010778
2.987	0.390	0.714	19.433	0.1032664 ± 0.03435814 ± 0.014305278
2.987	0.390	0.714	55.24427	0.07535726 ± 0.06348906 ± 0.014826822
2.987	0.390	0.714	95.27441	0.21340720 ± 0.1066241 ± 0.03136377
2.987	0.390	0.714	134.3823	-0.2684007 ± 0.2723481 ± 0.03863117
2.987	0.390	0.714	182.475	3.6842530 ± 5.592241 ± 0.03642855
2.987	0.390	0.714	232.2045	-0.3810377 ± 0.426418 ± 0.04691644
2.987	0.390	0.714	264.8367	-0.0853021 ± 0.1126019 ± 0.02026491
2.987	0.390	0.714	304.1341	-0.1678875 ± 0.04062397 ± 0.02296748
2.987	0.390	0.714	341.2705	-0.0649467 ± 0.03014188 ± 0.01568537

Table 6: Incoherent ALU in xB bins

$< Q^2 >$	$< x_B >$	$< -t >$	$< \phi >$	$A_{LU} \pm$ stat. $\pm$ syst.
1.823	0.213	0.145	22.36456	0.08044984 ± 0.044171 ± 0.013519389
1.823	0.213	0.145	57.76681	0.139094 ± 0.05252524 ± 0.019097037
1.823	0.213	0.145	97.34826	0.1215345 ± 0.05070444 ± 0.01794958
1.823	0.213	0.145	141.6077	0.1973951 ± 0.07158507 ± 0.0263301
1.823	0.213	0.145	180.9132	0.03301465 ± 0.087735 ± 0.01504234
1.823	0.213	0.145	219.6382	0.00344467 ± 0.07526837 ± 0.018209534
1.823	0.213	0.145	261.1274	-0.1527359 ± 0.05030086 ± 0.01958999
1.823	0.213	0.145	303.674	-0.1071745 ± 0.04406731 ± 0.0137369
1.823	0.213	0.145	337.0581	-0.06869941 ± 0.04715184 ± 0.01004524
2.127	0.255	0.282	21.36259	0.07262895 ± 0.04230211 ± 0.013126559
2.127	0.255	0.282	59.22203	0.03806518 ± 0.04905662 ± 0.012518665
2.127	0.255	0.282	95.55563	0.22988040 ± 0.05867932 ± 0.03380763
2.127	0.255	0.282	140.5704	-0.03154477 ± 0.08162287 ± 0.0178829
2.127	0.255	0.282	181.2953	-0.1565047 ± 0.10092 ± 0.0298368
2.127	0.255	0.282	219.844	-0.03787627 ± 0.09359193 ± 0.01834677
2.127	0.255	0.282	259.6599	-0.1349929 ± 0.05604338 ± 0.02535689
2.127	0.255	0.282	304.1345	-0.1822338 ± 0.03916768 ± 0.02481545
2.127	0.255	0.282	338.5113	-0.07208852 ± 0.04495988 ± 0.01711214
2.308	0.284	0.490	20.67062	0.129165 ± 0.0415758 ± 0.015497728
2.308	0.284	0.490	59.71279	0.113594 ± 0.05196332 ± 0.017545246
2.308	0.284	0.490	94.41645	0.1003674 ± 0.06511375 ± 0.01472001
2.308	0.284	0.490	137.7611	0.1088956 ± 0.1159367 ± 0.01662967
2.308	0.284	0.490	181.8561	0.3436873 ± 0.1353462 ± 0.03922332
2.308	0.284	0.490	225.1743	-0.06749131 ± 0.1106012 ± 0.01250426
2.308	0.284	0.490	259.4171	-0.2186645 ± 0.06202168 ± 0.02341567
2.308	0.284	0.490	302.9163	-0.1778958 ± 0.03422616 ± 0.01629588
2.308	0.284	0.490	338.8539	-0.04591294 ± 0.03922611 ± 0.017893601
2.406	0.308	0.90	20.16669	0.01851554 ± 0.03466921 ± 0.017815254
2.406	0.308	0.90	57.08842	0.167122 ± 0.06853916 ± 0.01086996
2.406	0.308	0.90	93.11341	0.07585309 ± 0.140148 ± 0.01108901
2.406	0.308	0.90	132.8371	-0.1390574 ± 0.4839775 ± 0.01772069
2.406	0.308	0.90	177.344	1.854154 ± 0.5453675 ± 0.01816686
2.406	0.308	0.90	228.2105	5.778605 ± 10.58589 ± 0.01512427
2.406	0.308	0.90	263.1194	0.02895751 ± 0.1390042 ± 0.017122356
2.406	0.308	0.90	305.0914	-0.1501369 ± 0.04840413 ± 0.01297528
2.406	0.308	0.90	340.095	-0.05253375 ± 0.03990596 ± 0.016446498

Table 7: Incoherent ALU in -t bins